QINGYUAN WANG

Broadband microstrip circuits, antennas, and antenna arrays for mobile satellite communications

Thèse

présentée

à la Faculté des études supérieures

de l'Université Laval

pour l'obtention

du grade de Philosophia Doctor (Ph. D.)

Département de génie électrique

et de génie informatique

FACULTÉ DES SCIENCES ET DE GÉNIE

UNIVERSITÉ LAVAL

QUÉBEC

AVRIL 2000

Acknowledgment

I would like to express my deep gratitude to Professor Michel Lecours, for giving me the opportunity of studying here, for the excellent project on the design of the electronically-scanned antenna arrays, for his guidance in each step of my design work, for his patience shown in the revision of this thesis, and finally, for his encouragement and recommendation in my job hunt.

Thanks to Professor Gilles-Y Delisle for his supervision over my course work. Thanks to Dr. Marcel Pelletier for his work on the configuration of the antenna array and his many suggestions. The suggestions from Mr. Claude Vergnolle were very important in my attempt to design microstrip switches, beam controllers and solid state amplifiers. I thank Dr. Martin Smith for his suggestions on the design of dual-band patch antennas with circular polarization. I thank Mr. Gilles Bisson for assembling most of my microstrip circuits and antenna arrays. Also thanks to Mr. Mario Le Blanc for his suggestions in the solid state amplifier design.

My thanks also to the many colleagues at the different design stages of the mobile satellite antenna array project: Pierre Lahaie, Tudor Breahna, Nathalie Robitaille, and Martin Lefebvre.

I also would like to thank Laval University for providing me a free and tolerant academic environment, in which I can concentrate in my study and design work and take some time visiting the sceneries around the beautiful Quebec City.

We also gratefully acknowledge the financial support of Davicom Technology Inc., the NSERC Technological Partnership Program, and the Nortel Global External Research Program.

Circuits microrubans à large bande, antennes et antennes-réseau pour communications mobiles par satellite

Sommaire

Les antennes à balayage mécanique pour communications mobiles par satellite de type géostationnaire couvrent typiquement des angles d'élévation allant jusqu'à 60 degrés. Cette limitation de couverture rend l'antenne peu utile dans plusieurs régions terrestres. Cette limitation peut être éliminée par une antenne-réseau à balayage électronique couvrant des angles d'élévation jusqu'à 90 degrés. De telles antennes-réseau possèdent également des avantages sur les antennes à balayage mécanique comme des durées d'acquisition et de pousuite plus courtes et une consommation de puissance CC moindre. Puisque l'antenne ne comporte pas de pièces mobiles, sa robustesse inhérente est également accrue. Cette thèse porte sur la conception et la réalisation d'une telle antenne-réseau globale, y inclus les techniques de conception large bande, les commutateurs à configuration radiale, le contrôle des faisceaux d'antenne et les antennes-plaque à couplage électromagnétique.

Dans les parties théoriques de la thèse, on développe plusieurs techniques pour la conception de circuits et d'antennes micro-rubans, on établit des critères pour le design d'un commutateur radial à large bande, on propose un concept novateur de réseau de formation de faisceaux, de même qu'un circuit diviseur de puissance simple, qui est utilisé pour le design d'une antenne-plaque à polarisation circulaire. Des simulations sur ordinateur sont faites pour vérifier les techniques et concepts et pour accélérer le design de circuits prototypes en utilisant HP-EEsof Series IV, MMICAD et Ensemble 4.02. Finalement les techniques et concepts sont implantés et testés.

Circuits microrubans à large bande, antennes et antennes-réseau pour communications mobiles par satellite

Résumé

Les antennes à balayage mécanique pour communications mobiles par satellite de type géostationnaire couvrent typiquement des angles d'élévation allant jusqu'à 60 degrés. Cette limitation de couverture rend l'antenne peu utile dans plusieurs régions terrestres. Cette limitation peut être éliminée par une antenne-réseau à balayage électronique couvrant des angles d'élévation jusqu'à 90 degrés. De telles antennes-réseau possèdent également des avantages sur les antennes à balayage mécanique comme des durées d'acquisition et de pousuite plus courtes et une consommation de puissance CC moindre. Puisque l'antenne ne comporte pas de pièces mobiles, sa robustesse inhérente est également accrue. Cette thèse porte sur la conception et la réalisation d'une telle antenne-réseau globale, y inclus les techniques de conception large bande, les commutateurs à configuration radiale, le contrôle des faisceaux d'antenne et les antennes à double plaque à couplage électromagnétique.

Dans les parties théoriques de la thèse, on développe plusieurs techniques pour la conception de circuits et d'antennes micro-rubans, on établit des critères pour le design d'un commutateur radial à large bande, on propose un concept novateur de réseau de formation de faisceaux, de même qu'un circuit diviseur de puissance simple, qui est utilisé pour le design d'une antenne-plaque à polarisation circulaire. Des simulations sur ordinateur sont faites pour vérifier les techniques et concepts et pour accélérer le design de circuits prototypes en utilisant HP-EEsof Series IV, MMICAD et Ensemble 4.02. Finalement les techniques et concepts sont implantés et testés.

Cette thèse comporte sept chapitres. Au chapitre 1, on introduit les satellites géostationnaires pour communications mobiles par satellite et les exigences pour les antennes et antennes-réseau. On présente un certain nombre d'exemples de réalisations.

Au chapitre 2, on dérive une matrice de transfert simple pour une ligne de transmission quart

d'onde, qui sert à développer et optimiser plusieurs techniques, soit un transformateur quart d'onde à deux segments, un stub parallèle ouvert de demi-longueur d'onde et un stub composite. Une technique de design basée sur trois points de mesure est aussi étudiée.

On étudie au chapitre 3 le design de commutateurs sur circuit microruban. On adopte une configuration simple de commutateur pour obtenir une perte d'insertion faible et un coût modéré. En vue de montrer les facteurs qui limitent la largeur de bande, on dérive une expression pour le Q d'un commutateur radial composé de lignes de transmission idéales et on l'utilise pour établir des critères pour la conception d'un commutateur à large bande.

Au chapitre 4, on introduit le concept d'un contrôleur de faisceau M/N pour fournir un signal commandé en phase dans M canaux activés sur les N canaux disponibles, avec une répartition de puissance mieux équilibrée par rapport à la configuration utilisée précédemment. Le processus du design d'un contrôleur de faisceau 3/8 basé sur ce concept est introduit.

Nous présentons au chapitre 5 une méthode pour le design d'une antenne-plaque double avec couplage électromagnétique pour polarisation circulaire. Nous dérivons d'abord un facteur de mésadaptation de polarisation en fonction du rapport axial d'une onde électromagnétique incidente et d'une antenne réceptrice. Nous proposons ensuite un circuit simple pour fournir des signaux contrôlés en phase et de puissance équilibrée aux deux alimentations de l'antenne plaque. Troisièmement, en supposant que la puissance à chaque port d'alimentation de l'antenne est spécifiée, nous dérivons des expressions pour montrer l'effet sur le rapport axial de la différence de phase entre les champs électriques orthogonaux rayonnés par l'antenne.

Au chapitre 6, nous présentons la configuration d'un prototype d'antenne-réseau à balayage électronique à couverture quasi-hémisphérique ou encore "globale", composé d'un contrôleur de faisceau, de 8 antennes à double plaque sur les 8 facettes d'un cône octogonal tronqué, et d'une antenne sur le dessus.

Le chapitre 7 présente quelques discussions et conclusions.

Broadband microstrip circuits, antennas, and antenna arrays for mobile satellite communications

Abstract

A typical mechanically-scanned antenna for geostationary satellite mobile communications covers elevation angles up to 60 degrees. This coverage limitation renders the antenna of little use in many areas of the earth. This limitation can be relieved by an electronically-scanned antenna array which covers elevation angles up to 90 degrees. Such an array also has advantages over a mechanically-scanned antenna such as faster satellite acquisition and tracking and lower DC power consumption. Because there is no moving component involved, it is inherently more robust as well. The design and test of such a global array is addressed in this thesis, together with the concepts and implementations of broadband design techniques, radial switches, beam controllers, and electromagnetically-coupled patch antennas.

Each step of the work is carried out under the guidance of microwave circuit theories. In the theoretical work, several techniques for broadband microstrip circuit and antenna design are developed, criteria for broadband radial switch design are established, the concept of a novel beam-forming network, called beam controller, is proposed, and a simple power dividing circuit, which is useful in the design of patch antennas with circular polarization, is also proposed. Computer simulations with HP-EEsof Series IV, MMICAD Version 2 and Ensemble 4.02 are used to verify the techniques and concepts and to expedite the design of circuit prototypes. Finally, the techniques and concepts are implemented according to the simulations and tested.

Broadband microstrip circuits, antennas, and antenna arrays for mobile satellite communications

Summary

A typical mechanically-scanned antenna for geostationary satellite mobile communications covers elevation angles up to 60 degrees. This coverage limitation renders the antenna of little use in many areas of the earth. This limitation can be relieved by an electronically-scanned antenna array which covers elevation angles up to 90 degrees. Such an array also has advantages over a mechanically-scanned antenna such as faster satellite acquisition and tracking and lower DC power consumption. Because there is no moving component involved, it is inherently more robust as well. The design and test of such a global array is addressed in this thesis, together with the concepts and implementations of broadband design techniques, radial switches, beam controllers, and electromagnetically-coupled stacked patch antennas.

Each step of the work is carried out under the guidance of microwave circuit theories. In the theoretical work, several techniques for broadband microstrip circuits and antennas design are developed, criteria for broadband radial switch design are established, the concept of a novel beam-forming network, called beam controller, is proposed, and a simple power dividing circuit, which is useful in the design of patch antennas with circular polarization, is also proposed. Computer simulations with HP-EEsof Series IV, Ensemble 4.02, and MMICAD Version 2 are used to verify the techniques and concepts and to expedite the design of circuit prototypes. Finally, the techniques and concepts are implemented according to the simulations and tested.

This thesis is composed of seven chapters. In Chapter 1, geo-stationary satellites for mobile satellite communications and the requirements on antennas and antenna arrays are introduced. A number of implementations in this field are also reviewed.

In chapter 2, a simple transferring matrix of a quarter-wavelength transmission line is derived.

Several techniques which arise from such a matrix, are proposed: an optimized two-stage quarter-wavelength transformer, an optimized shunt half-wavelength open stub, and a compound half-wavelength open stub. A three-point compromise technique is also addressed.

In Chapter 3, the design of microstrip switches is studied. A simple switching circuit is chosen to form the switches for lower cost and lower insertion loss. In order to show the factors limiting the bandwidth, the Q-factor of a radial switch composed of ideal transmission lines is derived and used to establish criteria for wide bandwidth switch design.

In Chapter 4, the concept of a M/N-channel radial beam controller is introduced to deliver phase-controlled power into M activated channels out of a total of N channels, with a power-delivering balance improved over what could be achieved by the previously suggested configuration. The process of the design of a 3/8-channel beam controller based on the above concept is presented.

In Chapter 5, we present a method for electronically-coupled circular polarization stacked patch antenna design. First we derive the polarization mismatch factor as a function of axial ratio of an incident electromagnetic wave and that of a receiving antenna. Second, we propose a simple circuit which is capable of delivering balanced phase-controlled power into the two feeds of a dual-feed patch antenna. Third, assuming the power fed into each port of the dual-feed antenna is specified, we derive formulae to show the effect on the axial ratio of the phase difference between the orthogonal electrical fields radiated from the antenna.

In Chapter 6, we present the configuration of a global electronically-scanned array prototype. It is composed of a beam controller, 8 patch antennas on the 8 facets of a truncated octagonal cone, and of a patch antenna on the top.

In Chapter 7 are some discussions and conclusions.

Table of Contents

Chapter 3

Chapter 4

Chapter 5

List of Figures

Chapter 1

Chapter 2

Chapter 3

Chapter 4

Chapter 5

Chapter 6

List of Tables

WE MUST KNOW,

WE SHALL KNOW.

----DAVID HILBERT

CHAPTER 1

Introduction

1.1 Mobile satellite communications

Wherever we are, satellite communications are advancing rapidly towards providing us with links such as telephone, fax and data, to other people at any other location, with an affordable per-minute cost. In the past three decades, hundreds of satellites have already been launched for global, regional and domestic satellite communications[1].

Satellites can be classified as Geostationary Earth Orbit (GEO), Medium Earth Orbit (MEO), and Low Earth Orbit (LEO) systems, according to their altitude above the earth. Each system has its own advantages and disadvantages, depending on the user's particular purpose. Because of their high latitude, a global coverage can be provided by as little as 3 GEO satellites. As for a LEO system, several tens to a few hundred satellites are required for a similar coverage. Also because the satellites in a GEO system appear stationary to the Earth, no tracking ability is necessary for station antennas and antennas on board for gateway links. Although GEO satellites, which are located 35,700 km above the Equator, are expensive to launch, and have an unpleas-

ant 0.37 second of transmission delay, it is anticipated that GEO systems will continue to be of major importance in the satellite communication markets in the following years.

While new global and regional GEO systems are continuing to be planned, the commercial use of GEO satellites for mobile communications is already available through several systems, such as Inmarsat, MSAT, and OPTUS. The first two systems use a relative bandwidth of 8.5% around a center frequency of 1.593 GHz for mobile-satellite links (1.5250 GHz ~ 1.5590 GHz for downlink from Satellite to Mobile users and 1.6265 GHz ~ 1.6605 GHz for uplinks from Mobile users to Satellite). The last system uses a relative bandwidth of 7.2% around a center frequency of 1.603 GHz for mobile satellite links (1.5450 GHz to 1.5590 GHz for downlink and 1.6465 GHz to 1.6605 GHz for uplink). Because of the different requirements on the bandwidth and elevation coverages, a mobile satellite antenna array for the first two systems will be technically more challenging than that for the third system.

1.2 Requirements on mobile satellite antennas and antenna arrays

The requirements on the mobile satellite antenna terminals are several folds: in the horizontal plane, any mobile terminal must have satellite tracking ability and should cover horizontal angles from 0 to 360 degrees. The requirement on the elevation angular coverage depends on the particular area in which the terminal is to be used. For instance, in the Australian OPTUS system, elevation angular coverage from 30° to 70° is enough, while for land mobile users in North America by Inmarsat or MSAT systems, elevation angular coverage from 20° to 70° is required. The highest requirement on the elevation angular coverage is put by the inter-continental voyagers, who may need to cross the Equator frequently. For them, a global terminal which covers elevation angles from 20° to 90° is required. Although there is no direct requirement on the axial ratio of the antenna, the compound gain, defined as the gain of the terminal antenna reduced by the polarization mismatch factor between the terminal antenna and the incident wave from the satellite, should be comparable to 7 dB over the operation band. The return loss of the antennas is usually required to be lower than -10 dB. In order to stand the vibrations of the car caused by bad road conditions or of the ship because of strong wind on the sea, the antenna should be mechanically robust. In order to be able to be mounted on top of a vehicle the

antenna should also be compact and light-weight. The antenna should also be low profile to minimize resistance to the wind should the vehicle be fast moving. The last requirement and also one of the most important one for a commercial product is that the antenna should be low cost so that a large enough market can be built up.

1.3 International efforts in the development of mobile satellite antennas and antenna arrays

In the past several years, because of their technical simplicity, mechanically-steered antennas have been designed and mobile satellite communication systems with such antennas are available on the market[2,3]. New designs are also continuing to be reported [4,5]. Such an antenna system typically uses an antenna such as a helical antenna or a microstrip patch array with a single broad beam. The beam is tilted downward from the vertical direction for better coverage in the lower elevation angles, with relatively wide beam width in elevation and narrower beam in azimuth (fan beam). A step motor is generally used to rotate the beam around the vertical axis, allowing any horizontal angle to be covered. Mitsubishi and Westinghouse antennas [3,4] are the most popular in this category. A Mitsubishi MSAT antenna, which uses a helical antenna as the radiation element, covers elevation angles from 15° to 60° with a minimum gain of about 8 dB. A mechanically-scanned antenna was tested by Charles D. McCarrick [5] which used a microstrip array. The antenna had a minimum gain of about 9.0 dB and covered elevation angles from 25° to 60°. Measured axial ratios of 4.5 to 5.7 dB, were reported. The antenna was designed to cover relatively high elevation angles only and the poor coverage at lower elevation angles was because the planar patch antenna array was not tilted but rather located in the horizontal plane. A tilted, mechanically-scanned antenna has been developed by JPL [6] for L-band mobile applications. The antenna consisted of a linear array of four square microstrip patches tilted with respect to the ground plane to provide elevation angle coverage from 20 to 60 degrees with a minimum gain of 10 dB. The antenna was 50.8 cm in diameter and 22.9 cm in height.

An electronically-scanned array has several advantages over a mechanically steered one such as faster acquisition and tracking, lower DC power consumption. Because there are no moving parts in the system, it will also be more robust and more reliable as well. Because of these ad-

vantages, in the past ten years, considerable effort has been devoted to the design of this kind of arrays for mobile satellite communications.

R. Milne at CRC [7] designed a kind of linearly-polarized adaptive array antenna. The antenna was composed of a quarter-wavelength monopole with two to five concentric rings of parasitic elements mounted on a ground plane. The gain of an antenna with five concentric rings varies between 12 and 14 dB in the receiving band from 1.53 GHz to 1.56 GHz, and between 9 and 13.5 dB in the transmitting band from 1.63 GHz to 1.66 GHz. Considering the polarization mismatch factor of 3 dB between circular and linear polarization, a compound gain higher than 6 dB can be achieved over the whole band. A power-handling-capacity as high as 100 W was reported. The antenna was 91 cm in diameter and about 5 cm in height.

Circular polarization using this concept has also been obtained at CRC by adding a polarizer (lens) to the linearly polarized array[8]. Maximum return loss is -11 dB. The most current data [9] for CRC's adaptive antenna indicated a gain of 6.0 to 10 dB, an elevation angular coverage from 0 to 90 degrees with a diameter of 35.6 cm and a height of 5.7 cm.

A six-element switched-element spherical array was reported in 1987 by Hori[10]. The antenna comprised a radiator section, a switching circuit and a controller. The radiation section was composed of 6 circularly-polarized elements. The gain was higher than 5.4 dB for elevation angles from 20 to 60 degrees. The array was 40 cm in diameter and 20 cm in height.

Another 14-channel switched-beam antenna for Australian Mobilesat was also reported by M. E. Bialkowski et al in 1996, [11]. The antenna worked in a 7.2% bandwidth with overall return loss lower than -10 dB. The antenna element was a cavity-enclosed dual-patch electromagnetically-coupled microstrip antenna. 3 adjacent channels were switched on to form a beam. No phase shifter was used in the array and a total of 14 beams can be formed by turning on each group of 3 adjacent channels. Satellite tracking was made possible by turning on the beam closest to the direction of the satellite.

A phased array was also reported in 1999 for the Australian Mobilesat by M. E. Bialkowski and N. C. Karmakar [12]. Compared with a switched-beam array, no switch was used in this phased

array. The scanning of the beam was made possible by different combinations of the phase shifters' states. The antenna was a multi-layer planar structure which was composed of 12 antenna elements and with a 3-bit phase shifter inserted before each element. The cost of the array was considerably lowered down from an earlier phased-array [13] by the use of cheap diodes. The antenna element was a dual-feed aperture-coupled patch antenna in which two substrates were spaced by a thick layer of foam for increased bandwidth. The gain of the antenna was 8.8 dB covering elevation angles from 30° to 70° for a relative bandwidth of about 7.2%. The axial ratio measured in any direction of interest was lower than 6 dB. The overall return loss was lower than -18 dB and the antenna was 46 cm in diameter and 4 cm in height.

Classified between a mechanically-scanned antenna and a electronically-scanned array, a semi-electronically-scanned array was designed by J. Aurinsalo [14] from the Technical Research Center of Finland (VTT). The array used 12 one-turn antenna (OTA's), which were installed on the facets of a 12-side truncated cone. In the array two elements radiated simultaneously. The tilt angle of the elements could be adjusted mechanically to point at elevation angles of 20, 30 and 40 degrees. By doing this, elevation angles from 10° up to from 50° were well covered with a gain of about 11 dB. The antenna was 42 cm in diameter and 20.5 cm in height. Cross-polar levels better than -20 dB were reported.

1.4 Challenges in economical electronically-scanned antenna array design

Although an electronically-scanned antenna array for mobile satellite communications is very attractive and considerable progress has already been made in this field, such antennas appear to be prototypes rather than fully commercial products. As for a global antenna or antenna array, which means an antenna with hemispheric coverage, no mechanically-scanned antenna or electronically-scanned array product is available in the market yet. Technical difficulties and high cost are two main reasons for the delay in the emergence of such commercial products.

For a commercially motivated development, it is important to lower down the price and to achieve good performance. Printed circuits are light-weight, robust, highly reproducible and low cost, especially when the manufacturing process is automated. In order to achieve low cost, al-

most all structures other than microstrip switches, phase shifters and patch antennas should be excluded from consideration. However, microstrip antennas are inherently characterized by narrow bandwidth and low radiation efficiency. The requirement of a relative bandwidth of 8.5% (7.2% for OPUS) for the whole system is a stringent one. To meet it, the bandwidth of the switches, phase shifters and antenna elements, should be considerably wider and care must also be taken to deal with the interaction between them when they are integrated together.

1.5 Objective and plan of the present work

The motivation of the work presented in this thesis is to explore the possibility of developing a global electronically-scanned antenna array which covers elevation angles from 20° to 90° at the lowest possible cost and with the electrical parameters meeting the performance requirements. In order to do so, efforts are devoted to the development of various techniques, sub-circuits and patch antennas, which can be used in the integration of such an array.

This thesis is composed of seven chapters.

After this introductory chapter, in chapter 2, a simple transferring matrix of a quarter-wavelength transmission line is derived. Several techniques which arise from such a matrix, are proposed: the optimized two-stage quarter-wavelength transformer, the optimized shunt half-wavelength open stub, and the compound half-wavelength open stub. A three point compromise technique is also addressed.

In Chapter 3, the design of microstrip switches is studied. A simple switching circuit is chosen to form the switches for lower cost and lower insertion loss. In order to show the factors limiting the bandwidth, the Q-factor of a radial switch composed of ideal transmission lines is derived and used to establish criteria for wide bandwidth switch design. From a sample switch implementation, the measured insertion loss is found to be lower than 0.50 dB, the reflection lower than -13.76 dB, and the isolation better than 28.45 dB, for the whole band from 1.525 GHz to 1.661 GHz. The measured power handling capacity from such an switch is also estimated.

In Chapter 4, the concept of a M/N-channel radial beam controller is introduced to deliver phase-controlled power into M activated channels out of a total of N channels, with a power-delivering balance improved over what could be achieved by a previously suggested configuration composed of separate switch and phase shifters. The process of the design of a 3/8-channel beam controller based on the above concept is presented. A tuning circuit using two compound half-wavelength open stubs is designed to increase the bandwidth. Four features of the beam controller are worth mentioning, namely low cost, good power-delivering balance, good isolation of the deactivated channels and phase difference flexibility. The measured results from a sample beam controller showed a return loss lower than -14.92 dB, an overall insertion loss lower than 2.08 dB, a power-delivering balance better than 0.92 dB, and an isolation better than 28.53 dB for the operation band from 1.525 GHz through 1.661 GHz. The phase differences were 103, 107, 114, 121, and 124 degrees, at 1.525, 1.559, 1.593, 1.627, and 1.661 GHz, respectively.

In Chapter 5, we present a method for economical circularly-polarized electromagnetically-coupled stacked patch antenna design. First we derive the polarization mismatch factor as a function of axial ratio of an incident electromagnetic wave and that of a receiving antenna. Second, we propose a simple circuit which is capable of delivering balanced phase-controlled power into the two feeds of a dual-feed patch antenna. Third, assuming the power fed into each port to the dual-feed antenna is specified, we derive formulae to show the effect on the axial ratio of the phase difference between the orthogonal electrical fields radiated from the antenna. A step-by-step method for electromagnetically-coupled patch antenna design based on simulations follows. Measured results from a sample antenna are: gains from 8.10 dB to 9.36 dB and axial ratios from 2.41 dB to 4.41 dB in the boresight direction for frequencies from 1.525 GHz to 1.661 GHz. The return losses are lower than -19.52 dB.

In Chapter 6, we present the configuration of a global electronically-scanned array prototype. It is composed of a beam controller, 8 patch antennas on the 8 facets of a truncated octagonal cone, and of a patch antenna on the top. It covers elevation angles from $\theta_E = 20°$ to $\theta_E = 90°$ with a gain higher than 4.6 dB and a measured return loss lower than -14.5 dB in the receiving and transmitting bands.

In Chapter 7 are some discussions and conclusions.

1.6 Configuration of an electronically-scanned antenna array

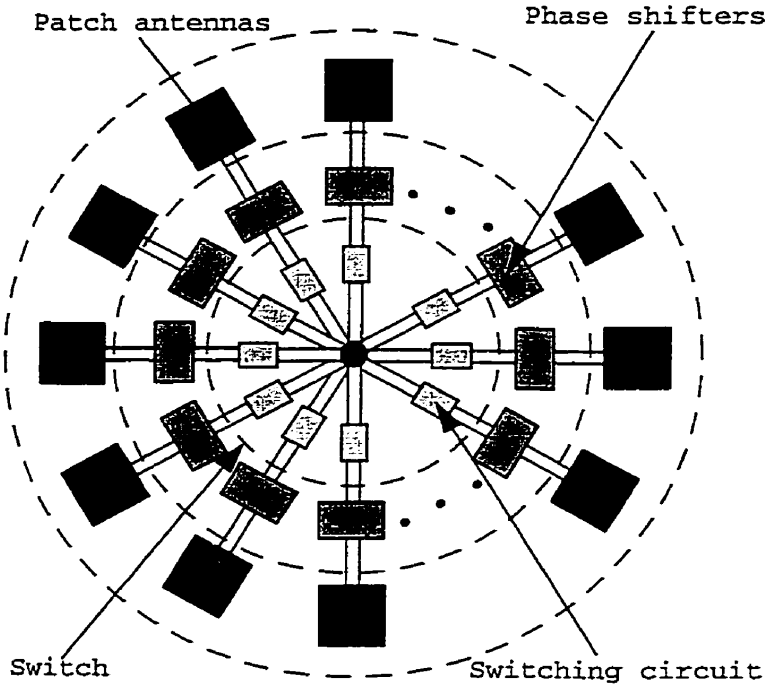

Figure 1.1 An N-channel electronically-scanned antenna array.

The present research project has been realized in the frame work of a team effort to develop an N-channel electronically-scanned antenna array[15-23]. The original configuration of the array, as shown in Figure 1.1, was proposed for an elevation coverage from 20° to 60°. It is composed of a total of N-channels joined together in parallel at the center of the panel. Each channel is again composed of a switching circuit[24] in series with a 1-bit phase shifter and a patch antenna. Each channel can be activated or deactivated by its switching circuit. In operation, 3 adjacent channels will be activated simultaneously. The 1-bit phase shifter can be on its "1" state with a larger electrical length in degrees or on its "0" state with a smaller electrical length. For each 3 activated channels, 3 beams, i.e the 110, the 010 and the 011 beams, which point in three different adjacent directions can be formed by assuming different combinations of the phase shifters. A total of 3N beams can be formed horizontally in this way. The array acquires the direction of the satellite by pointing the beam towards each of the total 3N directions and comparing the re-

ceived pilot signal from the satellite. The beam which receives the highest signal level will be used for communications. This process will be repeated every several tenth of a second and another beam will be used should the relative orientation of the satellite be changed because of the movement of the vehicle.

With the evolution of the project, two modifications to the configuration of the array have been made. First, a beam controller was proposed to replace the N-channel switch and a phase shifter in each channel. Second, a top patch antenna was added, making the array a global one which covers elevation angles from 20° to 90°.

1.7 Methodology used in the work

To avoid a time-consuming and costly try-and-error process, each step of the work was carried out under the guidance of microwave circuit theories. Theoretical work has been useful in the establishment of criteria for broadband radial switch design. Also because of the theoretical work, several techniques for broadband microwave circuits and antennas design were developed. These techniques were very helpful in our battle for improved bandwidth of the microstrip circuits and patch antennas to meet the bandwidth requirement on the whole array. Theoretical work has also been relied on to show the principal limitation of a technical avenue which was generally adopted by other groups, namely a central switch leading to separate phase shifters and antenna units. Consequently, the concept of a beam controller, where transmission-type phase shifters also function as switch, was proposed and implemented. Such a beam-forming network with low insertion loss, low return loss, high isolation and good power delivering balance, has proved crucial for the design of the global antenna array.

1.8 Contributions of the thesis

1. Several techniques for broadband microwave circuit and patch antenna design are established. A simple transferring matrix is derived and its applications lead to the concepts of an optimized two-stage quarter-wavelength transformer, an optimized shunt half-wavelength open stub, and

a compound half-wavelength open stub, which are useful in broadband circuit and antenna design. A three-point compromise technique for broadband matching is also proposed.

2. A simple switching circuit which can be used to form a microwave switch is proposed. Formulae are derived to show the limitations on the bandwidth and insertion loss of a microwave switch and broadband switch design criteria are established. An economical broadband microstrip switch with low insertion loss and good cross-channel isolation is designed under the guidance of the criteria.

3. Formulae are derived to show the difficulties in the design of the switch, phase shifter, and patch antenna for a beam-forming network with good power-delivering balance. The concept of a beam controller is proposed to solve the problem. A beam controller which has low insertion loss, increased bandwidth, good cross-channel isolation, with improved power delivering balance, is designed and tested.

4. Formulae are derived to show the dependence of the polarization mismatch factor on the axial ratio of a patch antenna. Formulae are also derived to show the dependence of the axial ratio of a double-feed patch antenna on the phase difference of the orthogonal electric fields. Using the software Ensemble, economical broadband electromagnetically-coupled patch antennas with enough bandwidth and relatively high gains were designed.

5.Based on the above work, an economical electronically-scanned patch antenna array covering elevation angles from 20° to 90° with a minimum gain of 4.6 dB was designed and tested.

1.9 History of the mobile satellite antenna array project

The circuit design concepts and implementations described in the following chapters constitute our contribution. We would like to state how these are linked to the whole mobile satellite antenna array project.

The basic impulse for an Msat/Inmarsat electronic steering antenna was given in 1995 by Davicom Technologies and its president R. Daviault, as a part of the company's business plan. A research proposal was then formulated by Professors Lecours and Delisle and Dr. Pelletier and submitted to NSERC's Technological Partnership Program which approved it at the end of 1996. The project started, first on a modest scale, at the beginning of 1997 with Dr. Pelletier being the main architect behind the antenna array configuration. P. Lahaie as design engineer was globally responsible for the project and especially the design of the reflection type phase shifters, with a resulting publication [15]. T. Breahna was designing and testing stacked patch antennas and performing different tests on the antenna, which were reported in his M.Sc. thesis [18]. G. Bisson and Y. Chalifour were the technicians attached to the project for its whole duration.

I joined the project in early November 1997 and started, with initial suggestions from C. Vergnolle, the design of the central switch for the first antenna array prototype: the design of that switch eventually led to a conference paper [20] and a Journal paper [21] and is reported in chapters 2 and 3 of this thesis. Work proceeded at an intense rate by the whole team during 1998: this first antenna array prototype was successfully implemented by the team, now including M. Lefebvre of Davicom, and the results reported by the team in a conference paper [19].

T. Breahna and P. Lahaie then left the project at the end of 1998 and work continued by Dr. Pelletier and M. Lefebvre on different tests and implementation aspects, in particular the design and implementation of a satellite pilot signal detection circuit for the antenna controller. N. Robitaille, who had joined the project in 1998 as an M.Sc. student, was responsible for designing and

implementing an antenna array controller, which was, during the first part of the year 2000, inserted in a micro-controller circuit with the assistance of S. Tremblay and J.M. Beaulieu.

Following my work with the switch of the first prototype, and following on an initial suggestion by C. Vergnolle, I proposed and developed the novel concept of the beam controller reported in Chapter 4 of this thesis, in which switches are used to produce a switching system which also acts as a phase shifting system.

I suggested then to complete this second antenna array prototype by designing air dielectric stacked patch antennas: this led to the optimization of the feed circuit and tuning stub designs for circular polarization (Chapter 5).

Finally, under the impulse of Professor Lecours, I designed and implemented the upper antenna and the switch circuit to achieve semi-hemisperic coverage, as reported in Chapter 6.

CHAPTER 2

Techniques for broadband microstrip circuits and patch antenna design*

2.1 Introduction

The transferring matrix of a transmission line is [25]

$$\begin{bmatrix} \cos\beta l & jZ_0 \sin\beta l \\ j\frac{1}{Z_0}\sin\beta l & \cos\beta l \end{bmatrix}, \tag{2.1}$$

where l is the length of the transmission line, Z_0 its characteristic impedance, and β its wave-number,

$$\beta = \frac{2\pi f}{c}\sqrt{\varepsilon_{eff}}. \tag{2.2}$$

* Some of the content of this chapter has been accepted for publication in the IEEE Transactions on Microwave Theory and Techniques [21].

Here f is the frequency of the wave and ε_{eff} the effective dielectric constant of the transmission line and c the speed of light in free space. For a low-dispersion transmission line, such as a microstrip, ε_{eff} can be assumed to be constant over a relatively wide bandwidth.

For a quarter-wavelength transmission line,

$$l = \frac{\lambda_g}{4} = \frac{c}{4\sqrt{\varepsilon_{eff}} f_0}, \tag{2.3}$$

where f_0 is the center frequency. At a frequency Δf away from f_0, we have $\beta l = \pi(1 + \Delta f / f_0)/2$ and

$$\cos\beta l = \cos\left(\frac{\pi}{2} + \frac{\pi}{2}\frac{\Delta f}{f_0}\right) = -\frac{\pi}{2}\frac{\Delta f}{f_0} = -\frac{1}{2}x \tag{2.4}$$

and

$$\sin\beta l = \sin\left(\frac{\pi}{2} + \frac{\pi}{2}\frac{\Delta f}{f_0}\right) = \cos\left(\frac{\pi}{2}\frac{\Delta f}{f_0}\right) = 1. \tag{2.5}$$

Equations (2.4) and (2.5) are accurate to the first order of $x = \pi\Delta f / f_0$. Using (2.4) and (2.5) in (2.1), the transferring matrix of the quarter-wavelength transmission line is,

$$\begin{bmatrix} -\frac{1}{2}x & jZ_0 \\ j\frac{1}{Z_0} & -\frac{1}{2}x \end{bmatrix}. \tag{2.6}$$

In this chapter, this transferring matrix will be used in several situations, resulting in the concepts of an optimized two-stage quarter-wavelength transformer, an optimized shunt half-wavelength open stub, and a compound half-wavelength open stub, which are useful in broadband circuit and antenna design. We will also suggest a three-point compromise technique for broadband matching. In Section 2.2, we will give the expression of the impedances of the two quarter-wavelength transformers required for wide bandwidth. In Section 2.3, the three-point compromise technique in choosing the feed impedance for a narrow-band will be suggested for improved bandwidth. In Section 2.4, the impedance of the optimized quarter-wavelength open

stub used for broadband matching will be derived. In Section 2.5, the compound half-wavelength open stub which can be realized with a wider range of impedance than can be done with a conventional one will be introduced. In the last section are some discussions and conclusions.

2.2 An optimized two-stage quarter-wavelength transformer

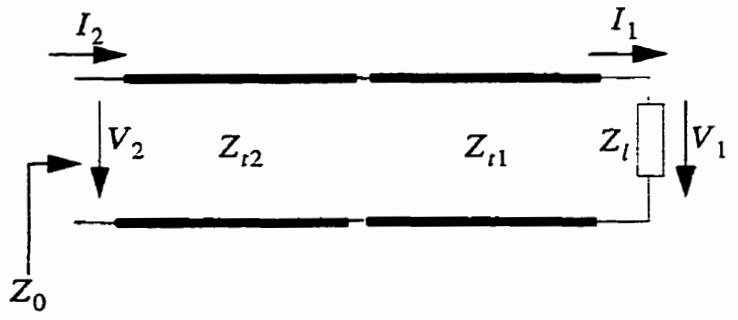

Figure 2.1 Matching a load with a feed impedance using a two-stage quarter-wavelength transformer.

It is well known that a quarter-wavelength transformer can be used to match a load Z_l to a feed impedance Z_0. This kind of match is usually broadband when the two impedances are not very different. In practice we sometimes need to match a transmission line with a load impedance which is several times higher or lower. For example, in the design of electromagnetically-coupled patch antennas, the input impedance of the antenna can be 10 to 20 Ω whereas the impedance of the feeding lines can be as high as 130 Ω. The reason for using such a high impedance for the feeding lines is that the losses of the feeding circuits are usually dominated by the radiation losses of the T junctions and rectangular bends. This kind of radiation loss decreases with the use of microstrips with high impedances [26]. A two-stage quarter-wavelength transformer, as shown in Figure 2.1, can be used to match two very different impedances with broader bandwidth.

Using the transferring matrix for the two transformers in Figure 2.1, we have,

$$\begin{bmatrix} V_2 \\ I_2 \end{bmatrix} = \begin{bmatrix} -\frac{1}{2}x & jZ_{t2} \\ j\frac{1}{Z_{t2}} & -\frac{1}{2}x \end{bmatrix} \begin{bmatrix} -\frac{1}{2}x & jZ_{t1} \\ j\frac{1}{Z_{t1}} & -\frac{1}{2}x \end{bmatrix} \begin{bmatrix} V_1 \\ I_1 \end{bmatrix} = \begin{bmatrix} -\frac{Z_{t2}}{Z_{t1}} & -\frac{1}{2}x(Z_{t1}+Z_{t2}) \\ -\frac{1}{2}x\left(\frac{1}{Z_{t1}}+\frac{1}{Z_{t2}}\right) & -\frac{Z_{t1}}{Z_{t2}} \end{bmatrix} \begin{bmatrix} V_1 \\ I_1 \end{bmatrix}, \quad (2.7)$$

where V_2, I_2, V_1 and I_1 are the voltages and currents at the input end and at the load, respectively. The input admittance at the input end is

$$Y_{in} = \frac{V_2}{I_2} = \left(\frac{Z_{t1}}{Z_{t2}}\right)^2 \frac{1}{Z_l} + i\frac{x}{2}\left(\frac{Z_{t1}}{Z_{t2}Z_l}\right)^2 \left(\frac{Z_l^2 Z_{t2}}{Z_{t1}^2} + \frac{Z_l^2}{Z_{t1}} - \frac{Z_{t1}^2}{Z_{t2}} - Z_{t1}\right). \quad (2.8)$$

In obtaining (2.8) from (2.7), we have used $Z_l = V_1/I_1$ for the load.

For a parallel LRC circuit, when the frequency is close to its oscillating frequency $f_0 = 1/(2\pi\sqrt{LC})$, its input admittance can be written as:

$$Y_{in} = \frac{1}{R} + j4f_0 Cx \quad (2.9)$$

and its Q-factor is:

$$Q = 2\pi f_0 RC. \quad (2.10)$$

In the same way, from Equation (2.8), the Q-factor of the circuit shown in Figure 2.1 is:

$$Q = \frac{\pi}{4}\left(\frac{Z_l Z_{t2}}{Z_{t1}^2} + \frac{Z_l}{Z_{t1}} - \frac{Z_{t1}^2}{Z_{t2}Z_l} - \frac{Z_{t1}}{Z_l}\right). \quad (2.11)$$

For impedance matching requirement, we also have

$$Z_0 = Z_l\left(\frac{Z_{t2}}{Z_{t1}}\right)^2. \quad (2.12)$$

From (2.11), we know that, when

$$Z_{t1} = Z_l^{3/4} Z_0^{1/4} \tag{2.13}$$

and

$$Z_{t2} = Z_l^{1/4} Z_0^{3/4}, \tag{2.14}$$

the Q-factor is zero. This means an infinite bandwidth can be achieved in principle. In practice a very broadband matching can be realized.

As an example, let us look at the case of matching a microstrip of impedance 130 Ω with a load of impedance 20 Ω. Figure 2.2 shows the return loss curves for the case of a single-stage transformer and three two-stage quarter-wavelength transformers. The impedance of the single-stage transformer is 51 Ω and the impedances of the third two-stage quarter-wavelength transformer are chosen according to (2.13) and (2.14) for the maximum bandwidth. By doing so, the bandwidth for a -30 dB return loss is increased from about 70 MHz to about 340 MHz.

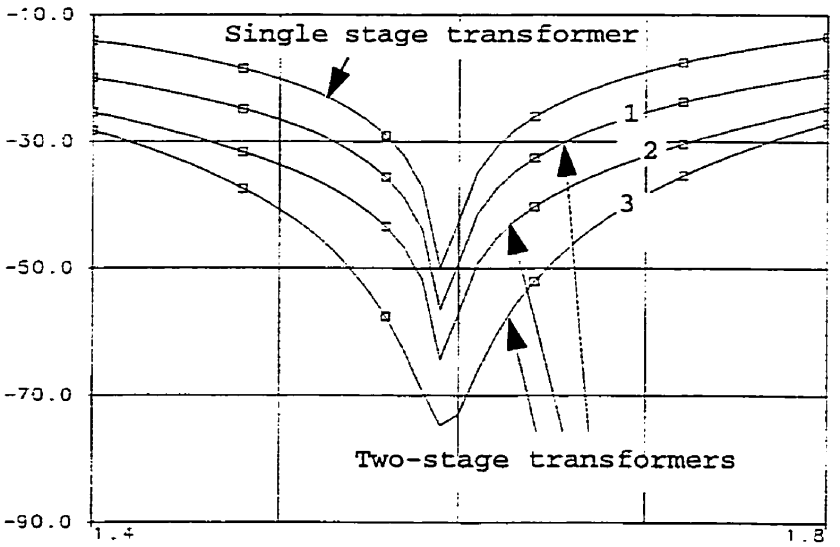

Figure 2.2 The return loss in dB vs. frequency in GHz for a single-stage transformer and three two-stage transformers.

In the case of a feeding circuit for a large scale antenna array, we sometimes need to use several transformers in series and the bandwidth can become narrower. The concept of two-stage quarter-wavelength transformers can be used for broader bandwidth. The only disadvantage with two-stage quarter-wavelength transformers is that the length of the transformer is doubled and so does the loss of the line. Two-stage quarter-wavelength transformers can also find other applications in microwave circuits. For example, in Paratek Microwave Inc. [27], efforts are being made to develop a kind of continuously electrically tunable phase shifters using ferroelectric material for satellite communications. Because the dielectric constant of the material is usually 200 to 300, the impedance of the microstrip fabricated with such ferroelectric material is very low. A typical characteristic impedance of such microstrips is 5 Ω. One has to match this microstrip with a conventional microstrip of 50 to 130 Ω impedance.

2.3 A three-point compromise technique

In the design of microwave circuits and antennas, we often encounter the case that the input impedance of the circuit is $Z_{in}(f) = R(f) + iX(f)$, where R and X have a shape as shown in Figure 2.3. The resistance of the input impedance has an even symmetry with respect to the center frequency f_0 and the reactance X an odd symmetry with respect to f_0. Our question is how to choose the feeding circuit impedance to obtain a lower overall return loss in the bandwidth of interest from f_1 to f_2.

We assume the input impedances at f_1, f_0 and f_2 are $R_2 + iX_0$, R_1, and $R_2 - iX_0$, respectively. The optimized impedance of the input line is derived out as

$$\frac{Z_0}{R_1} = \sqrt{\frac{R_2}{R_1} - \frac{1}{1 - \frac{R_2}{R_1}}\left(\frac{X_0}{R_1}\right)^2} \tag{2.15}$$

and the maximum return loss from f_1 to f_2 is

$$20lg(|\Gamma|) = 20lg\left|\frac{1 - Z_0/R_1}{1 + Z_0/R_1}\right|(dB). \tag{2.16}$$

In this case, the return loss curve will take the shape as shown by the dashed curve in Figure 2.3. When $\frac{R_2}{R_1} \geq 1$, i.e. when the resistance of the input impedance has a minimum value at f_0, the above technique is always available. When $\frac{R_2}{R_1} < 1$, i.e. the resistance of the input impedance has a maximum value at f_0, as in the case shown in Figure 2.3, the above technique is valid only when $X_0/R_1 \leq 1/2$ and $1/2 - \sqrt{1/4 - (X_0/R_1)^2} < R_2/R_1 < 1/2 + \sqrt{1/4 - (X_0/R_1)^2}$. These conditions limit the maximum reactance X_0 for this technique to be valid when R_2/R_1 is specified.

A special case is when the reactance is much smaller than R_1. We then have $Z_0 = \sqrt{R_1 R_2}$ and the maximum return loss is

$$20lg(|\Gamma|) = 20lg\left|\frac{1-\sqrt{R_2/R_1}}{1+\sqrt{R_2/R_1}}\right|(dB). \tag{2.17}$$

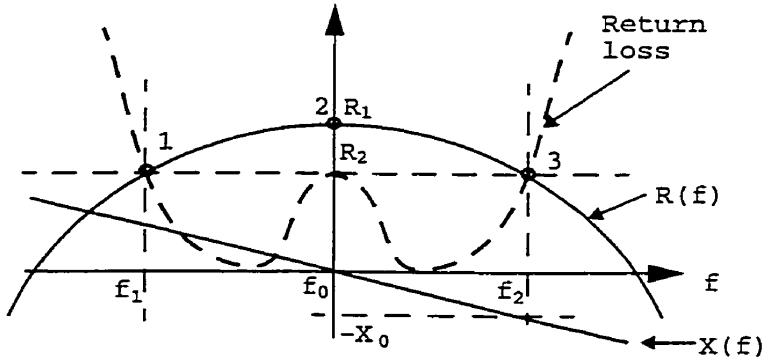

Figure 2.3 Typical input impedance of a narrow-band microwave circuit (solid lines) and the return loss curve (dashed line) when the feed impedance is chosen according to the three-point compromise technique.

For example, in the bandwidth of interest, if $R_1/R_2 = 2$ and the reactance of the input impedance is negligible, a return loss lower than -15.3 dB can be obtained.

2.4 An optimized shunt half-wavelength open stub

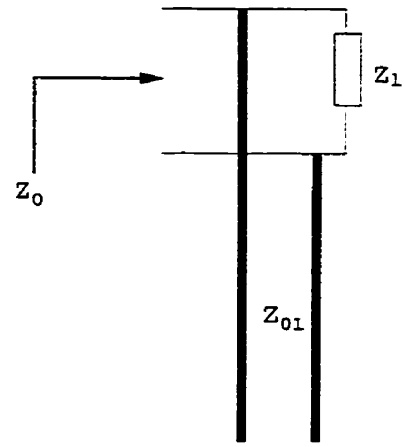

Figure 2.4 The equivalent circuit of a narrow-band circuit or an antenna.

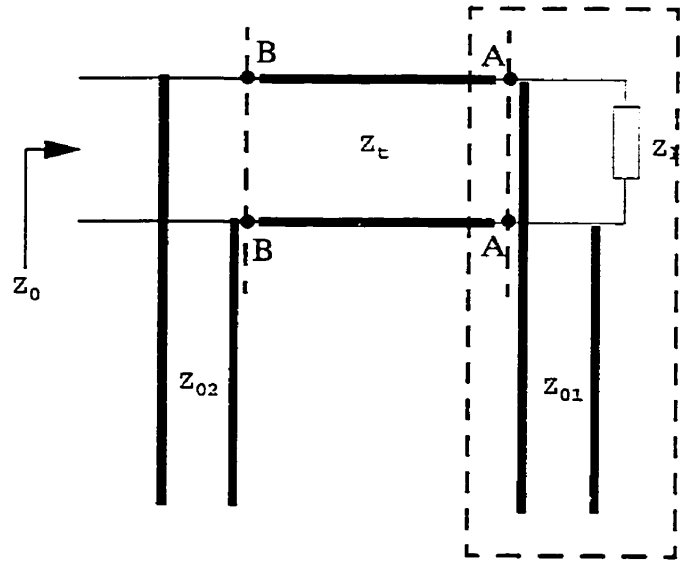

Figure 2.5 Broadband matching to a narrow-band circuit or antenna.

In the design of microwave circuits and antennas, we often need to increase the bandwidth. One important case is when the equivalent circuit of the circuit or antenna can be represented by a load in parallel with a shunt half-wavelength open stub, as shown in Figure 2.4. Another shunt half-wavelength open stub of impedance Z_{02} can be used a quarter-wavelength away to increase

the bandwidth, as shown in Figure 2.5. Our question is, what is the optimized impedance Z_{02} for broad bandwidth, when Z_l, Z_{01} and Z_0 are specified?

From (2.6), the transferring matrix of a half-wavelength transmission line of impedance Z_{01} is

$$\begin{bmatrix} -1 & -jxZ_{01} \\ -j\dfrac{x}{Z_{01}} & -1 \end{bmatrix}. \tag{2.18}$$

Using the same steps as for obtaining (2.8), the input admittance of the half-wavelength open stub can be derived to be

$$Y_{in01} = \frac{jx}{Z_{01}}. \tag{2.19}$$

The input impedance seen at plane A-A is

$$Z_{inA-A} = \frac{1}{\dfrac{1}{Z_l} + j\dfrac{x}{Z_{01}}}. \tag{2.20}$$

Using a similar transferring matrix for the quarter-wavelength transformer with impedance Z_t and along the same way as for obtaining (2.8), the input impedance at plane B-B is

$$Z_{inB-B} = \frac{-\dfrac{1}{2}x\dfrac{1}{\dfrac{1}{Z_l} + j\dfrac{x}{Z_{01}}} + jZ_t}{j\dfrac{1}{Z_t}\dfrac{1}{\dfrac{1}{Z_l} + j\dfrac{x}{Z_{01}}} - \dfrac{1}{2}x}. \tag{2.21}$$

Similar to (2.19), the admittance of the half-wavelength open stub with impedance of Z_{02} will be

$$Y_{in02} = \frac{jx}{Z_{02}}. \tag{2.22}$$

The input admittance of the whole circuit in Figure 2.5 is

$$Y_{in} = \frac{j\frac{1}{Z_t}\frac{1}{\frac{1}{Z_l}+j\frac{x}{Z_{01}}} - \frac{1}{2}x}{-\frac{1}{2}x\frac{1}{\frac{1}{Z_l}+j\frac{x}{Z_{01}}} + jZ_t} + j\frac{x}{Z_{02}} \tag{2.23}$$

or

$$Y_{in} = \frac{1}{Z_0} + jx\left[\frac{Z_0}{Z_{02}} - \frac{Z_l}{Z_{01}} + \left(\sqrt{\frac{Z_0}{Z_l}} - \sqrt{\frac{Z_l}{Z_0}}\right)\right]. \tag{2.24}$$

In deriving (2.24) from (2.23), we use the matching condition for Z_t,

$$Z_t = \sqrt{Z_0 Z_l}, \tag{2.25}$$

and again, all higher order terms of x were neglected. From (2.24), we can obtain the Q-factor of the whole circuit:

$$Q = \frac{\pi}{2}\left[\frac{Z_0}{Z_{02}} - \frac{Z_l}{Z_{01}} + \left(\sqrt{\frac{Z_0}{Z_l}} - \sqrt{\frac{Z_l}{Z_0}}\right)\right]. \tag{2.26}$$

From (2.26) the Q-factor will be zero and a broadband matching can be achieved when

$$Z_{02} = \frac{Z_0}{\frac{Z_l}{Z_{01}} - \frac{1}{2}\left(\sqrt{\frac{Z_0}{Z_l}} - \sqrt{\frac{Z_l}{Z_0}}\right)}. \tag{2.27}$$

When the feeding impedance is as required by (2.27), a single dip return loss with broader bandwidth will be achieved. The bandwidth can be further increased by increasing the feeding impedance a little bit, according to the three point compromise technique described in the last section. This will cause the return loss at the center frequency to increase and the return loss at both lower and higher boundary frequencies of the band to decrease, resulting in a wider matching for a specified return loss level.

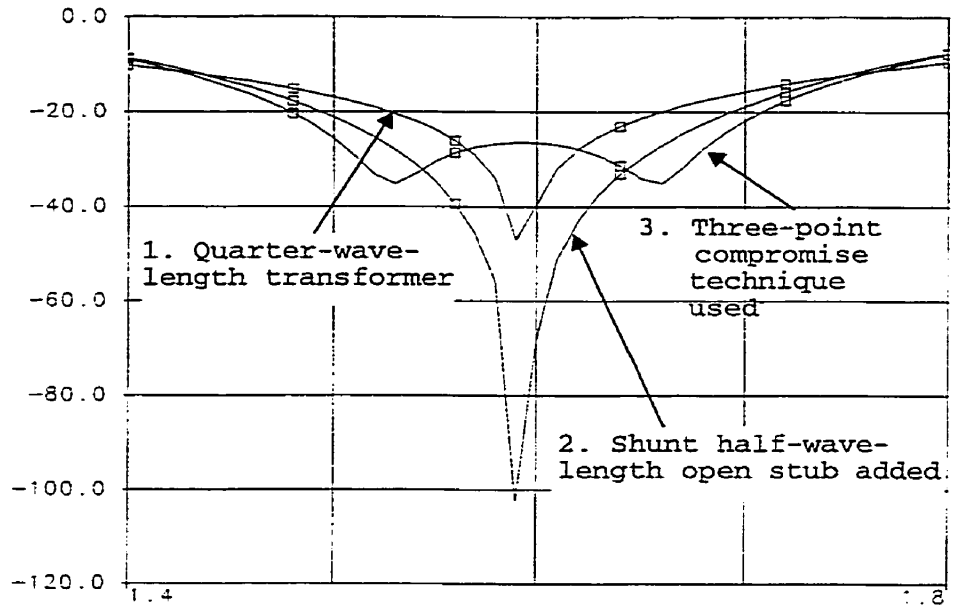

Figure 2.6 Return loss in dB vs. frequency in GHz for three kinds of matching.

Figure 2.6 shows the return losses vs. frequency for several cases of matching a narrow band circuit with $Z_l = 20\Omega$ and $Z_{01} = 10\ \Omega$ to a feeding impedance of 50 Ω. The first case used a quarter-wavelength transformer of impedance 31.6 Ω only and the second case used a quarter-wavelength transformer of 31.6 Ω and a shunt half-wavelength open stub of 32.7 Ω, which was calculated from (2.27). For the third case, the three point compromise technique was used. The impedance of the feeding circuit was increased from 50 Ω to 55 Ω. The -24 dB return loss bandwidth was increased from about 55 MHz to 125 MHz and finally to about 155 MHz.

2.5 A compound half-wavelength microstrip open stub

As discussed in Section 2.4, a shunt half-wavelength open stub can be used to match a feeding circuit to a narrow band microwave circuit or antenna with increased bandwidth. In the case of printed circuits, the highest and lowest impedances of a realizable for broad bandwidth is subject to technical limitations. When the width of a microstrip is increased, its radiation from the open end will increase. This radiation will interfere with the radiation pattern of a patch antenna, increase the sidelobe level of a patch antenna array, and result in lower gain. For a 30 mil GIL 1000 substrate which has a dielectric constant of 3.34 and a thickness of 0.76 mm, we suggest

to limit the largest width of the microstrip to 3 mm. The limitation on the highest realizable impedance comes from the fabrication error. When the microstrip is too narrow, the impedance of the fabricated microstrip can be quite different from the design value because of limited photolithography fabrication precision. We suggest that the narrowest microstrip width be about 0.17 mm. For this substrate, the above widths of the microstrip correspond to a lowest impedance of about $Z_l = 35.2\ \Omega$ and a highest realizable impedance $Z_h = 130\ \Omega$.

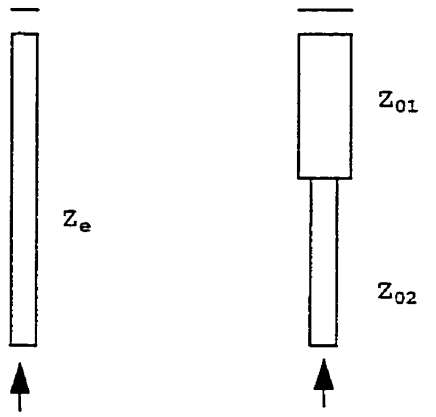

Figure 2.7 A conventional and a compound half-wavelength open stub.

In practice we sometimes need to realize a half-wavelength microstrip tuning stub using a microstrip of impedance beyond these impedance limits. A compound half-wavelength microstrip open stub, as shown in Figure 2.7, is proposed for use in this case. Also shown in Figure 2.7 is a conventional half-wavelength microstrip open stub. Please note that the impedance of a open stub in this case means the characteristic impedance of the microstrip from which an open stub is made. The compound open stub is composed of a quarter-wavelength transformer of impedance Z_{02} in series with a quarter-wavelength microstrip of impedance Z_{01} with open end. According to (2.6) and along similar steps as in the last section, the input admittance of a half-wavelength open stub of impedance Z_e is

$$Y_{in1} = \frac{jx}{Z_e}, \tag{2.28}$$

and the input admittance of the compound half-wavelength open stub is

$$Y_{in2} = jx\frac{Z_{01}+Z_{02}}{2Z_{02}^2}. \tag{2.29}$$

The compound open stub is equivalent to a conventional half-wavelength microstrip open stub made of microstrip with impedance $Z_e = \frac{2Z_{02}^2}{Z_{01}+Z_{02}}$. If we choose Z_{01} to be that of the narrowest microstrip $Z_h = 130\ \Omega$ and Z_{02} to be that of the widest microstrip $Z_l = 35.2\ \Omega$, a compound open stub of impedance of as low as 15.0 Ω can be realized. If we choose Z_{01} to be that of the widest microstrip $Z_l = 35.2\ \Omega$ and Z_{02} to be that of the narrowest microstrip $Z_h = 130\ \Omega$, a compound open stub of impedance as high as 204.6 Ω can be realized.

This compound half-wavelength microstrip open stub is critical in our design of broadband microstrip switches and beam controllers. To optimize the bandwidth of each of these two circuits, two parallel half-wavelength microstrip open stubs with an impedance around 22 Ω are used.

2.6 Discussion and conclusion

To obtain (2.6), the transferring matrix of the quarter-wavelength transmission line, we assumed that the effective dielectric constant ε_{eff} of the transmission line is constant. In a practical case, this is true in a relatively wide but still limited bandwidth. This bandwidth poses a limitation on the bandwidth for which our discussions presented in this chapter will be valid. Furthermore, the transferring matrix (2.6) is accurate only to the first order of x. When the frequency is farther away from the center frequency, the validity of the discussions will be impaired. Fortunately, the bandwidth limitation from the above two aspects is relatively loose for most of our designs with microstrip circuits and patch antennas, which work in a relative bandwidth of less than 10%.

In conclusion, a simple transferring matrix of a quarter-wavelength transmission line was derived. The use of such a matrix led to several techniques for broadband matching of microstrip circuits and patch antennas, i.e., the optimized two-stage quarter-wavelength transformer, the

optimized shunt half-wavelength open stub, and the compound half-wavelength open stub. A three point compromise technique was also addressed. These techniques have been used in our design of broadband microstrip switches, beam controllers, and patch antennas. The application of these techniques also led to the design of unique dual-band patch antennas with orthogonal polarization and circular polarization in the 12 GHz/18 GHz bands, which can be integrated into arrays.

CHAPTER 3

Broadband radial microstrip switches *

3.1 Introduction

The advantages of an electronically-steered array over a mechanically-steered antenna include robustness, faster scanning, acquisition and tracking, lower DC power consumption, but the potential for cost reduction is of paramount importance.

Let us first consider a switched-beam electronically-scanned horizontal array composed of m channels. When it is in operation, n (n<m) adjacent channels are combined to form a beam in the direction closest to the satellite. By activating different n channels, a total of m beams can be formed horizontally. The switched-beam array reported by Bialkowski et al. at the University of Queensland in 1996 [11] is a good example of the this kind of array. The array has 14 channels in which 3 adjacent channels are activated when it is in operation. Consider now a phased

* The main part of this chapter has been accepted for publication in the IEEE Transactions on Microwave Theory and Techniques [21].

array, which is very similar to the switched-beam array except that a phase shifter is used in each channel. For n activated adjacent channel, N beams can be formed. Higher overall gain can be achieved with this kind of array. The phased array recently reported by Karmakar and Bialkowski at the University of Queensland [12] belongs to this type of array. It is composed of 8 channels and 2 channels are activated when it is in operation. In each channel, a 1-bit phase shifter is used. A total of 24 beams can be formed horizontally by activating different channels and by choosing different states of the phase shifters.

In both arrays, radial switches are used to activate certain channels while deactivating the others. In order to design a good electronically-scanned array, the return loss, the insertion losses for the activated channels, and the isolations for the deactivated channel, need to be optimized in the whole operation band.

A first radial microstrip switch design with an insertion loss of 1.5 dB and reflection coefficient of -10 dB in the 1.54 GHz to 1.66 GHz band has been reported in [11,24] for such an application. We now explore the possibility of a microstrip switch with substantially lower insertion loss and reflection, by carefully designing the unit switching circuit for each channel. We also discuss the power handling capacity of such switches and present estimated results from sample microstrip switches.

3.2 Selection of the unit switch circuit

The switch under consideration is composed of m channels with a unit switching circuit in each channel. All channels join together at the switch junction and are fed by a common perpendicular coaxial line of assumed impedance Z_0. The switching circuit can open a channel, allowing the signal to propagate through it, or close it, causing the signal to be reflected. For lower insertion loss and lower cost, a simple switching circuit is preferred. The application of lumped components such as capacitors and resistors should be avoided and the total length of the microwave channel should also be as short as possible to reduce ohmic losses.

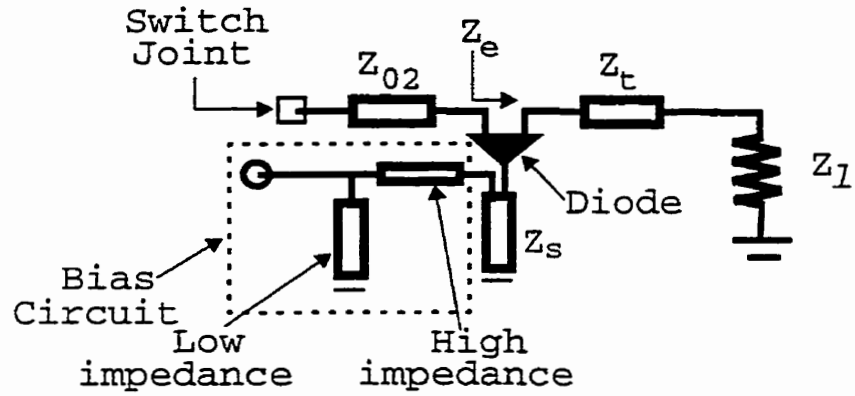

Figure 3.1 Unit switching circuit used in the switch.

Figure 3.1 shows the unit switching circuit proposed for the design. This switching circuit is composed of a quarter-wavelength transformer of impedance Z_{02}, of another quarter-wavelength transformer of impedance Z_t and is terminated by a load Z_l. A third quarter-wavelength open stub of impedance Z_s is connected in parallel with each channel through a diode. This open stub provides a virtual ground for microwave signals at the cathode of the diode. The effect of the bias circuit defined by the dotted square in Figure 3.1 is neglected. For generality, in this section and in the following one, ideal transmission lines will be used instead of practical transmission lines such as waveguides or microstrips.

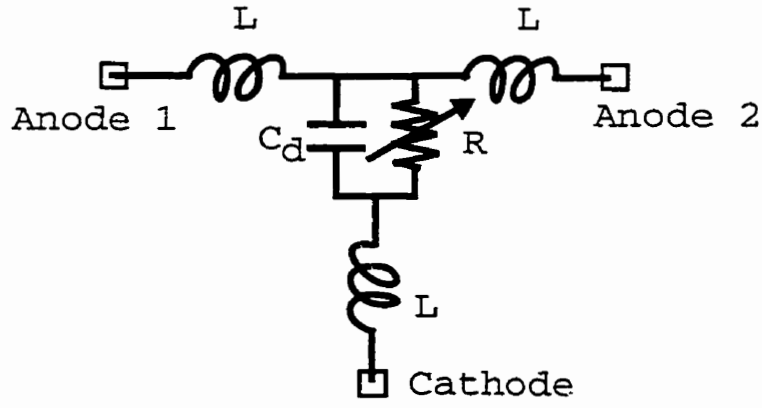

Figure 3.2 Equivalent circuit of a PIN diode.

A dual-anode diode is used to close each channel or to open it by forward or reverse biasing. Figure 3.2 gives the equivalent circuit of such a diode. The inductance L is the inductance of each lead of the diode. The variable resistor R has a small forward residue resistance r_d when the diode is forward biased and the channel is closed. The effect of the shunt capacitance C_d is negligible in this case. When the diode is reverse biased, the variable resistor R is very high (it is assumed to be 10,000 Ω in our design) and the shunt capacitance becomes important. The channel is open with some reflection and insertion loss caused by the shunt capacitor.

A good diode for such an application would have a very small forward residue resistance r_d and a very small shunt capacitance C_d. However, this is not the case for commercially available diodes. Diodes with small forward residue resistance r_d usually have a high shunt capacitance C_d, or vice versa. A higher residue resistance will cause power leaking through the closed channels, resulting in poor isolation. A higher shunt capacitance, on the other hand, will cause reflection in an open channel, resulting in higher insertion loss. A compromise was achieved by using a diode with a small residue resistance and by using a compensation inductance for the high shunt capacitance.

To compensate for the shunt capacitance, a so-called constant-k low-pass filter should be formed which requires the anode lead inductance to be [28]:

$$L = \frac{Z^2}{2} C_d, \tag{3.1}$$

where Z is the impedance of the transmission lines connected to both anodes of the diode. The effect of the cathode lead is neglected considering that it can be compensated by adjusting the length of the open stub connected to it.

For a HSMP 4820 PIN diode with $r_d = 0.6\ \Omega$, $C_d = 0.75$ pF, Figure 3.3 shows the resulting insertion loss versus frequency for different choices of lead inductance. The transmission line impedance is assumed to be $Z = 50\ \Omega$. When $L = 0$ nH, in the band from 1.525 GHz to 1.661 GHz, the shunt capacitance will cause in each open channel an insertion loss as high as 0.16 dB and a reflection of as high as -14.35 dB. Whereas when $L = 0.94$ nH is chosen, the insertion loss

is lower than 1.43×10^{-4} dB, and the reflection is lower than -42.50 dB over the whole band. When the diode is used at higher frequencies, the improvement in increasing the anode lead inductance will be more apparent. The improvement is also more important in the case of a higher diode shunt capacitance. In the case of $C_d = 2.2$ pF[24], and with $Z = 50\ \Omega$, when $L = 0$ nH, the insertion loss will be as high as 1.25 dB and the reflection -6.08 dB. If the compensation inductors are chosen according to Equation (3.1), with $L = 2.75$ nH, the insertion loss will be lower than 0.18 dB and the reflection -14.66 dB.

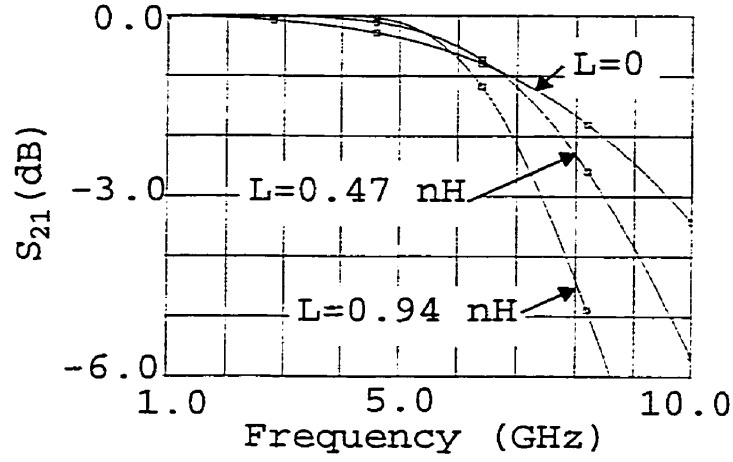

Figure 3.3 Insertion loss caused by a reverse biased diode, with its anode lead inductance as the parameter.

3.3 The bandwidth and insertion loss of an ideal transmission line switch

Let us now consider a radial switch having a total of m channels, among which n channels are open and the other $m - n$ channels are closed. Each channel has the configuration shown in Figure 3.1 and an ideal transmission line model for each microwave channel is again used here for generality.

The transfer matrix of a quarter-wavelength transmission line of center frequency f_0 and arbitrary impedance Z_{00}, at a normalized frequency difference $= \pi \Delta f / f$, is:

$$\begin{bmatrix} -\frac{1}{2}x & jZ_{00} \\ jY_{00} & -\frac{1}{2}x \end{bmatrix}. \tag{3.2}$$

Using such a matrix for each of the transmission lines, the input admittance for n open channels in parallel can be calculated to be:

$$Y_{open} = \frac{1}{Z_0} + j\frac{x}{2Z_0}\frac{\left(\sqrt{\overline{Z_1}} + \sqrt{n}\right)\left(\sqrt{n\overline{Z_1}} - \overline{Z_e}\right)}{\sqrt{n\overline{Z_1}\overline{Z_e}}}. \tag{3.3}$$

Here $Z_e = Z_t^2/Z_1$, as defined in Figure 3.1, is the equivalent load impedance seen at the diode. The impedances with over-bars are normalized with respect to the feed line impedance Z_0. In order to match the switch to the feed line, we have:

$$Z_{02} = \sqrt{nZ_0 Z_e}. \tag{3.4}$$

In the same way, for the $m-n$ closed channels, we have:

$$Y_{close} = \frac{(m-n)\overline{r_d}}{nZ_0(\overline{r_d} + \overline{Z_e})} + j\frac{x}{2Z_0}\left[\frac{(m-n)\left(\overline{Z_s} + \sqrt{n\overline{Z_e}}\right)}{n\overline{Z_e}} - \frac{(m-n)\overline{r_d}^2\sqrt{\overline{Z_e}}}{n^{3/2}(\overline{r_d} + \overline{Z_e})^2}\right]. \tag{3.5}$$

The total admittance of the switch from the feed point is:

$$Y_{in} = Y_{open} + Y_{close}. \tag{3.6}$$

For a parallel LRC circuit, when the frequency is close to its oscillating frequency $f_0 = 1/2\pi\sqrt{LC}$, the input admittance can be written as:

$$Y_{in} = \frac{1}{R} + j4f_0Cx \tag{3.7}$$

and its Q-factor is:

$$Q = 2\pi f_0 RC. \tag{3.8}$$

In the same way, from Equation (3.5), the Q-factor of the switch is:

$$Q = \frac{\pi}{4}\frac{1}{1 + \frac{(m-n)\overline{r_d}}{n(\overline{r_d} + \overline{Z_e})}}\left(\frac{\left(\sqrt{\overline{Z_1}} + \sqrt{n}\right)\left[\sqrt{n\overline{Z_1}} - \overline{Z_e}\right]}{\sqrt{n\overline{Z_1}\overline{Z_e}}} + \frac{(m-n)\left[\overline{Z_s} + \sqrt{n\overline{Z_e}}\right]}{n\overline{Z_e}} - \frac{(m-n)\overline{r_d}^2\sqrt{\overline{Z_e}}}{n^{3/2}(\overline{r_d} + \overline{Z_e})^2}\right) \tag{3.9}$$

If the switch is matched at its center frequency, the relative bandwidth for a VSWR lower than S is [29]:

$$BW = \frac{1}{Q}\frac{S-1}{\sqrt{S}}. \tag{3.10}$$

Broad bandwidth is achieved when the Q-factor in Equation (3.9) is small. Accordingly, we can establish the following criteria for wide band switch design:

1. Large n or small m-n when m is fixed. This is easy to understand because this case is tending towards matching a transmission line with n parallel transmission lines with quarter-wavelength transformers.

2. Low impedance of the open stubs, Z_s. In Equation (3.9), we recognize that the contribution of the m-n closed channels to the Q-factor is represented by the second term in the large bracket. Lowering Z_s, the Q-factor will be decreased.

3. High equivalent load impedance, Z_e. In the same large bracket in Equation (3.9), both the second term and the first term, which represent the contribution of the n open channels to the Q-factor, will decrease with increased Z_e, resulting in a wider bandwidth. The third term in the bracket, the contribution of the residue resistances of the diodes when they are forward biased, is usually very small compared to the other two terms.

For each open channel, at the center frequency of the switch, the residue resistance of each forward-biased diode in parallel with Z_e provides a shunt impedance of $Z_{02}^2(r_d + Z_e)/(r_d Z_e)$ at the feed port of the switch. The total $m-n$ open channels provide a shunt resistance of $Z_{02}^2(r_d + Z_e)/[r_d Z_e(m-n)]$ to the n channels which are matched to the feed line. The insertion loss due to the m-n deactivated channels at the center frequency is:

$$IL(dB) = 20\log\left(1 - \frac{(m-n)\overline{r_d}}{2n(\overline{r_d} + \overline{Z_e})}\right). \tag{3.11}$$

According to Equation (3.11), for the insertion loss, we can draw the following criteria:

1. When n, the number of activated channels, is fixed, the insertion loss will increase with m-n, the number of deactivated channels.

2. When m-n, the number of deactivated channels, is fixed, the insertion loss will decrease with n, the number of activated channels.

3. The insertion loss can be decreased by increasing the equivalent load impedance Z_e at the PIN diodes.

3.4 Simulation results from a switch designed under the guidance of the design criteria

The above design criteria were used to guide the design of microstrip switches. The PIN diodes used are HPSM 4820 PIN diodes, which have a shunt capacitance of $C_d = 0.75pF$ and a residue resistance of $r_d = 0.6\ \Omega$. The inductances of each of the two anode leads and of the cathode lead were measured to be $L = 0.47nH$. In Section 3.2, according to the unit switching circuit shown in Figure 3.1, it was calculated that the total inductance of the anode leads should be 0.94 nH. The extra 0.47 nH plus the microstrip transformer of impedance Z_{02}, on the left side of the diode, behaves as the same microstrip line with reduced length. The extra 0.47 nH inductance on the right side of the diode was provided by a narrow microstrip Z_i. As pointed out in Section 3.2, the inductance of the cathode lead was compensated by a quarter-wavelength open stub with reduced length.

We then create the HP-EEsof circuit network for a sample switch with parameters $Z_s = 43.8\Omega$, $Z_e = 50\Omega$, and $Z_{02} = 86.7\Omega$. The substrate used is GML 1000 laminate from Glasteel Industrial Laminates with both sides clad with 1 oz. copper. The nominal parameters of the substrate are: Dielectric constant=3.20±0.05, Thickness=0.762 mm, Copper thickness=0.035 mm, Dissipation factor=0.003. For such a substrate, the calculation tool provided by HP-EEsof is used to calculate the widths and quarter wavelengths corresponding to the above three impedances.

Table 3.1 Microstrip widths and quarter wavelengths calculated using HP-EEsof.

Impedance (Ω)	Microstrip width (mm)	Quarter wavelength (mm)
86.6	0.62	30.75
50	1.79	29.55
43.8	2.20	29.29

With Table 3.1, we can create the HP-EEsof circuit network for this sample microstrip switch. We begin our work by assuming the length of Z_{02}, Z_t and Z_s to be all quarter wavelengths. The width of Z_i is chosen the same as Z_{02}, and the equivalent inductance of 0.47 nH would require a length of about 1.00 mm for the equivalent impedance of $Z_e = 50\ \Omega$. First we adjust the length of Z_s to 26.90 mm to center the simulated transmission curve for a deactivated channel at 1.593 GHz, the center frequency of the operation band. Second, we adjust the length of Z_{02} to 30.03 mm to center the simulated return loss curve for the switch at the same center frequency of the operation band. The final parameters of the switch are as shown in Figure 3.4, where the shunt capacitance C_s is due to the spurious effect of soldering a perpendicular coaxial cable to the joint of the switch. Such a capacitance is suggested by correlating the simulated results with the measured results. The coaxial cable used is a 50 Ω UT 141-A coaxial cable from Micro-Coax Components Inc., which has a center conductor diameter of 0.91 mm and a dielectric diameter of 2.98 mm, with PTFE as the dielectric material

Figure 3.5 shows the S-parameters of a microstrip switch. Here the S_{21} parameter for a deactivated channel is the isolation from the feed of the switch to this channel. The overall insertion loss was obtained by subtracting 4.771 dB from the S_{21} parameter for an activated channel because of the 3 activated channels. From Figure 3.5 we can see that in the whole operation band, the return loss was lower than -14.48 dB, the insertion loss lower than 0.45 dB, and the isolation better than 28.76 dB.

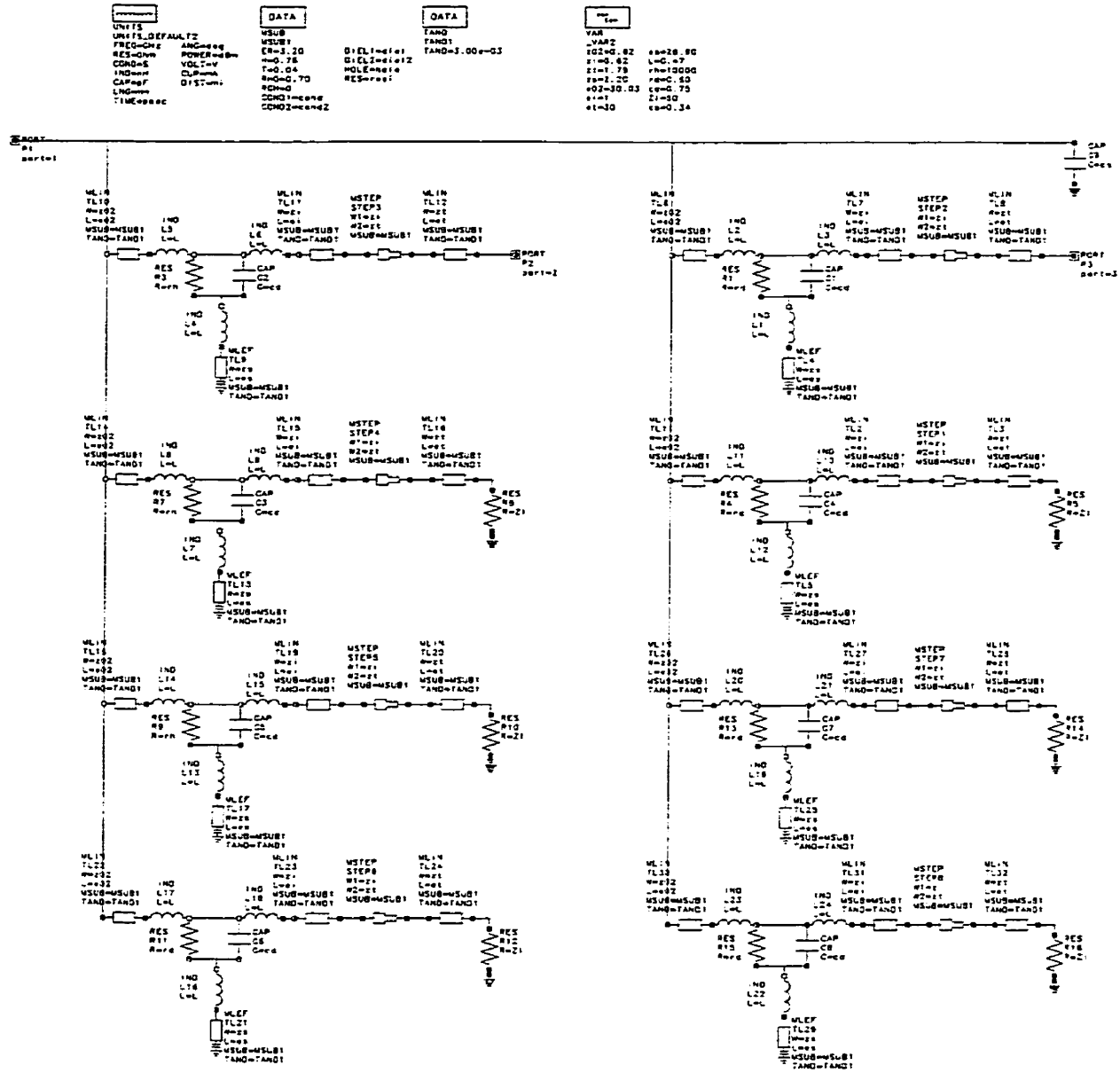

Figure 3.4 . HP-EEsof circuit network for the microstrip switch

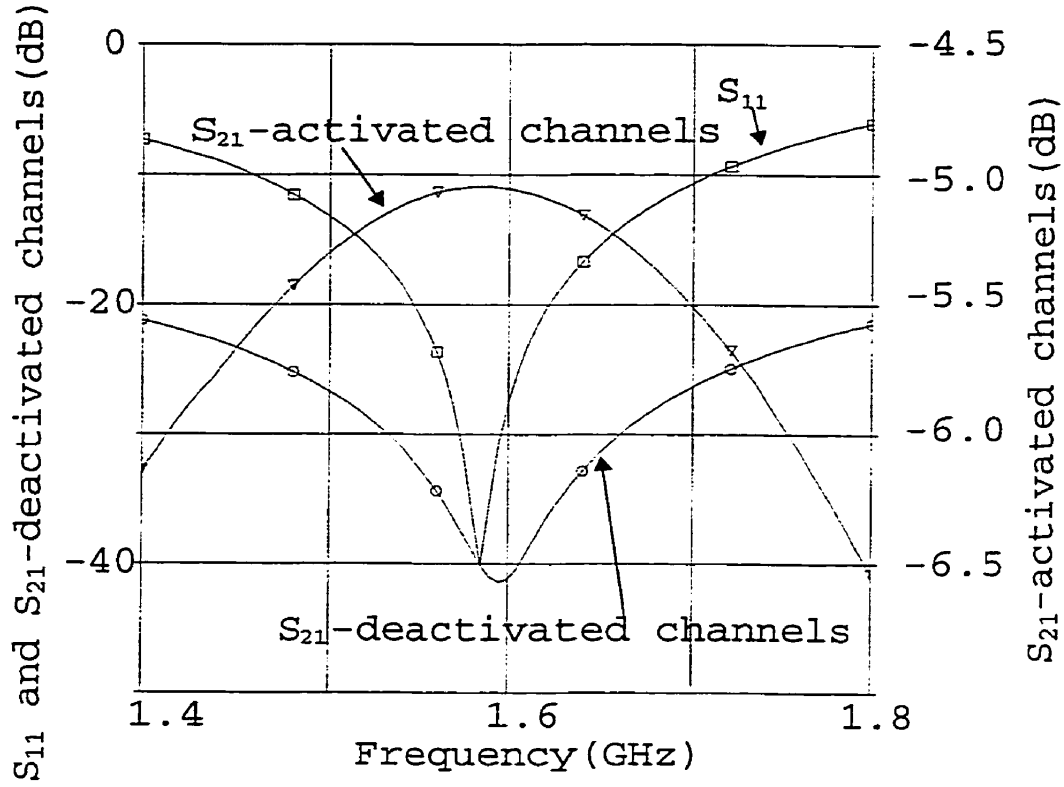

Figure 3.5 Simulated S-parameters of a sample switch with an equivalent load impedance of 50 Ω

In Section 3, it was mentioned that both bandwidth and insertion loss will decrease with the effective load impedance Z_e. This has been verified by the simulation of a second sample switch. Compared with the first one, Z_e was increased from 50 Ω to 70 Ω, and from the matching condition of Equation (3.4), Z_{02} was increased from 86.7 Ω to 102.47 Ω. The simulated results are shown in Figure 3.6. The return loss was lower than -16.41 dB, the insertion loss lower than 0.39 dB, and the isolation better than 32.07 dB.

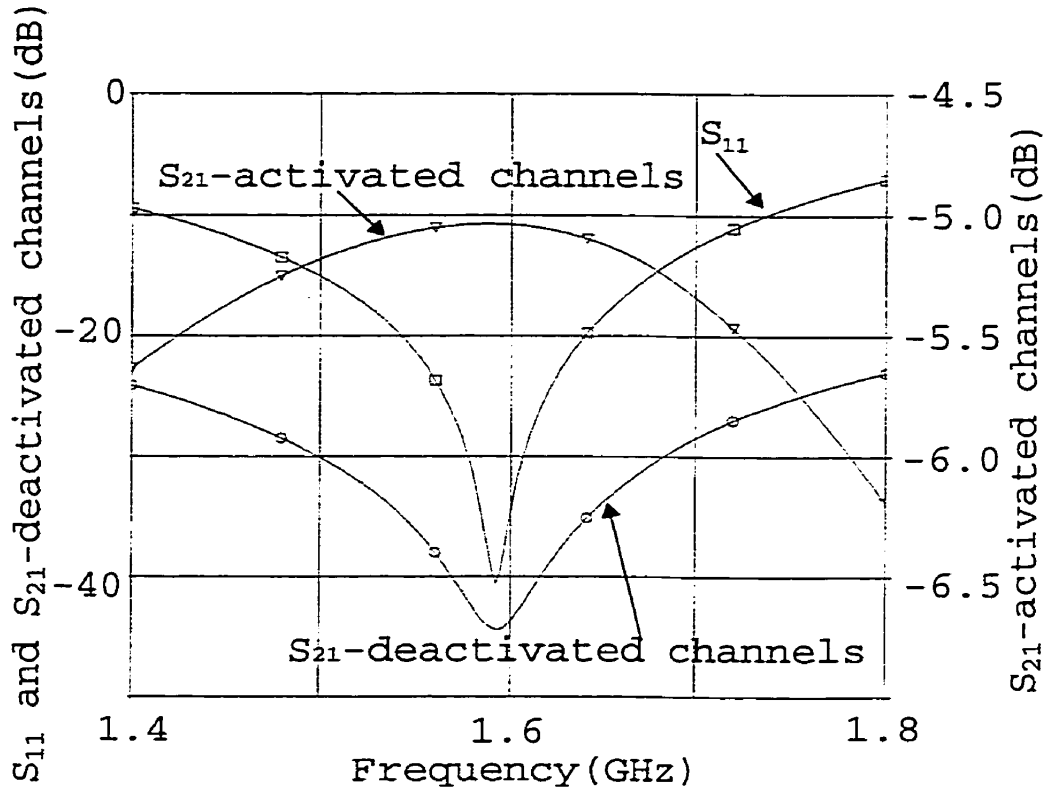

Figure 3.6 Simulated S-parameters of a sample switch with an equivalent load impedance of 70 Ω.

3.5 Microstrip switch realization and the measured results

Figure 3.7 L-band microstrip switch with an effective load impedance of 50 Ω *under test.*

The first sample switch, whose simulation results were given in Figure 3.5, was implemented and Figure 3.7 shows the testing switch, with one channel connected to Port 2 of a HP 8703 Light-Wave Component Analyzer and the other 7 channels terminated by 50Ω matched loads. Figure 3.8 shows the return loss, the insertion loss and the isolation measured by the analyzer. From Figure 3.8, for the whole band from 1.525 GHz through 1.661 GHz, the insertion loss was lower than 0.50 dB, the reflection lower than -13.76 dB and the isolation better than 28.45 dB. Compared with the simulations, all results agree with each other very well. The switch was also found to be very symmetrical and the measurements at each of the 3 open channels gave essentially the same results.

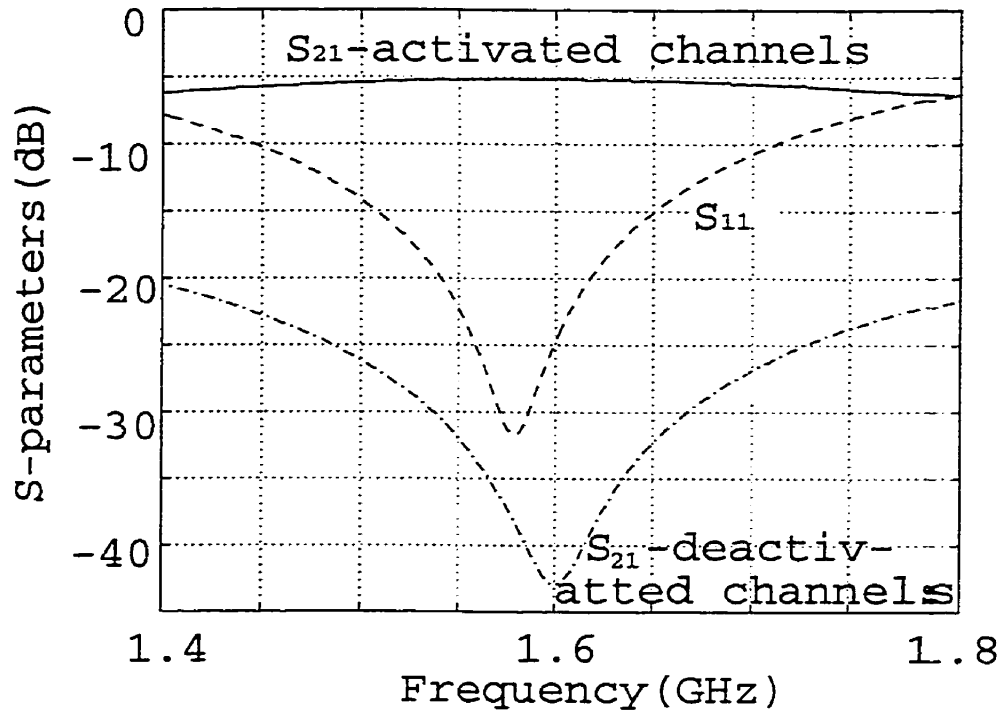

Figure 3.8 Measured return loss, insertion loss and isolation of a switch with an effective load impedance of 50 Ω.

3.6 Power handling capacity of microstrip switches: measurements and analysis

The power handling capacity of the switch is mainly a function of the reverse bias voltage for an activated channel and of the forward current for a deactivated channel. The insertion losses of the first sample switch using HSMP 4820 diodes was measured experimentally. The switch was used in a mismatched way where only one channel was activated. For the results the lowest required voltage and current are estimated. Using an HSMP 4890 diode in the single activated channel of the same sample switch instead of an HSMP 4820 diode, the lowest required bias voltage for a switch using HSMP 4890 diodes is also estimated.

3.6.1 Measurement setups

The test setup is shown schematically in Figure 3.9.

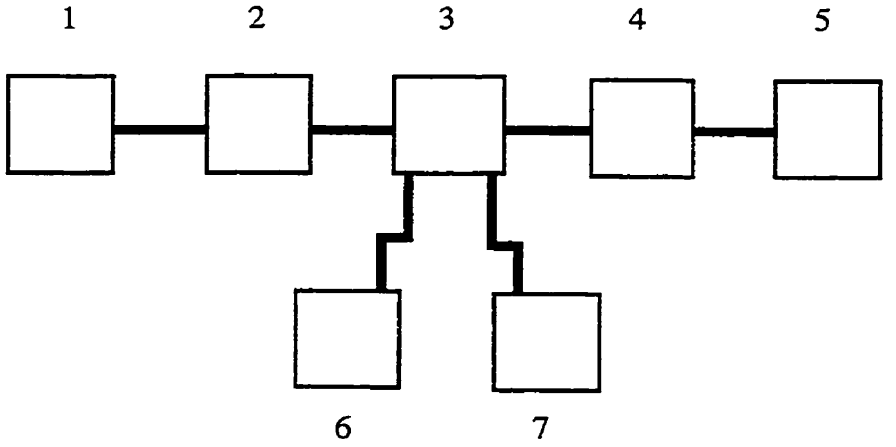

1. Signal generator: Fluke 6062 A 100kHz-2.1 GHz.
2. Microwave amplifier: PST AR 1929-20.
3. Microstrip switch under test.
4. High power attenuator (20 dB nominal).
5. Power meter: HP 4378.
6. DC voltage source: PAB 32-2A.
7. DC current source: HP 62058

Figure 3.9 Test setup for switch power handling capacity measurements.

A microwave signal at power level P_s is generated by the signal generator 1 and then amplified to P_{in} by the microwave amplifier 2. The amplified power is fed to the microstrip switch through its coaxial feeding port. Part of the power is reflected at the switch and the rest propagates with some loss through the activated channel and is attenuated by the high power attenuator 4 and is finally measured by the power meter 5. The DC voltage source 6 provides reverse bias for the diode of the activated channel and the DC current source 7 provides forward current for all the 7 diodes in the 7 deactivated channels.

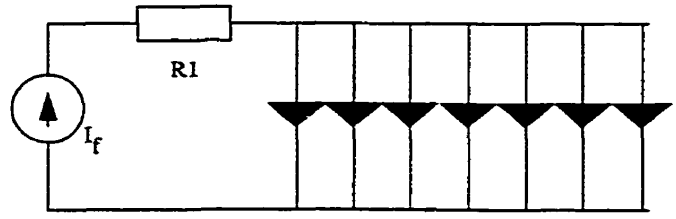

a.Forward bias for the 7 deactivated channels

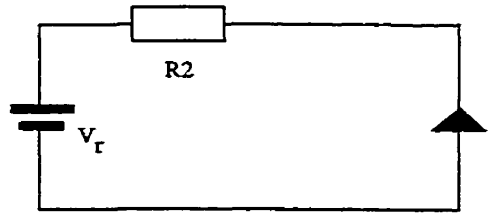

b.Reverse bias for the activated channel

Figure 3.10 Forward and reverse bias circuits.

The diodes in the switch were biased as shown in Figure 3.10. In the forward bias circuit, R1 was composed of seven 1-Watt resistors of 120 Ω and, in the reverse bias circuit, R2 was a resistor of 1 k Ω to protect the diode.

3.6.2 Measured results

The power levels P_{in} input to the switch at different power levels P_s from the signal generator 1, were calculated from the power levels P_m read from the power meter 5, by removing the switch and connecting the high power attenuator 4 directly to the microwave amplifier 2. The input power level P_{in} was calculated out by using the nominal attenuation of 20 dB of the high power attenuator 4. The power levels P_m and P_{in}, for different power levels from the power source P_s, are shown in Table 3.2. The frequency was fixed at 1.600 GHz and the input power was valued from 0.66 W to about 10 W.

The power handling capacity of a single channel of the microstrip switch shown in Figure 3.7 was measured, by measuring the insertion loss of such a channel. In the measurements, only the channel under measurement was activated and the other 7 channels were all deactivated. The

insertion losses of a channel using a HPSM 4820 PIN diode is shown in Figure 3.11 with different reverse bias voltage as the parameter. All other seven channels used HPSM 4820 PIN diodes and were deactivated by applying to each diode a forward bias current of 7 mA. Figure 3.12 shows similar curves for the case where all the forward bias currents were increased to 14 mA. Note that the dotted line in Figure 3.11, 3.12 and 3.13 is related to the low power insertion loss and represents a loss criteria A_{cr} which will be used in the discussion later in this chapter.

Table 3.2 Input power levels for different power levels from the power generator.

P_s(dBm)	-30	-27	-24	-21	-20	-19	-18
P_m(dBm)	8.20	11.20	14.14	17.15	18.11	19.07	20.02
P_{in}(W)	0.66	1.318	2.59	5.19	6.47	8.07	10.05

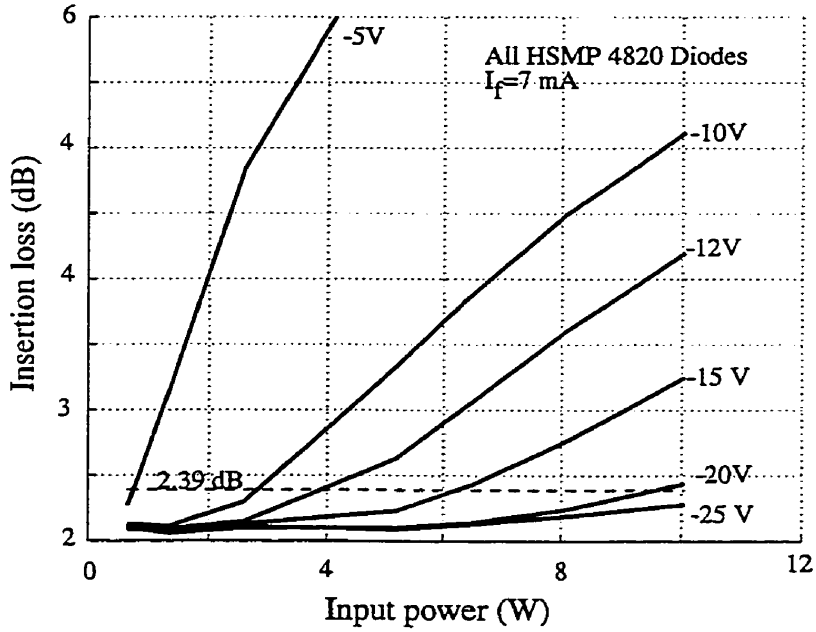

Figure 3.11 Measured insertion loss of a mismatched switch vs. input power for different reverse bias voltages. The forward bias currents were all 7 mA.

By comparing Figure 3.11 and Figure 3.12, we can see that the insertion loss of the channel changed little when the forward bias currents for the other channels increased from 7 mA to 14 mA. This means that the power handling capacity of a switch is mainly determined by the re-

verse bias voltages of the activated channels and is not sensitive to the forward bias current of the deactivated channels.

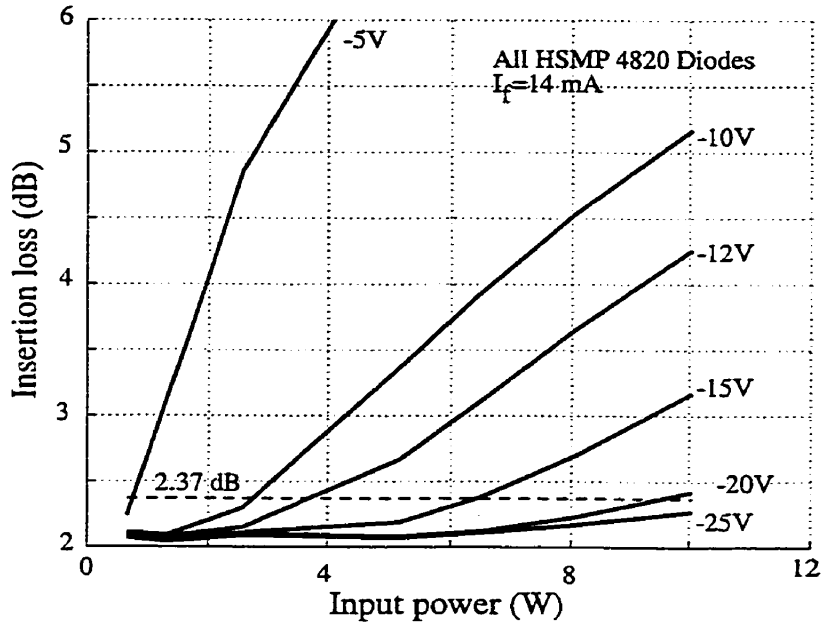

Figure 3.12 Measured insertion loss of a mismatched switch vs. input power for different reverse bias voltages. The forward bias currents were all 14 mA.

We used the same setup to measure the insertion loss at different reverse bias voltages when an HSMP 4890 diode was used instead of an HSMP 4820 diode in the activated channel. Figure 3.13 shows the insertion loss of such a mismatched switch vs. input power.

Comparing Figure 3.11 with Figure 3.12 and Figure 3.13, an activated channel using a HSMP 4890 diode generally has a lower insertion loss than that using an HSMP 4820 diode at the same reverse bias voltage.

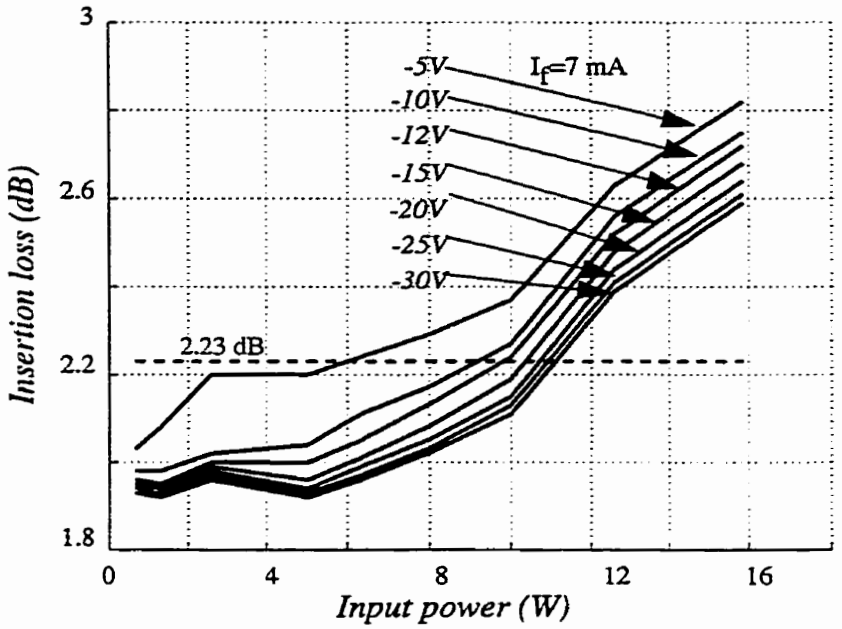

Figure 3.13 Measured insertion loss of a mismatched switch vs. input power for different reverse bias voltages. The forward bias currents were all 7 mA. The 7 diodes in the 7 activated channels were HSMP 4820 diodes and the diode in the activated channel was a HSMP 4890 diode.

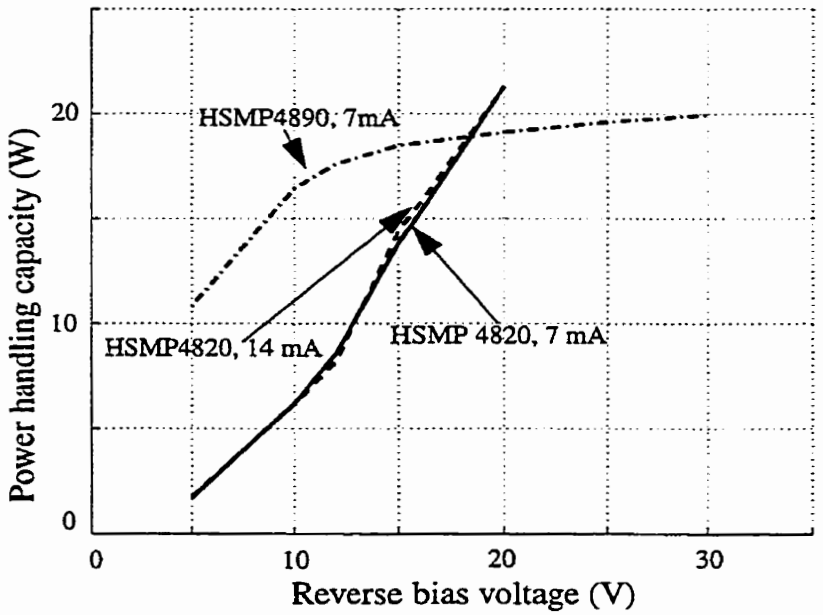

Figure 3.14 Estimated power handling capacity of microstrip switches with HSMP 4820 or HSMP 4890 diodes vs. reverse bias voltage.

For fixed values of reverse biased voltages and forward bias current, the insertion loss of a single channel increased with the input power. For each curve in Figure 3.11, the input power level P_{inc} at which the insertion loss is equal to the criterion loss A_{cr}, which is 0.3 dB higher than the insertion loss of 2.09 dB, the insertion loss of the channel when the input power is low, is used to estimate the power handling capacity of the channel at the corresponding reverse bias voltage. The choice of the value of 0.3 dB is somewhat arbitrary and an other small value around 0.3 dB could be taken. According to this estimation then, the power handling capacity of a switch when 3 adjacent channels are activated simultaneously is:

$$P_{max} = 3P_{inc} \times 10^{-A_{cr}/10} \tag{3.12}$$

The factor 3 is due to the 3 channels being activated simultaneously when the switch is used.

The estimated power handling capacity of different switches with different biases are shown in Figure 3.14. For the cases shown in Figure 3.12 and in Figure 3.13, A_{cr}=2.37 dB and A_{cr}=2.23 dB are used respectively. From Figure 3.14 we know that, for a specified transmission power level, using HSMP 4890 diodes can lower down the required reverse bias voltages. If the transmission power is 6 W, a reverse bias voltage of 5 V will be good enough for a switch using HSMP 4890 diodes. When HSMP 4820 diodes are used, a reverse bias voltage of about 9 V will be required.

3.6.3 Power handling capacity versus the equivalent load impedance

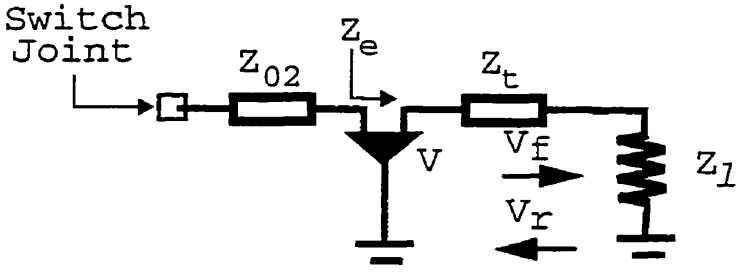

Figure 3.15 A reverse biased switching circuit.

For the switching circuit shown in Figure 3.15, the power absorbed by the load is

$$P = \frac{|V_f^2| - |V_r^2|}{Z_t}, \tag{3.13}$$

where V_f and V_r are the complex voltages of the microwaves propagating to the load and reflected from the load, respectively. For the voltage across the diode, V, we have $V = V_f + V_r$ and $V_r = \Gamma V_f$. Here Γ is the reflection coefficient measured at the diode. Equation (3.13) can be rewritten as,

$$P = \frac{|V^2|}{Z_t} \frac{[1 - |\Gamma|^2]}{|1 + \Gamma|^2}. \tag{3.14}$$

When the reverse bias voltage and the operation frequency are specified, there exists a maximum microwave voltage V_{max} across the diode in order for the cathode and anode of the diode to be well isolated. For the case shown in Figure 3.15, we have $\Gamma = (Z_t - Z_l)/(Z_t - Z_l)$. The final expression of the power handling capacity of the channel is

$$P_{max} = \frac{V_{max}^2}{Z_e}. \tag{3.15}$$

This means that the power handling capacity of an activated channel will decrease with the equivalent load impedance z_e. From Equation (3.15), if the switch needs to be operated at a power level of 6W, because of the increase of Z_e from 50 Ω to 70 Ω, the corresponding V_{max} will give a power level of 8.4 W when Z_e is 50 Ω. From Figure 3.14, a reverse bias voltage of 5 V is still good for switches using HSMP 4890 diodes. For switches using HSMP 4820 diodes, the reverse voltage will be about 12.5 V.

3.7 Conclusion

In this chapter we addressed the design of microstrip switches for applications in electronically-scanned antenna arrays for satellite communications. A simple switching circuit has been chosen to form the switches for lower cost and lower insertion loss. For HSMP 4890 PIN diodes, which have relatively high shunt capacitance, extra anode lead inductance is suggested to com-

pensate for the shunt capacitance of the diode, which will otherwise cause a high insertion loss and a high return loss in an open channel. In order to show the factors limiting the bandwidth, the Q-factor of a radial switch composed of ideal transmission lines was derived and used to establish criteria for wide bandwidth switch design. According to the formula, the number of closed channels should be small and the number of open channels large to give a wide bandwidth. When these numbers are specified, lowering the impedance of the open stubs and increasing the equivalent load impedance seen at each diode will also increase the bandwidth.

The design criteria were verified by simulations and were used to guide the implementation of microstrip switches. In the low-cost test switch presented in this thesis, the measured insertion loss was lower than 0.50 dB, reflection lower than -13.76 dB, and the isolation better than 28.45 dB, for the whole band from 1.525 GHz to 1.661 GHz.

The power handling capacity has been estimated experimentally. For a switch using HSMP 4820 diodes, reverse bias voltage of about 9 V would be required to give a power handling capacity of 6W. If we use HSMP 4890 diodes, 5 V of reverse bias voltage will be high enough. A forward bias current of 7 mA will be sufficient for power levels as high as 20 W.

We have also shown that the power handling capacity is inversely proportional to the equivalent load impedance Z_e. While increasing Z_e can increase the bandwidth and lower down the insertion loss, it has a negative effect from the view point of power handling capacity. If we increase Z_e from 50 Ω to 70 Ω, for a switch using HSMP 4890 diodes, a reverse bias voltage as high as 5 V will still be good enough. If we use HSMP 4820 diodes, the required reverse bias voltage will be about 12.5V.

CHAPTER 4

Beam controller for phased antenna arrays*

4.1 Introduction

In this chapter, we present a novel concept for a M/N-channel radial beam controller to deliver phase-controlled power into M activated channels out of a total of N channels. The design of the beam controller is discussed in details. Simulations show its performance, in particular the power delivering balance in the different branches. Finally, the beam controller is implemented and its performance is discussed.

The suggested M/N-channel phased antenna array is shown schematically in Figure 4.1, which is composed of an M/N-channel switch, and in each channel a 1-bit phase shifter and a patch antenna. Each channel is activated or deactivated by its switching circuit. In operation, a group of adjacent M channels out of the total N channels are activated while the other channels are

* The main part of this chapter has been submitted to the IEEE Transactions on Microwave Theory and Techniques [23].

deactivated. Each 1-bit phase shifter can be in its 1 state with a larger electrical length in degrees or in its 0 state with a smaller electrical length. For the case of M=3, 3 beams which point in 3 adjacent directions can be formed when the states of the phase shifters are 110, 010, and 011, respectively. A total of 3N beams can be formed horizontally.

A phased antenna array is under development in our laboratory for MSAT and INMARSAT mobile communications. A first configuration chosen was similar to that shown in Figure 4.1 with N=8 and M=3, and a 3/8-channel radial switch[20] and 8 hybrid reflection-type phase shifters were designed. However, the radiation pattern of the antenna was found to be somewhat different from expected. A reason for this was the different power levels delivered into each of the 3 activated channels. In order to understand this, let us look at the power delivering error into several shunt channels. Assuming the input admittance of an arbitrary channel is Y_j, the power delivered to it has the relation:

$$P_j \propto Re(Y_j). \tag{4.1}$$

For any two shunt channels which do not have identical impedances in the whole operation band, different powers will be delivered.

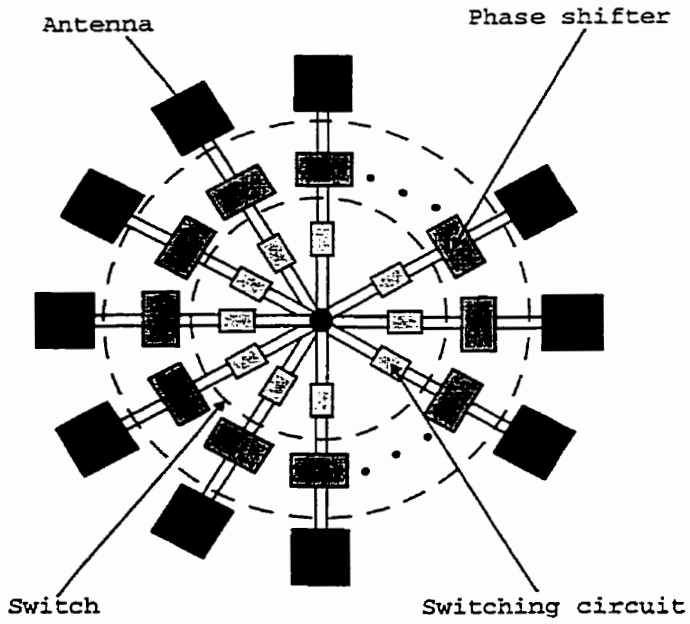

Figure 4.1 An M/N-channel phased antenna array.

In the case of Figure 4.1, if each activated channel could be matched to a common feed impedance, with maximum return loss R in the operation band, we know from a Smith chart that

$$\frac{1-\sqrt{R}}{1+\sqrt{R}} \le Re(Y_j) \le \frac{1+\sqrt{R}}{1-\sqrt{R}} \tag{4.2}$$

and the maximum power delivering error would be

$$\delta = 20\log\frac{1+\sqrt{R}}{1-\sqrt{R}}(\text{dB}). \tag{4.3}$$

Figure 4.2 gives the maximum power delivering error vs. maximum return loss.

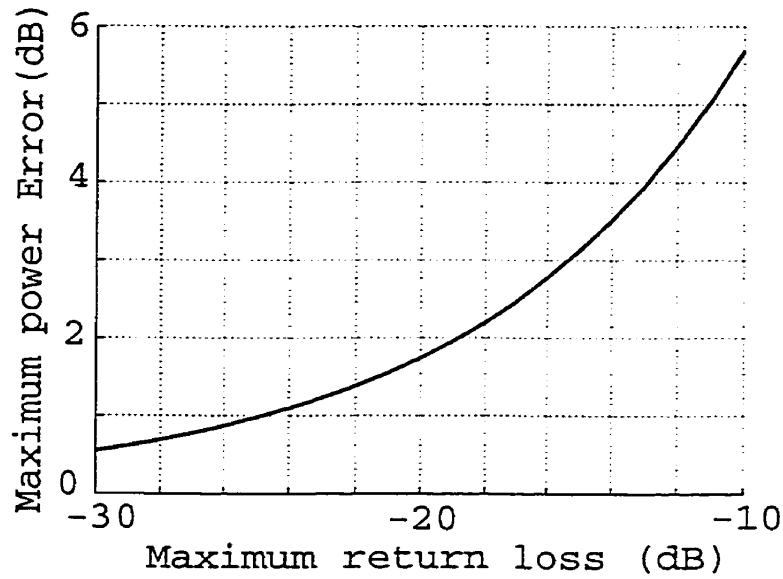

Figure 4.2 Maximum power-delivering error vs. maximum return loss.

For the configuration shown in Figure 4.1, in order to guarantee a power delivering error within 1 dB, each activated channel, including its switching circuit, phase shifter, and antenna in series, should be matched to a common impedance (150 Ω for our case of 3 channels activated and a feed impedance of 50 Ω), with a return loss lower than about -24.8 dB for the whole operation band. This is difficult for microstrip circuits.

In order to solve this problem, the concept of an M/N channel beam controller was proposed. In order to increase the bandwidth of the beam controller, the concepts of an optimized half-wavelength open stub and of a compound half-wavelength open stub, introduced in Chapter 2, were implemented.

4.2 The beam controller

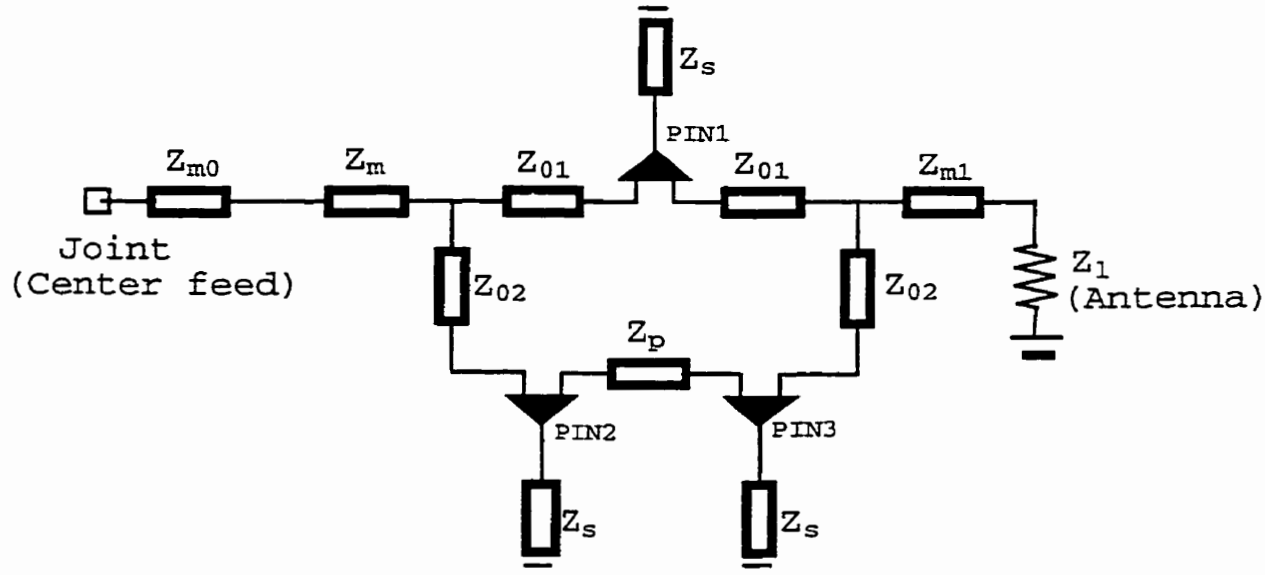

Figure 4.3 Transmission type phase-shifter used to form a beam controller.

The proposed M/N-channel beam controller is composed of N transmission-type phase shifters[30] as shown in Figure 4.3. Each phase shifter forms a channel, which is composed of two sub-channels, Sub-channel 0 and Sub-channel 1, and three PIN diodes. Each sub-channel can be activated or deactivated by its PIN diode(diodes) in series with a quarter-wavelength open stub. Sub-channel 0 is activated when PIN1 is reversely biased and PIN2 and PIN3 forward biased. Sub-channel 1 is activated when PIN1 is forward biased and PIN2 and PIN3 reversely biased. Both sub-channels are deactivated and therefore the channel is deactivated when all three diodes are forward biased. The length of each transmission line is around a quarter-wavelength except that of Z_p. The length of Z_p is decided according to the required phase difference between the two states of the phase shifter. Transmission lines Z_{m0} and Z_m are used to match the beam controller to the feed line at its center. Double transformers are required here to make

a deactivated channel an open circuit at the feed line. Transmission line Z_{m1} is used to match a channel to a patch antenna which will be added when an antenna array is formed.

As an example, let us consider the case of a 3/8-channel transmission line beam controller, in which 3 channels are activated simultaneously. For the 3 activated channels, the three combinations of phase shifter states are 110, 010, and 011, which correspond to a left, a middle, and a right beam in the array. HPSM 4890 Dual-anode PIN diodes are used and their equivalent circuit is the same as shown in Figure 3.2, where $L = 0.5\ nH$ is the lead inductance of the anode and of the cathode, $C_d = 0.33\ pF$ the shunt capacitance and R_d the shunt resistance, which is variable between $R_{dl} = 2.5\ \Omega$ when it is forward biased and $R_{dh} = 10000\Omega$ when it is reversely biased. A compromise value of 70 Ω is selected for the impedance of the two sub-channels in each phase shifter. A higher impedance would cause more reflection when the sub-channel is activated and its diode is featured as a shunt capacitance C_d. A lower impedance, on the other hand, would lead to power leaking through the sub-channel when its diode is forward biased and featured by its shunt resistance R_{dl}. The impedance of the transformer Z_{m0} is chosen to be 100 Ω. Assuming $Z_0 = 50\ \Omega$, according to the matching condition, we have $Z_m = 68\ \Omega$ and $Z_{m1} = 59\ \Omega$. The impedance of the quarter-wavelength open stubs is chosen to be $Z_s = 45\ \Omega$. HP-EEsof is used to simulate the operation of the beam controller. From the simulations, we see that in order to compensate for the lead inductance of the diodes, the length of Z_{01} and Z_s should be 78.6 and 83.7 degrees, a little less than 90 degrees. The length of Z_p is chosen to be 80 degrees to obtain a center phase difference of 102 degrees, which is required by our antenna array.

One important feature is that Z_{01} and Z_{02} can be adjusted around their initial values for better power-delivering balance between a channel with phase shift state 1 and a channel with phase shift state 0. Accordingly, $Z_{01} = 75\ \Omega$ and $Z_{02} = 67\ \Omega$ are chosen. Figure 4.4 is the HP-EEsof circuit network for this beam controller for its 010 beam. The impedance and electrical length of each transmission line are listed in Table 4.1. Also in Table 4.1 are the width and length of the microstrip corresponding to each transmission line, for the same substrate used for the microstrip switch design, i.e., GML 1000 laminate with nominal parameters: Dielectric con-

stant=3.20±0.05, Thickness=0.762 mm, Copper thickness=0.035 mm, Dissipation factor=0.003.

Table 4.1 Transmission lines used to form the beam controller and the widths and lengths of their corresponding microstrips.

Transmission line	Impedance (Ω)	Electrical length (degrees)	Width (mm)	Length (mm)
Z_{01}	75	78.6	.86	26.56
Z_{02}	67	90	1.07	30.17
Z_{m0}	100	90	.43	31.08
Z_m	68	90	1.04	30.20
Z_p	67	80	1.07	26.81
Z_{m1}	59	90	1.35	29.89
Z_s	45	83.7	2.11	27.29

Figure 4.5 (a), (b), and (c) show the return loss, insertion loss and phase shift in function of frequency for 1-channels and 0-channels. In simulations, the results for a 110 beam are exactly the same as for a 011 beam and therefore only the results for a 011 beams are shown. Only the phase shift for a 010 beam is shown because the phase difference between a 1-channel and a 0-channel for a 011 beam is almost the same. The overall insertion loss of a beam, which is the sum of the power delivered into each of the three activated channels divided by the power fed into the beam controller, can be calculated from the figures. It is between 0.90 dB and 1.43 dB for all beams. The difference in the power delivered into a 1-channel and a 0-channel is lower than 0.28 dB. The isolation, which is the insertion loss between the feed and a deactivated channel, is better than 33 dB. The phase shift between a 1-channel and a 0-channel for a 010 beam is 93, 97, 104, 109, and 113 degrees at 1.525, 1.559, 1.593, 1.627, and 1.661 GHz, respectively. The phase shift for the 011 or 110 beam is the same (within 1 degree) as for the 010 beam.

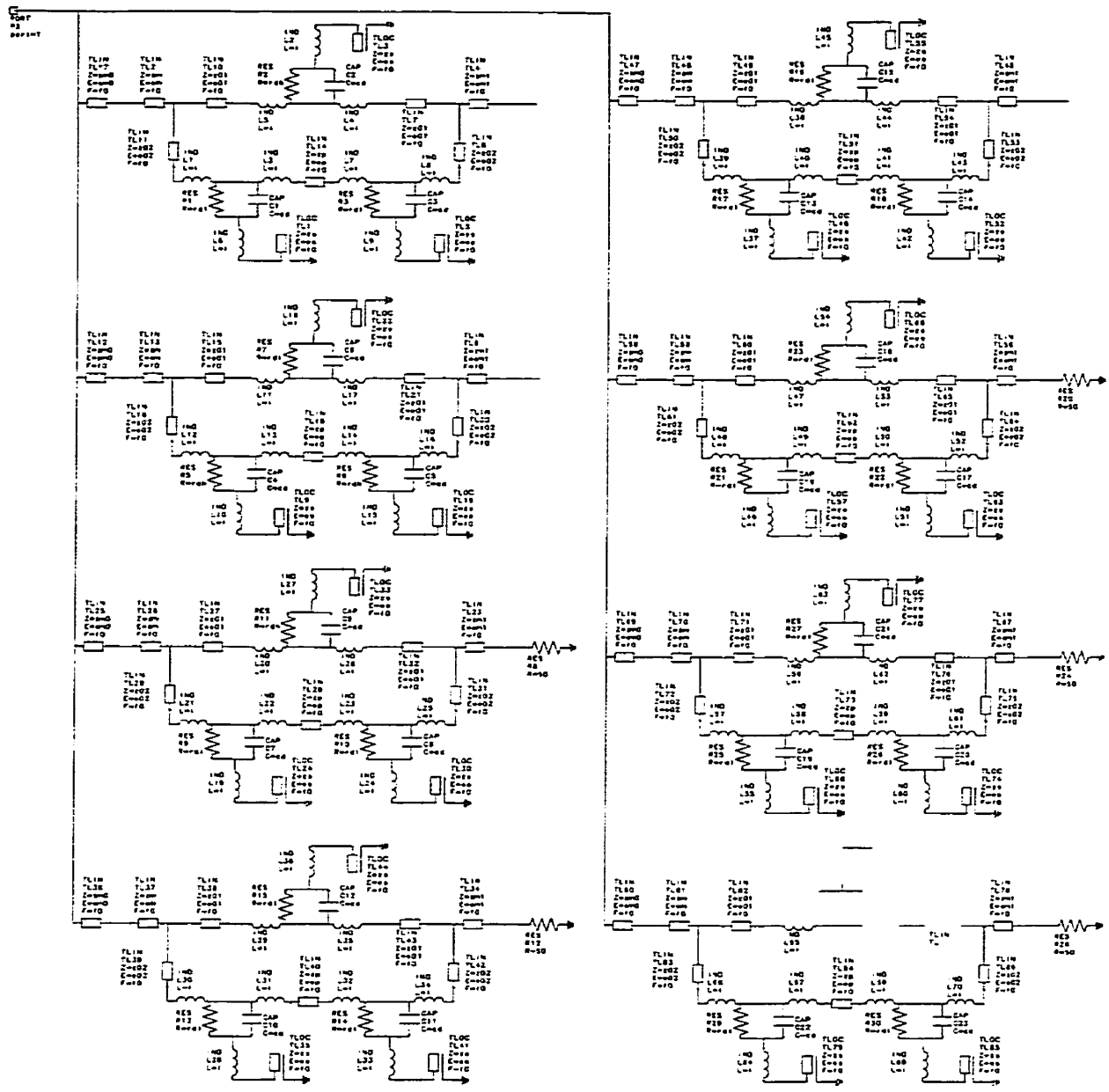

Figure 4.4 HP-EEsof circuit network for the beam controller for its 010 beam.

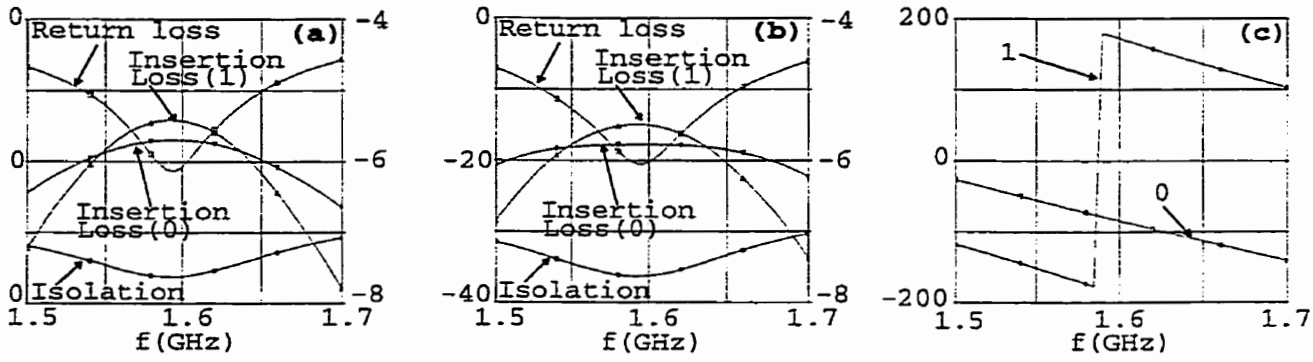

Figure 4.5 Simulated results: (a) S-parameters in dB for a 010 beam, (b) S-parameters in dB for a 011 beam, and (c) phase shift of a 1- and 0-channel for a 010 beam. For the insertion losses, please refer to the right axis.

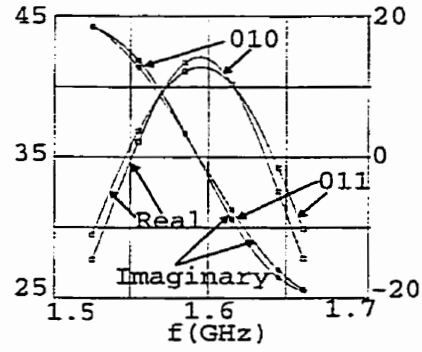

Figure 4.6 Real (left axis) and imaginary (right axis) parts of the input impedance in Ω.

Because of the frequency-dependent behavior of all the quarter-wavelength transmission lines, the return loss increases when the frequency is away from the center frequency and, at the lower boundary of the band, it is -8.83 dB, which is considerably higher than -14 dB, the maximum return loss objective for the array. For the same reason, the overall insertion loss at the lower boundary frequency is 0.53 dB higher than that at the center frequency. In order to lower down

the overall return loss in the whole operation band, an optimized tuning circuit based on the optimized half-wavelength tuning stub described in Chapter 2 is designed.

The input impedances of the beam controller for the 010 and 011 beams are calculated and are shown in Figure 4.6. The input impedance vs. frequency characteristics are similar for both beams. The equivalent parameters Z_l and Z_{01} (please see Figure 2.5) for the beam controller can be calculated. At the center frequency of 1.593 GHz, the value of the shunt resistances is about $Z_l = 41.8\ \Omega$. The imaginary parts of the impedances have an averaged slope of $\Delta X/\Delta\omega = -6.26x10^{-8}\Omega s$. For the equivalent circuit enclosed in the dashed square of Figure 2.5, the imaginary part of the impedance has a slope of $\Delta X/\Delta\omega = -(Z_l^2\pi)/(\omega_0 Z_{01})$. Correlating these two slopes, we have $Z_{01} = 8.7\ \Omega$. In our case we have $Z_t = 50\ \Omega$ and according to Equation (2.27), we have $Z_{02} = 13.0\ \Omega$.

An open stub of impedance 13.0 Ω would be too wide to be implemented using microstrip circuits. In this case, a tuning circuit shown in Figure 4.7 is designed, based on two shunt compound half-wavelength tuning stubs described in Chapter 2. The length of each transmission line is around a quarter-wavelength. According to Equation (2.29), if we choose $Z_{sb} = 45\ \Omega$, $Z_e = 26\ \Omega$, we have $Z_{sa} = 111\ \Omega$. In Chapter 2.2 the value of Z_t was lowered from its matching value for lower overall return loss. This is achieved here by keeping the impedance of Z_t to be 50 Ω while increasing the effective load impedance. For this purpose the value of the transformer Z_{c1} is increased from its matching value of 50 Ω to 63.5 Ω.

Adding the tuning circuit to the beam controller, the simulated S-parameters of the beam controller are as shown in Figure 4.8. The return loss for both 010 and 011 beams is lower than -15.81 dB, the overall insertion loss between 0.85 dB and 0.94 dB, the power delivering balance better than 0.37 dB, and the isolation between the feed and a deactivated channel better than 32 dB. The phase differences for each phase shifter are almost the same as when no tuning circuit is added. At frequencies 1.525, 1.559, 1.593, 1.627, and 1.661 GHz, they are 93, 97, 102, 108 and 113 degrees, respectively.

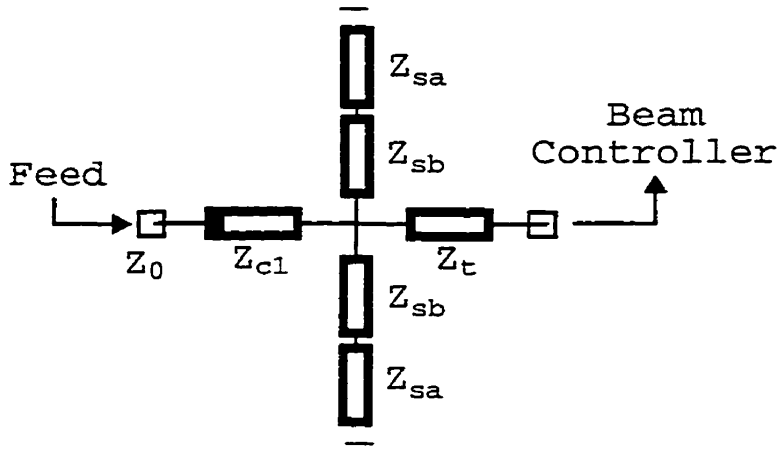

Figure 4.7 The tuning circuit.

In the case analyzed here the length of Z_p is chosen to be 80 degrees in order for the beam controller to have a phase difference off 102 degrees at the center frequency of the band. Simulations show that the beam controller will work well for other phase differences. The only parameter which needs to be changed is the length of Z_p. If we choose the length of Z_p to be 70, 80, and 90 degrees, the phase difference at the center frequency will be 92, 102 and 113 degrees, respectively. Little effects can be found on the return loss, the power delivered into each activated channel, and the isolation.

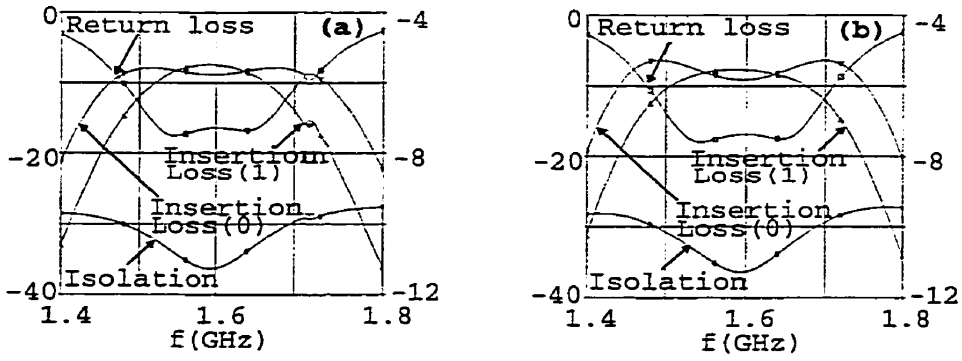

Figure 4.8 Simulated results: (a) S-parameters in dB for 010 beam, (b) S-parameters in dB for 011 beam. For all the insertion losses, please refer to the right axis.

4.3 Beam controller realization and measured results

The beam controller simulations based on transmission lines similar to those described in the Section 4.2 were used to guide the design of a microstrip beam controller. HP-EEsof has been used to calculate the width and length of the microstrip corresponding to each transmission line used in the tuning circuit, as has been done for Table 4.1. Figure 4.9 is a photo of the beam controller and the tuning circuit. The tuning circuit is perpendicularly connected to the joint of the beam controller through a section of coaxial cable of 50 Ω impedance. Here Z_t was composed of this section of coaxial cable and a section of microstrip of the same impedance 50 Ω. The total electrical length was 90 degrees as was required by the tuning circuit. A DC block consisting of a capacitor with a nominal 10 pF capacitance was also mounted on the tuning circuit board. In order to compensate for the capacitance, a section of microstrip of width 0.70mm and length 1.4 mm was added at each side of the capacitor. A SMA connector was finally used as the feed for the whole circuit.

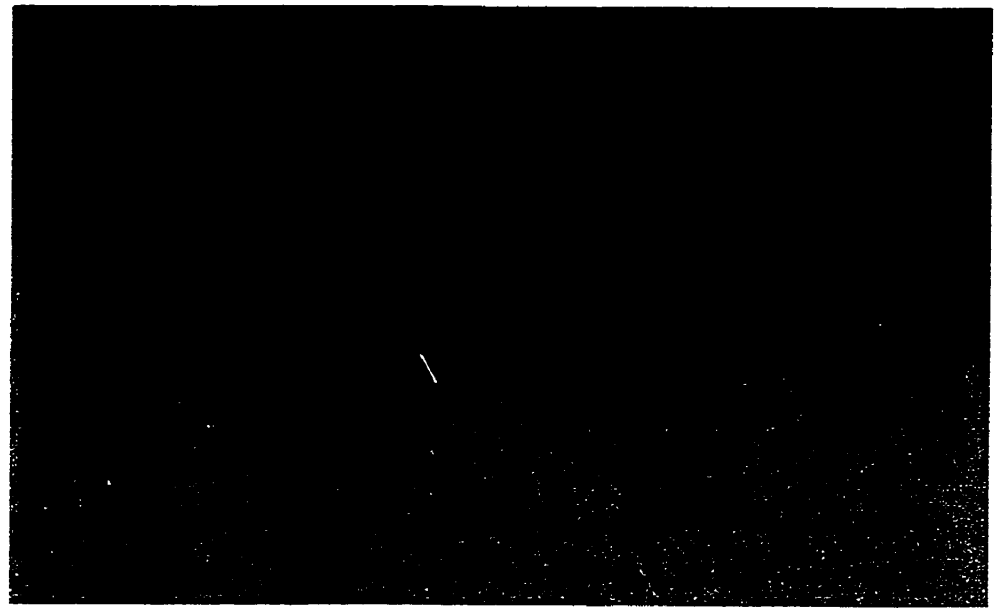

Figure 4.9 A photo of the beam controller and the tuning circuit.

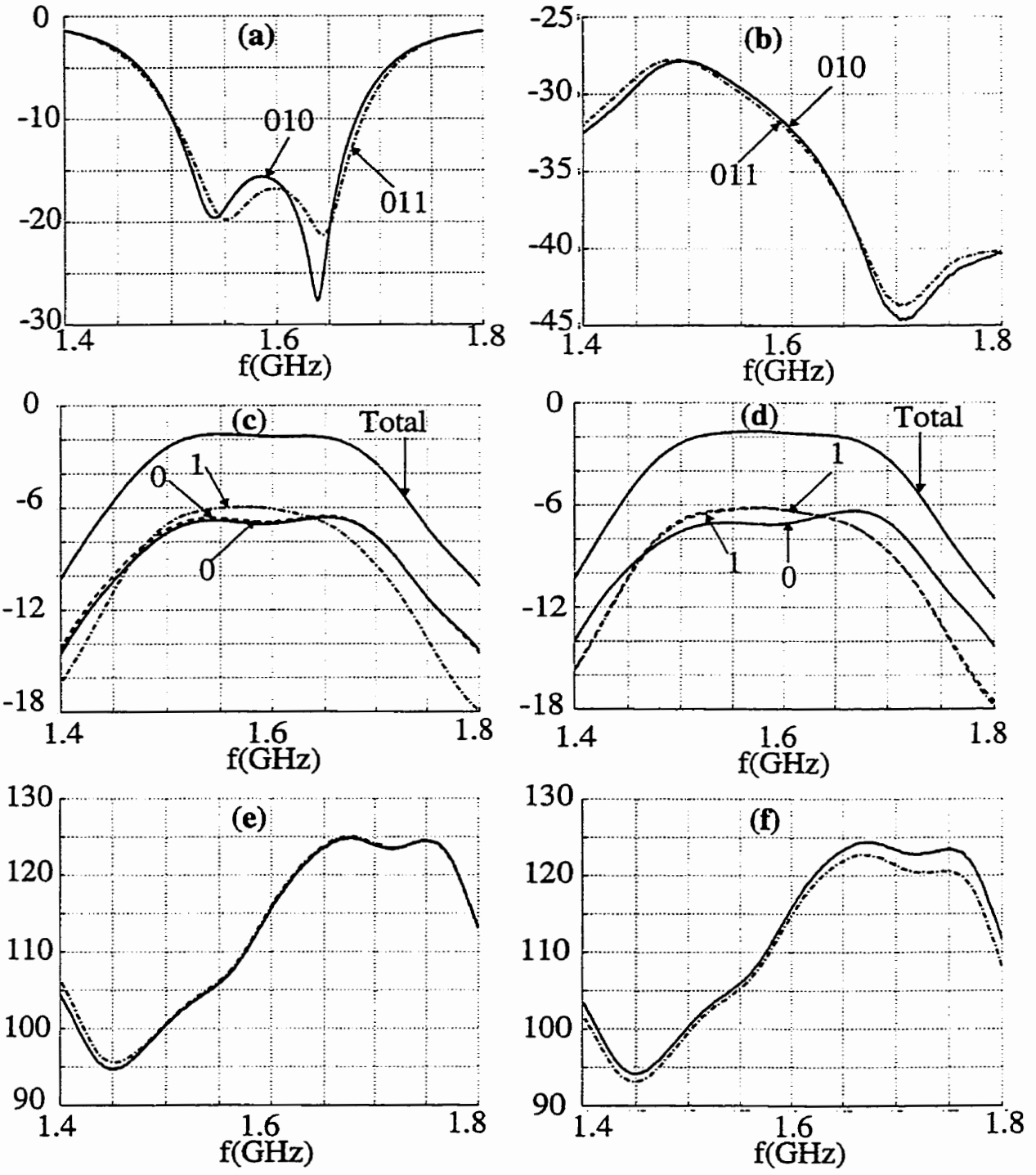

Figure 4.10 Measured results: (a) return loss in dB for a 010 beam and a 011 beam, (b) isolation for a 010 beam and a 011 beam, (c) insertion loss in dB for the 0-, 1-channel and all activated channels for a 010 beam, (d) insertion loss in dB for the 0-, 1-channel and all activated channels for a 011 beam, (e) phase differences between 1-channel and 0-channel for a 010 beam, and (f) phase differences between 1-channel and 0-channel for a 011 beam.

Measurements for return loss, isolation, insertion loss and phase difference from the beam controller with the tuning circuit and the DC block are shown in Figure 4.10. The return loss was lower than -14.92 dB, the overall insertion loss lower than 2.08 dB, the power-delivering balance better than 0.92 dB, and the isolation better than 28.53 dB for the operation band from 1.525 GHz to 1.661 GHz. The phase differences for both 010 and 011 beams were 103, 107, 114, 121, and 124 degrees, at 1.525, 1.559, 1.593, 1.627, and 1.661 GHz, respectively.

4.4 Conclusion

In this chapter, the concept of a M/N-channel radial beam controller was introduced to deliver phase-controlled power into M activated channels out of a total of N channels, with improved power-delivering balance than what could be achieved by the first suggested configuration of an M/N channel central switch with a 1-bit phase shifter in each channel.

The process of the design of a 3/8-channel beam controller based on the above concept was presented. A tuning circuit using two compound half-wavelength open stubs was designed to increase the bandwidth. Four features of the beam controller are worth mentioning, namely low cost, good power-delivering balance, good isolation of the deactivated channels and phase difference flexibility. As pointed in [12], the cost of a microstrip antenna array highly depends on the number of diodes used. Only 24 PIN diodes were used in our case. The impedances of the two sub-channels in each channel enable optimizing the power-delivering balance: a power delivering-balance as good as 0.37 dB was achieved from the simulations. An isolation better than 32 dB is possible for a deactivated channel. Finally one can simply change the length of Z_p in the design when another phase difference is required.

A microstrip beam controller has been implemented under the guidance of simulations. The measurements showed a return loss lower than -14.92 dB, an overall insertion loss lower than 2.08 dB, a power-delivering balance better than 0.92 dB, and an isolation better than 28.53 dB for the operation band from 1.525 GHz through 1.661 GHz. The phase differences were 103, 107, 114, 121, and 124 degrees, at 1.525, 1.559, 1.593, 1.627, and 1.661 GHz, respectively. The

operation parameters of the beam controller are already good enough for our antenna array application.

Compared to the simulations, the measured overall insertion loss was about 1 dB higher than simulated. The power-delivering balance was different from the simulated one by 0.55 dB. The phase difference was 6 to 8 degrees more than that from the simulations. The isolations, from Figure 4.10 (b), were centered at a frequency higher than 1.7 GHz, and therefore, the overall isolation in the operation band was 3.5 dB lower than the simulated one. Among the reasons which could account for these discrepancies, first, we found that the behavior of the beam controller, especially its phase difference and insertion loss, was quite sensitive to the anode lead inductance. In practice, the anode lead inductance actually depends on the way the diode is soldered to a microstrip, while in the simulations they were all assumed 0.5 nH according to the parameters provided by the company. Another reason was the effects of the microstrip T-, cross-, and step-junction circuits, which were not included in the simulations. The operation of the microstrip beam controller could be further improved, after carefully dealing with these issues.

CHAPTER 5

Broadband electromagnetically-coupled patch antennas with circular polarization

5.1 Introduction

Patch antennas have been chosen as the unit antennas for our electronically-scanned arrays because of their low cost and compatibility with our printed circuit beam-forming network. The technical challenges in designing such patch antennas are several folds. First, because Inmarsat/ Msat geostationary satellites use right-hand circularly-polarized microwave signals to communicate with earth terminal, circularly-polarized antennas are preferred. A linearly-polarized antenna will lead to about 3 dB or more loss because of the mismatch factor between the wave and the antenna. Second, the required relative bandwidth is about 8.5%, which poses a stringent requirement for patch antennas. A thick substrate can be used to increase the bandwidth but it also tends to increase the cost and weight of the antenna arrays. As a result, electromagnetically-coupled patch antennas using a thin substrate are preferred.

A single-fed and a dual-fed electromagnetically-coupled patch antennas were reported by Karmakar and Bialkowski last year [31]. As expected, the single-fed antenna was somewhat limited in bandwidth. The 3 dB axial ratio bandwidth is only 4.1%, which is not enough for our application. The dual-fed patch antenna was a two substrate structure spaced by a foam layer. A circular patch was etched on the upper side of the top substrate. The foam layer was used to support the first layer. Two coupling slots were etched on the upper side of the second substrate and the whole antenna was fed by a 3 dB hybrid coupler on the lower side of the second substrate through the two coupling slots.

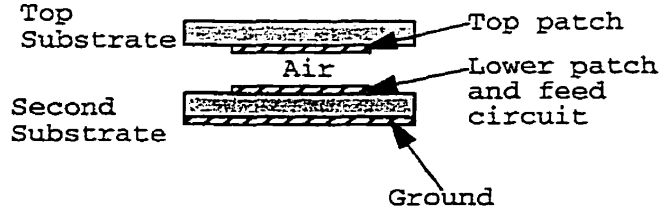

Figure 5.1 Configuration of an electromagnetically-coupled patch antenna.

In this chapter a simpler structure as shown in Figure 5.1, will be proposed for the antenna. First we suggest not to use any foam layer because of its somehow unstable electric characteristics which makes it difficult to control the center frequency of the antenna and adds to its cost. Instead, an air gap will be provided. A square patch will be etched on the lower side of the top substrate and another square patch etched on the upper side of the second substrate. The top substrate will be fixed to the second substrate at several places by thin plastic pins. The locations of the pins should be far enough from the patches to avoid interfering with their field distributions. A simple power dividing circuit, which will also be proposed in this chapter, will be used to feed the lower patch for circular polarization. Although a 3 dB hybrid coupler can be used for better axial ratio, it will also lead to higher circuit loss which leads to a reduced gain of the antenna. For such a coupler, a resistor is usually needed to absorb the reflected power and it will further add to the cost of the antenna array because of the cost of the components and the cost of the labor needed to solder it to each unit antenna. Our solution also does not increase the design difficulties related to low axial ratios because it is the gain of the antenna and the polarization mismatch factor which will control the performance of an antenna.

In the first part of our antenna array project, an economical electromagnetically-coupled patch antenna has been designed and tested[18]. In that antenna, a thin copper patch was glued on a patch of construction foam, which was then glued to a thin substrate having an antenna patch on the upper side and the ground plane on the lower side. This antenna unit has given good results and was the starting point for the design of the air-dielectric electromagnetically-coupled patch antenna reported here.

The remainder of this chapter is managed as follows. In Section 5.2, the polarization mismatch factor for a wave and an antenna will be derived, as a function of their axial ratios and the orientation of their polarization. This formula can be used to evaluate the negative effect of an increased axial ratio of the antenna. In Section 5.3, a simple dual-feed circuit will be proposed for applications in circularly-polarized antenna design. In Section 5.4, assuming that the power fed into the each feed is specified, we will derive the relationship between the axial ratio of a dual-feed antenna and the phase difference between its orthogonal electric field components. In Section 5.5, according to the above sections, a step-by-step method for circularly-polarized antenna design will be presented with the design of a sample patch antenna using a commercial software: Ensemble. In Section 5.6, the measured results from the sample antenna will be presented. In Section 5.7, measured results from another sample antenna with improved axial ratio will be presented. In Section 5.8, some discussions and conclusions are provided.

5.2 The dependence of the mismatch factor on the axial ratio of an antenna

Suppose an incident circularly-polarized, or to be more general, an elliptically-polarized plane wave with electric field

$$\vec{E} = E_1 e^{i\omega t}\hat{e}_1 + E_2 e^{i(\omega t + \phi_E)}\hat{e}_2 \tag{5.1}$$

is intercepted by an antenna with effective length

$$\vec{A} = A_I e^{i\omega t}\hat{e}_I + A_{II} e^{i(\omega t + \phi_A)}\hat{e}_{II}, \tag{5.2}$$

the polarization mismatch factor will be [32]:

$$p = \frac{\left|A_I E_1 \hat{e}_I \bullet \hat{e}_1 + A_I E_2 \hat{e}_I \bullet \hat{e}_2 e^{i\phi_E} + A_{II} E_1 \hat{e}_{II} \bullet \hat{e}_1 e^{-i\phi_A} + A_{II} E_2 \hat{e}_{II} \bullet \hat{e}_2 e^{i(\phi_E - \phi_A)}\right|^2}{(A_I^2 + A_{II}^2)(E_1^2 + E_2^2)} \tag{5.3}$$

In (5.1) E_1 and E_2 are the amplitudes of the fields in the $\hat{e}_1$ and $\hat{e}_2$ directions, the orthogonal unit vectors in the direction of the long and short axis of the wave polarization ellipsoid and $\phi_E = \pm 90°$, where the "+" and "-" signs correspond to a right-hand and a left-hand polarization, respectively. The axial ratio of the wave is:

$$A_E = E_1 / E_2 \tag{5.4}$$

In (5.3) A_I and A_{II} are the components of the antenna effective length in $\hat{e}_I$ and $\hat{e}_{II}$, the unit vectors in the direction of the long and short axis of the antenna polarization ellipsoid, and $\phi_A = \pm 90°$, where the "+" and "-" signs correspond to a right-hand and left-hand polarization, respectively. The axial ratio of the antenna is:

$$A_A = A_I / A_{II} \tag{5.5}$$

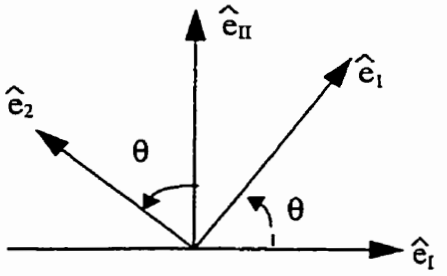

Figure 5.2 Unit vectors of the wave field and of the antenna effective length.

Figure 5.2 shows the orientations of the four unit vectors and from it we have: $\hat{e}_I \bullet \hat{e}_1 = \cos\theta$, $\hat{e}_{II} \bullet \hat{e}_1 = \sin\theta$, $\hat{e}_I \bullet \hat{e}_2 = -\sin\theta$, and $\hat{e}_{II} \bullet \hat{e}_2 = \cos\theta$ and therefore:

$$p = \frac{(A_I E_1 \pm A_{II} E_2)^2 \cos^2\theta + (A_I E_2 \pm A_{II} E_1)^2 \sin^2\theta}{(A_I^2 + A_{II}^2)(E_1^2 + E_2^2)} \tag{5.6}$$

or

$$p = \frac{(1 \pm A_E A_A)^2 \cos^2\theta + (A_E \pm A_A)^2 \sin^2\theta}{(1 + A_A^2)(1 + A_E^2)}. \tag{5.7}$$

In (5.6) and (5.7), if the polarizations of the wave and of the antenna are in the same sense (same right hand or left-hand polarization), the "+" sign will be used. Otherwise, the "-" sign will be used.

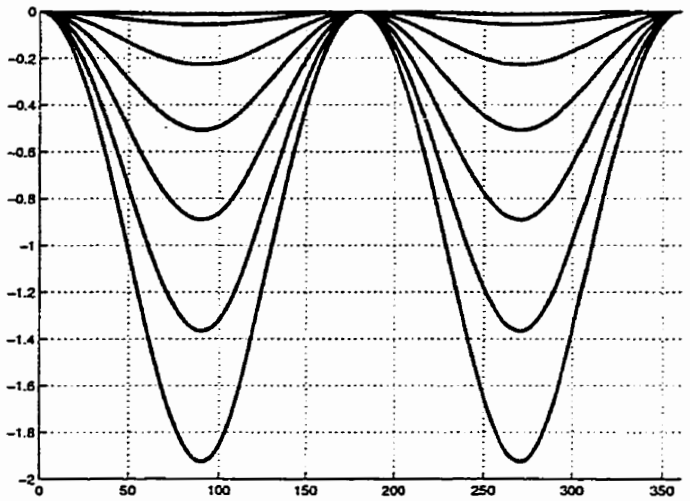

Figure 5.3 Mismatch factor in dB vs. orientation angle in degrees for axial ratios of the wave and of the antenna as parameter. Both axial ratios are assumed to be the same. For curves from top to bottom, $A_E = A_A = 0.5, 1, 3, 6, 9, 12, 15$ dB.

Figure 5.3 shows the mismatch factor vs. orientation angle for different axial ratios of the wave and of the antenna. The axial ratio of the wave is assumed to be the same as that of the antenna. When their polarizations are orientated in the same direction, $\theta = 0°$ or $180°$, they are matched in polarization and we will have the highest mismatch factor 1, or 0 dB. When their polarizations are orientated orthogonally, $\theta = 90°$ or $270°$, we will have the lowest polarization mismatch factor, which depends on the axial ratio of the wave and of the antenna. The lowest mismatch factors are -0.06, -0.23, -0.52, -0.89, -1.36, -1.92 dB, for $A_E = A_A = 1, 3, 6, 9, 12, and 15$ dB.

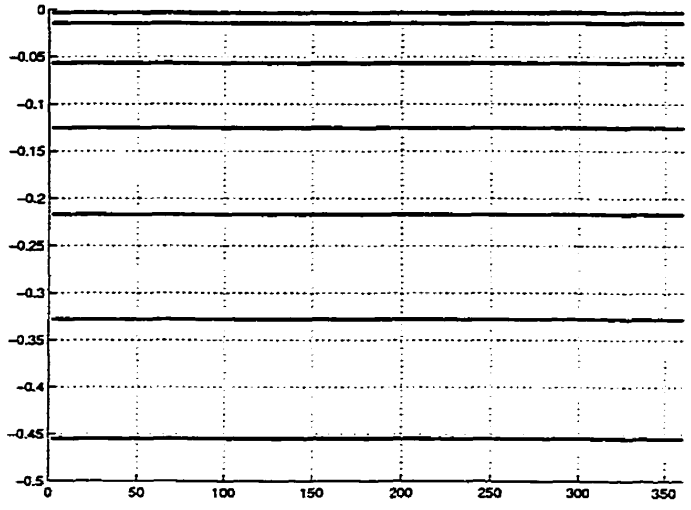

Figure 5.4 Mismatch factor in dB vs. orientation angle in degrees for different axial ratio of the antenna as parameter. The axial ratio of the wave is assumed to be 0 dB. For curves from top to bottom, A_A = 0.5, 1, 2, 3, 4, 5, 6 dB.

Figure 5.4 shows the mismatch factor vs. orientation angle for different axial ratios of the antenna as parameter. The axial ratio of the wave is assumed to be 0 dB, corresponding to an ideal circularly-polarized wave. In this case, the orientation of the wave polarization can be supposed in any direction and therefore, the mismatch factors are constant for any polarization orientation of the antenna. The mismatch factors are -0.005, -0.02, -0.06, -0.15, -0.22, -0.33 and 0.46 dB, for A_A = 1, 2, 3, 4, 5, 6 dB.

Figure 5.5 shows the mismatch factor vs. orientation angle for different axial ratios of the antenna as parameter. The axial ratio of the wave is assumed to be 3 dB for all curves. When their polarizations are orientated in the same direction, θ = 0° or 180°, we will have the highest mismatch factors, which are -0.09, -0.06, -0.02, 0, -0.02, -0.05, -0.10 dB, for A_A = 1, 2, 3, 4, 5, 6 dB. When their polarizations are orientated orthogonally, θ = 90° or 270°, we will have the lowest polarization mismatch factors, which also depend on the axial ratios of the wave and of the antenna. The lowest mismatch factors are -0.16, -0.24, -0.34, -0.51, -0.68, -0.88 and -1.09 dB, for A_A = 0.5, 1, 2, 3, 4, 5, 6 dB .

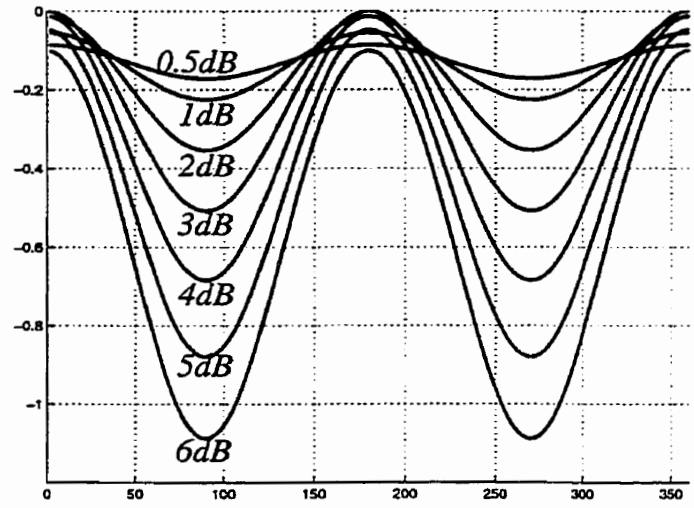

Figure 5.5 Mismatch factor in dB vs. orientation angle in degrees for different axial ratios of the antenna as parameter. The axial ratio of the wave is assumed to be 3dB.

For mobile satellite communications, the wave from a satellite is not of perfect circular polarization and neither is that of a terminal antenna. It is not practical to adjust the polarization of the antenna according to that of the wave from the satellite. Therefore, the lowest mismatch factor will be compared for different antennas.

5.3 A simple power distribution circuit for dual-feed antennas with circular polarization

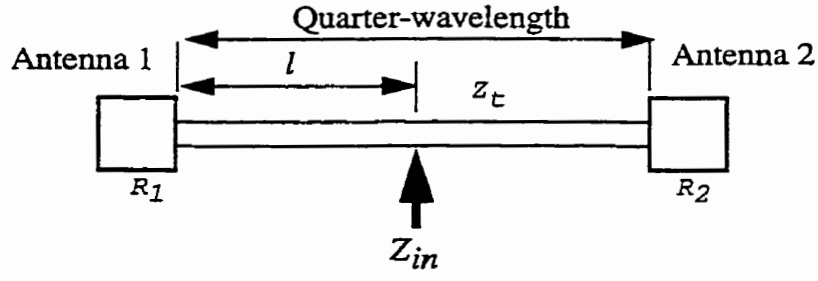

Figure 5.6 Simple dual-feed circuit for circular polarization.

A dual-feed circularly-polarized antenna can be constructed by dividing power into two feeds on a single antenna or on two separate antennas. The two feeds excite orthogonal modes in the single antenna or in the two antennas which radiate/receive orthogonal fields to/from the space. Here we propose a simple circuit, shown in Figure 5.6, as power dividing circuit. The circuit is a quarter-wavelength transformer connecting the two antennas represented by two resistive loads, fed by another transmission line at a certain point on the transformer. We will first prove that the input impedance of such a circuit will always be real wherever the feeding point is located, allowing the circuit to be matched to a 50Ω connector, provided that the input impedances of the two feeds are purely resistive. This also gives the flexibility to change the feeding location to adjust the phase difference between the orthogonal fields for circular polarization. Second, we will prove that the power divided into each load will always be the same.

The impedance of the quarter-wavelength transmission line is $Z_t = \sqrt{R_1 R_2}$. If we feed the two antennas at some point l away from load R_1, then the input impedances of the two feeds seen at the feeding point are

$$Z_{in1} = Z_t \frac{R_1 + iZ_t tg\beta l}{Z_t + iR_1 tg\beta l} \tag{5.8}$$

and

$$Z_{in2} = Z_t \frac{R_2 + iZ_t ctg\beta l}{Z_t + iR_2 ctg\beta l}. \tag{5.9}$$

Here we used $tg\left(\frac{\pi}{2} - \beta l\right) = ctg\beta l$. After some manipulations, the input impedance of the whole circuit is:

$$Z_{in} = \frac{1}{2} \frac{R_1 + R_2 tg^2 \beta l}{1 + tg^2 \beta l}. \tag{5.10}$$

From (5.10) we can see that the input impedance is always real for any l and therefore, we can easily match it with a 50Ω connector using a quarter-wavelength transformer. We can further show that the input impedance is between $R_1/2$ and $R_2/2$ and the closer the feed point is to

Antenna 1, the closer the input impedance will be to $R_1/2$. This is also true for Antenna 2. If we feed at the center of the transformer, we have

$$Z_{in} = \frac{R_1 + R_2}{4}. \tag{5.11}$$

From Section 4.1 we know that the power absorbed by each load is given by the relation

$$P_j \propto Re(Y_{inj}) \tag{5.12}$$

where $j = 1$ or 2. From (5.8) and (5.9) we have

$$R_e(Y_{in1}) = \frac{1}{Z_t}\frac{Z_t R_1 + R_1 Z_t tg^2\beta l}{R_1^2 + Z_t^2 tg^2\beta l} \tag{5.13}$$

and

$$R_e(Y_{in2}) = \frac{1}{Z_t}\frac{Z_t R_2 + R_2 Z_t ctg^2\beta l}{R_2^2 + Z_t^2 ctg^2\beta l} \tag{5.14}$$

From (5.13), (5.14) and (5.12), we can easily obtain:

$$P_1 = P_2, \tag{5.15}$$

i.e., the power divided into each antenna will always be the same. Accordingly we suggest the following steps in the design of an antenna with circular polarization:

1. Convert the input impedances of two orthogonal feeds on a single antenna or on two separate antennas into real impedances and cancel their imaginary part, using an appropriate circuit.

2. Connect the two feeds with a quarter-wavelength transformer. The impedance of the transformer is the same as that of a transformer which would match the two feeds.

3. Feed the circuit at some point on the transformer. The location is chosen to create a 90° phase difference between the orthogonal fields.

The ideal case is when the input impedances of the two feeds are constant and purely resistive over the whole operation band and the isolation between the two feeds is perfect. For such a case, the axial ratio of the antenna will be 0 dB over the operation band. In our case, the two feeds are on the same square patch antenna. Instead of being constant, the real part of the input impedance of each antenna changes over the operation band, the imaginary part is not zero, and the isolation between the two feeds for the single antenna is also not perfect. Consequently, the axial ratio of the antenna will depend on how close the situation can be to the ideal case.

5.4 The dependence of the axial ratio on the phase difference between orthogonal fields.

In the design of a dual-feed circularly-polarized antenna, when the power fed into each feed is decided, the axial ratio of the antenna will still change with the phase difference between the orthogonal electric fields. Here we will discuss the effect of such a phase difference.

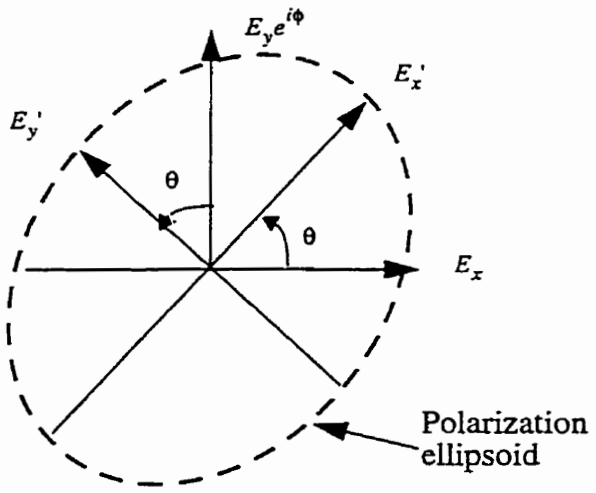

Figure 5.7 Orthogonal electric fields with a given phase difference and the resulting polarization ellipsoid.

The electric field of a plane wave can be expressed as:

$$\vec{E} = E_x \hat{e}_x + E_y e^{i\phi} \hat{e}_y \tag{5.16}$$

where $\hat{e}_x$ and $\hat{e}_y$ are two orthogonal unit vectors. In general, we can choose $\hat{e}_x$ or the direction in which the electric field component is larger and we have

$$A_0 = \frac{E_y}{E_x} > 1 . \tag{5.17}$$

According to Figure 5.7, the electric field can also be expressed as:

$$\vec{E} = (E_x \cos\theta + E_y e^{i\phi} \sin\theta)\hat{e}_{x'} + (-E_x \sin\theta + E_y e^{i\phi} \cos\theta)\hat{e}_{y'}, \tag{5.18}$$

where $\hat{e}_{x'}$ and $\hat{e}_{y'}$ are the two orthogonal unit vectors in the directions of the two axis of the polarization ellipsoid, which are obtained by rotating $\hat{e}_x$ and $\hat{e}_y$ anti-clockwise by θ, which is decided by the condition that the phase difference between the two components in (5.18) should be $\pm\pi/2$. The phases of the two components in (5.18) are:

$$tg\phi_{x'} = \frac{E_y \sin\theta \sin\phi}{E_x \cos\theta + Ey \sin\theta \cos\phi} \tag{5.19}$$

and

$$tg\phi_{y'} = \frac{E_y \cos\theta \sin\phi}{-E_x \sin\theta + Ey \cos\theta \cos\phi} \tag{5.20}$$

and the following conditions should be satisfied:

$$\phi_{x'} = \phi_{x'} \pm \frac{\pi}{2} \tag{5.21}$$

or

$$tg\phi_{x'} = -ctg\phi_{y'} . \tag{5.22}$$

From (5.19), (5.20), and (5.22) we have:

$$tg2\theta = \frac{2E_y E_x \cos\phi}{E_x^2 - E_y^2} . \tag{5.23}$$

From (5.17) we have

$$tg2\theta = \frac{2A_0\cos\phi}{1-A_0^2}. \tag{5.24}$$

From (5.24) $tg\theta$ can be calculated:

$$tg\theta = \frac{-1\pm\sqrt{1+tg^2 2\theta}}{tg^2 2\theta}. \tag{5.25}$$

The axial ratio of the wave is therefore defined by the ratio of the two components in (5.18)

$$A' = \left|\frac{\cos\theta + A_0 e^{i\phi}\sin\theta}{-\sin\theta + A_0 e^{i\phi}\cos\theta}\right| = \sqrt{\frac{(1+A_0 tg\theta\cos\phi)^2 + (A_0 tg\theta\sin\phi)^2}{(-tg\theta + A_0\cos\phi)^2 + (A_0\sin\phi)^2}}, \tag{5.26}$$

and the axial ratio of the wave is

$$A = max\left(A', \frac{1}{A'}\right). \tag{5.27}$$

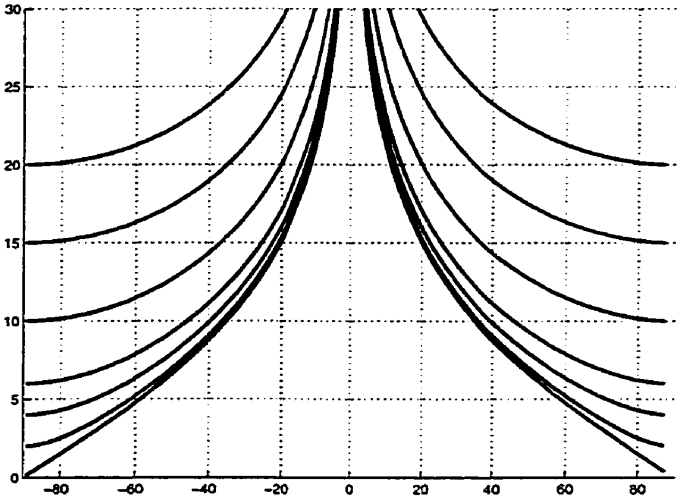

Figure 5.8 Axial ratio in dB vs. phase difference in degrees of the orthogonal fields with the power ratio between the two feeds as the parameter. For curves from bottom to top, A_0 = 0, 2, 4, 6, 10, 15, 20 dB.

Figure (5.8) shows the dependence of the axial ratio in dB on the phase difference ϕ for different values of A_0. From it we can see that the minimum axial ratio is simply A_0 when $\phi = \pm\pi/2$,

where the "+" sign corresponds to a right-hand circular polarization while the "-" sign corresponds to a left-hand circular polarization. When the phase difference between the two orthogonal field components is away from $\phi = \pm\pi/2$, the axial ratio tends to increase. As an extreme case, when $\phi = 0, \pm\pi$, the axial ratio is infinity, corresponding to a linearly-polarized wave. From Figure 5.8 we can also see that the effect of the phase difference away from $\phi = \pm\pi/2$ on the increase of the axial ratio will be more severe for smaller minimum axial ratios. For example, if the phase is $10°$ away from $\phi = \pm\pi/2$, the increase in the axial ratio will be 1.75 dB, 0.50 dB and 0.25 dB for $A_0 = 0, 2, 4$ dB.

5.5 Electromagnetically-coupled circularly-polarized patch antenna design using Ensemble

In this section we will present a step-by-step method for the design of an electronically-coupled patch antenna, based on the previous sections in this chapter. The software we will use is Ensemble Version 4.02 as provided in 1997 by Boulder Microwave Technologies, Inc. The method will be explained in the design of a sample patch antenna. The parameters of the substrate used in the simulation are from those of the GML 1000 laminate from Glasteel Industrial Laminates, which is also used in the design of our beam-forming network: dielectric constant=3.20 ± 0.05, thickness=0.762 mm, copper thickness=0.035 mm, dissipation factor=0.003.

The configuration of the patch antenna is shown in Figure 5.1, which is a two-substrate structure separated by air. There are two square patches in which the lower patch is the active one with feeding circuit while the top patch is passive. The whole design process involves decisions on the sizes of the two patches, the width of the gap between them, and on the design of the whole feeding circuit described in Section 5.3.

In a simulation, the circuit on each layer is automatically divided into small cells by the Grid command of the software, in which an optimal cell size is recommended according to a user-input parameter Maximum Frequency. Theoretically, the calculated results should be independent of the gridding process but in practice different simulation results are obtained for different gridding processes. In our case, the relative bandwidth is 8.5% and this poses a high requirement on

the precision of the calculated center frequency of the antenna. To meet this requirement, a higher Maximum Frequency and smaller recommended cell sizes are chosen to control the simulation errors. Consequently, we will choose the Maximum Frequency to be 3 GHz in Steps 1, 2 and 3 although the highest frequency of interest is 1.610 GHz. For better accuracy, in Step 4 we use 5 GHz as the Maximum Frequency.

In Section 5.3 we assumed that the input impedances of both antennas are purely resistive. The two antennas are actually a single square patch antenna fed orthogonally. Therefore, the first step is to adjust the parameters of a single-feed square patch antenna, the sizes of the two patches and the thickness of the gap between them, for a minimum variation of real part of the input impedance over the bands of interest, i.e. from 1.525 to 1.559 GHz (receiving band) and from 1.627 to 1.661 GHz (transmitting band). After this step the configuration is shown schematically in Figure 5.9. The top patch and the lower patch is 74.40 mm and 52.70 mm in size, spaced by 10 mm. The width of the feed microstrip is 2.08 mm.

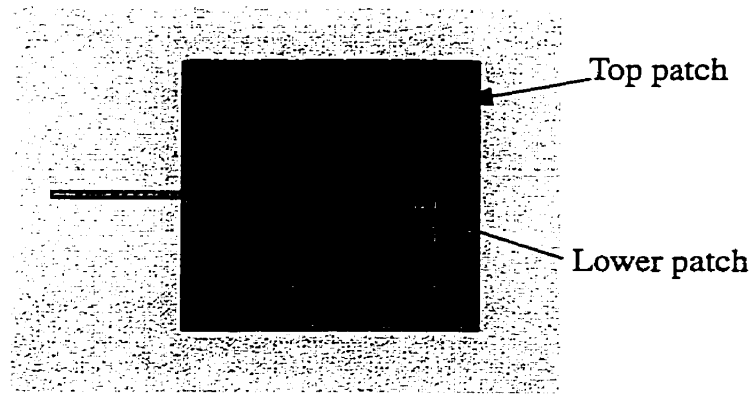

Figure 5.9 A single-feed patch antenna with a minimum variation in the real part of the input impedance over the bands of interest.

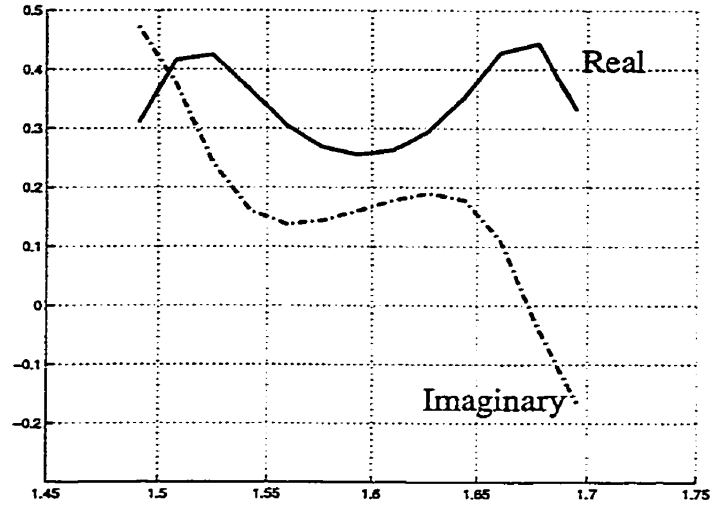

Figure 5.10 The simulated input impedance normalized to 46.69 Ω, *the impedance of the feed microstrip, for the antenna shown in Figure 5.9*

The simulated real and imaginary parts of the input impedance for the antenna is shown in Figure 5.10. The real part is symmetrical with respect to 1.593 GHz, the center frequency of the whole band from 1.525 to 1.661 GHz. We can see two peaks at about 1.542 GHz and 1.644 GHz, the center frequencies of the receiving and transmitting band. In these two bands, the real part of the normalized input impedance varies between 0.295 and 0.428.

Figure 5.10 shows that the imaginary part of the input impedance is high in the receive band and a little lower in the transmit band. In order to obtain an impedance very close to a purely resistive one, the absolute values of the imaginary part of the normalized impedance in the receiving and transmitting bands should be kept as small as possible. From a Smith chart we know that a transmission line a little shorter than a quarter-wavelength can be used for this purpose, resulting in the smallest absolute imaginary part of the impedance in the receiving band and in the transmitting band. This is realized in Step 2 by adding Microstrip 1 of width 2.08 mm and length 26.10 mm to the patch antenna. The antenna is now as shown in Figure 5.11.

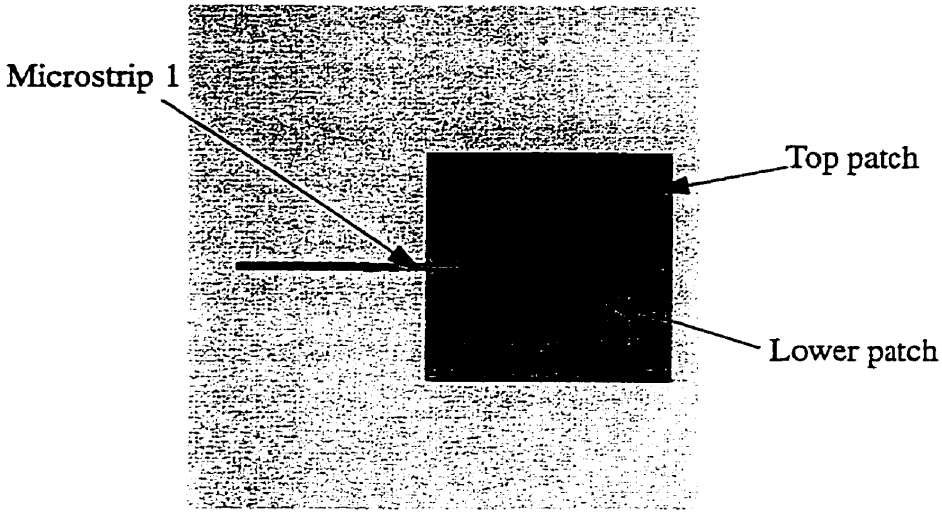

Figure 5.11 A single-feed patch antenna with minimization of the imaginary part of the input impedance over the bands of interest.

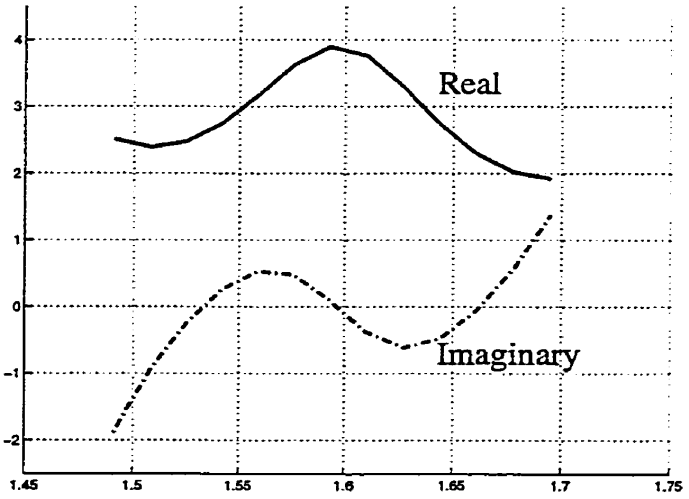

Figure 5.12 The simulated input impedance normalized to 46.69 Ω, *the impedance of the feed microstrip, for the antenna shown in Figure 5.11.*

Figure 5.12 shows that the imaginary part of the input impedance is between -0.6 and 0.5, which is relatively low compared with 2.30, the minimum real part of the normalized impedance. The real part of the impedance varies from 2.30 to 3.20, which is also an improvement from that shown in Figure 5.10. After Step 2, the input impedance has a small imaginary part and a real

part which varies less over the receiving and transmitting band. This impedance is close to the design goal, a constant purely resistive impedance over the whole bands of interest.

In Step 3, a microstrip Microstrip 2, which is the same as Microstrip 1, is connected to the other feed of the antenna. Both Microstrip 1 and Microstrip 2 are bent by 90° for connection. The two microstrips are then connected by a bent half-wavelength microstrip, Microstrip 3. The characteristic impedance of this microstrip is chosen to give a reasonable input impedance which is readily matched to a 50Ω connector. For this purpose, the width and length of Microstrip 3 are 0.50 mm and 61.44 mm, with a characteristic impedance of 98.70Ω. This half-wavelength microstrip can be looked at as two quarter-wavelength transformers, each transformer matching the loads at both ends. According to Section 5.3, the input impedance of the circuit will be close to a purely resistive one wherever we feed the circuit on Microstrip 3. The feed point is finally chosen by monitoring the calculated phases of the horizontal and vertical electrical fields. According to Section 5.4, this phase difference over the receiving band and over the transmitting band is adjusted to be as close to 90° as possible for lowest axial ratio. A quarter-wavelength transformer, Microstrip 4 of width 1.90 mm and length of 29.42 mm is finally used to match the whole structure with a 50Ω connector. The whole circuit after Step 3 is as shown in Figure 5.13.

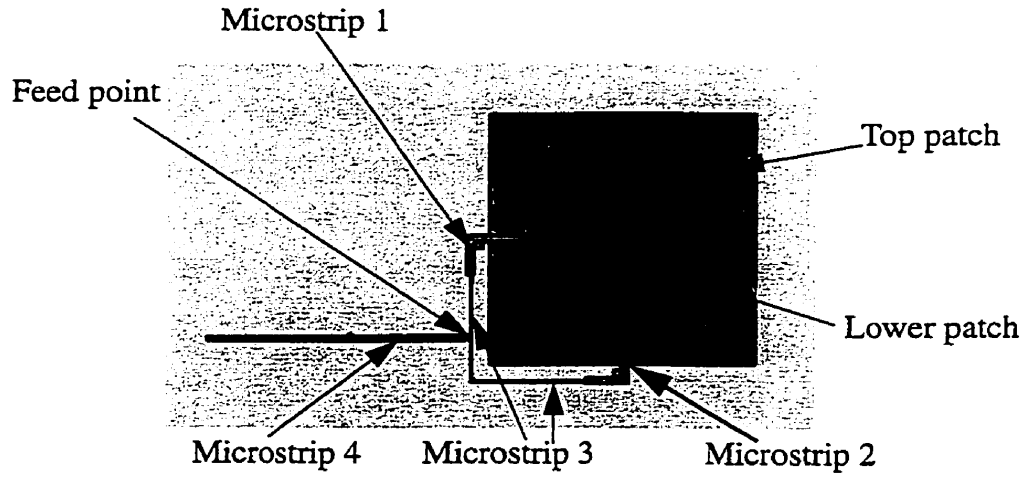

Figure 5.13 A right-hand circular polarization patch antenna.

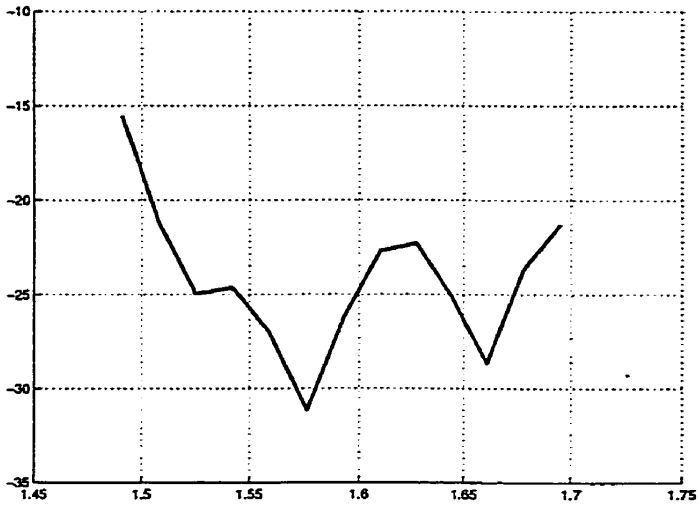

Figure 5.14 Simulated return loss in dB vs. frequency in GHz for the antenna shown in Figure 5.13.

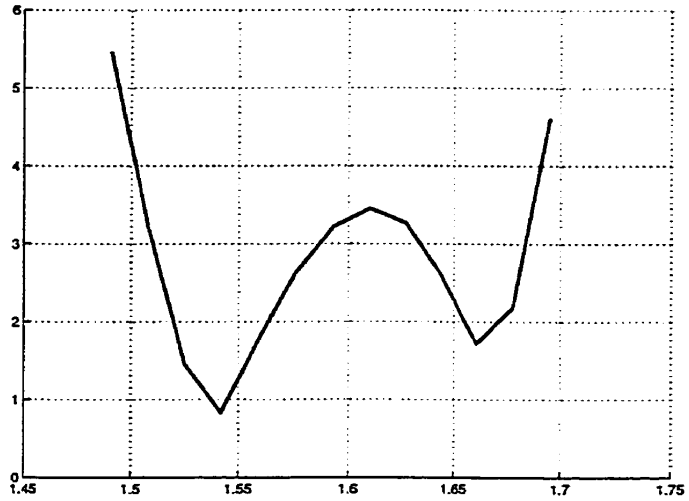

Figure 5.15 Simulated axial ratio in dB vs. frequency in GHz for the antenna shown in Figure 5.13.

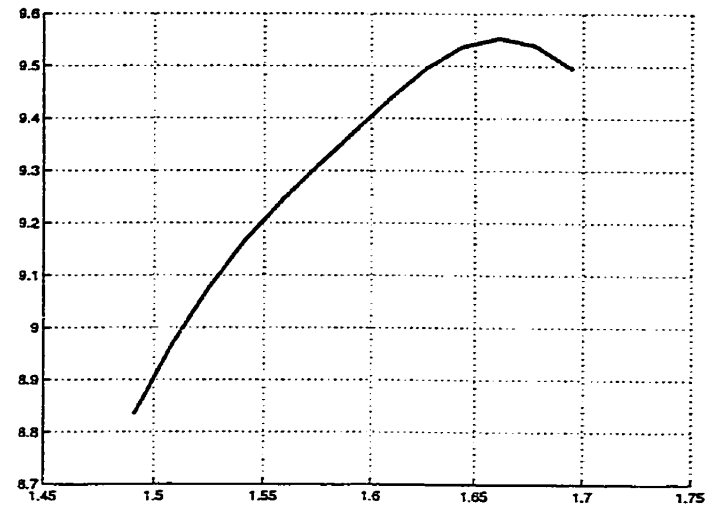

Figure 5.16 Simulated realized gain in dB vs. frequency in GHz for the antenna shown in Figure 5.13.

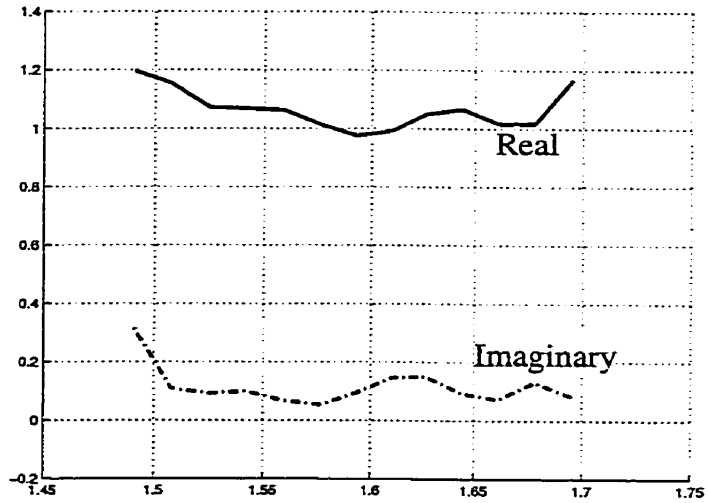

Figure 5.17 Simulated input impedance normalized to 50Ω vs. frequency in GHz for the antenna shown in Figure 5.13.

Figures 5.14 to 5.16 shows the calculated return loss, axial ratio, and gain for the antenna shown in Figure 5.13. The return loss is lower than -22.25 dB, the axial ratio lower than 3.35 dB, and the gain higher than 9.05 dB from 1.525 GHz to 1.661 GHz. Figure 5.17 shows the input impedance normalized to 50Ω. Please note that, in Figure 5.17, the imaginary part of the whole structure is lower than that of each feed at the feed point. The imaginary parts of the two impedances in parallel tend to cancel each other. Consequently, the return loss of a dual-feed patch

antenna can be lower in the whole operation band than that of the corresponding single-feed linearly-polarized square patch antenna.

In Steps 1, 2, and 3, the Maximum Frequency used in the simulations was 3 GHz. This is the result of a trade-off between calculation precision and the time needed for the calculation of the antenna at one frequency. The higher the Maximum Frequency, the better the precision but, unfortunately, the calculation time will also be longer. In the last step, Step 4, the same antenna structure shown in Figure 5.13 is simulated for a Maximum Frequency of 5 GHz. This lead to a calculation speed about 3 times lower than in the case for a Maximum Frequency of 3 GHz.

Figures 5.18 to 5.20 show the calculated return loss, the axial ratio, and the gain obtained from these calculations. The return loss is lower than -23.60 dB, the axial ratio lower than 3.65 dB, and the gain higher than 9.05 dB. Figure 5.21 shows the input impedance normalized to 50Ω, which is comparable to the input impedance shown in Figure 5.17.

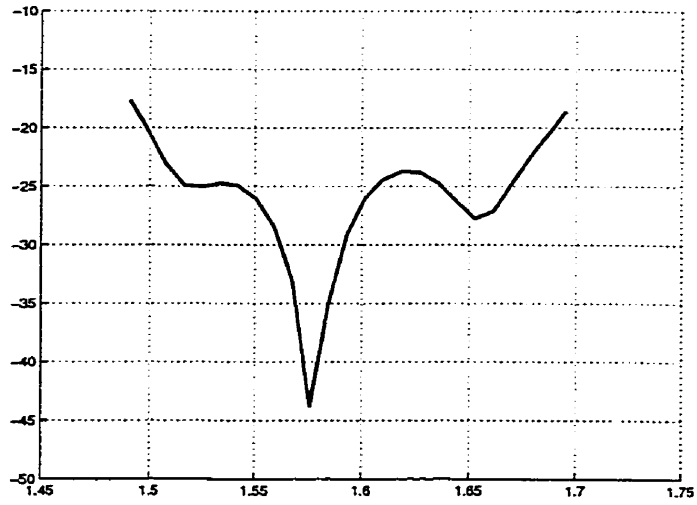

Figure 5.18 Simulated return loss in dB vs. frequency in GHz for the antenna shown in Figure 5.13. $f_m = 5GHz$.

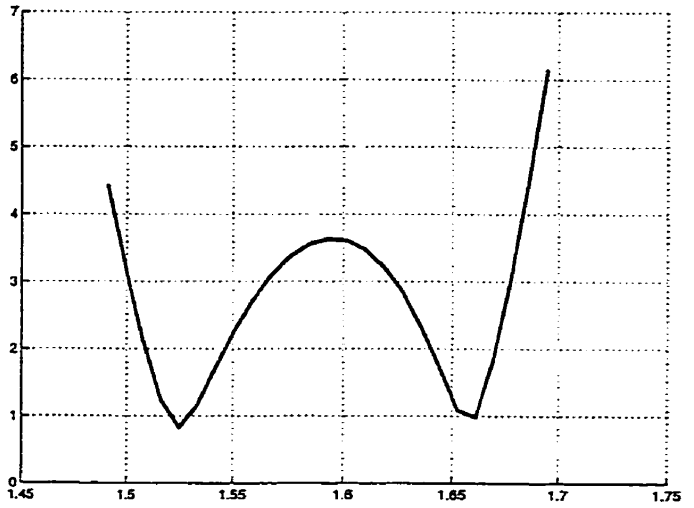

Figure 5.19 Simulated axial ratio in dB vs. frequency in GHz for the antenna shown in Figure 5.13. $f_m = 5GHz$.

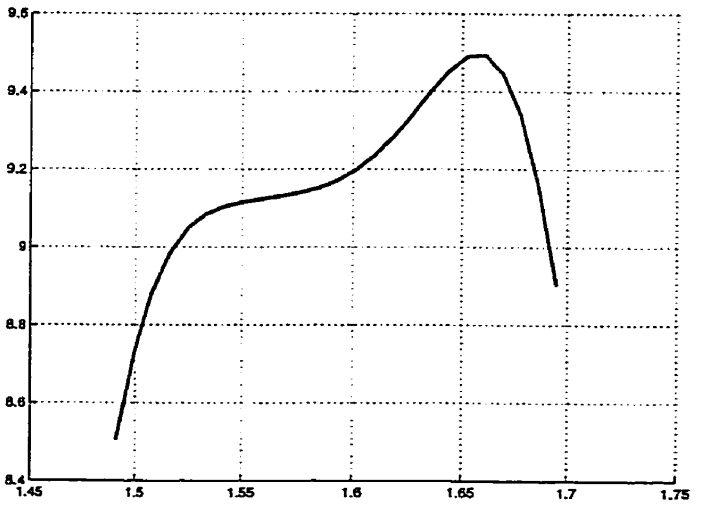

Figure 5.20 Simulated realized gain in dB vs. frequency in GHz for the antenna shown in Figure 5.13. $f_m = 5GHz$.

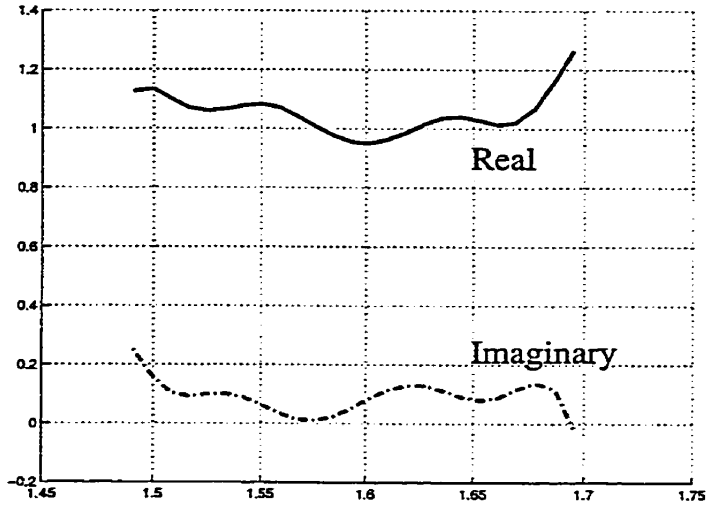

Figure 5.21 Simulated input impedance normalized to 50Ω vs. frequency in GHz for the antenna shown in Figure 5.13. $f_m = 5GHz$.

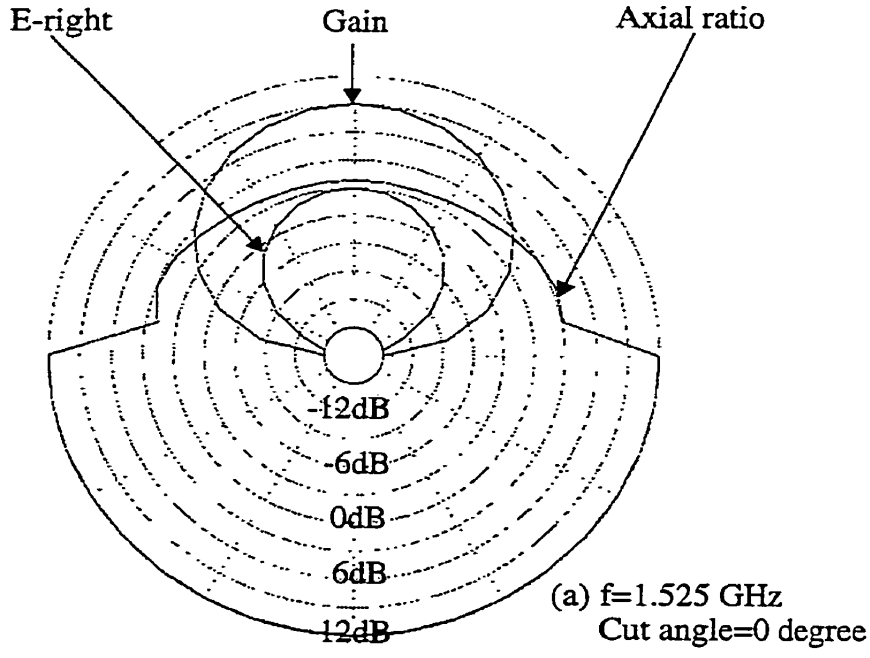

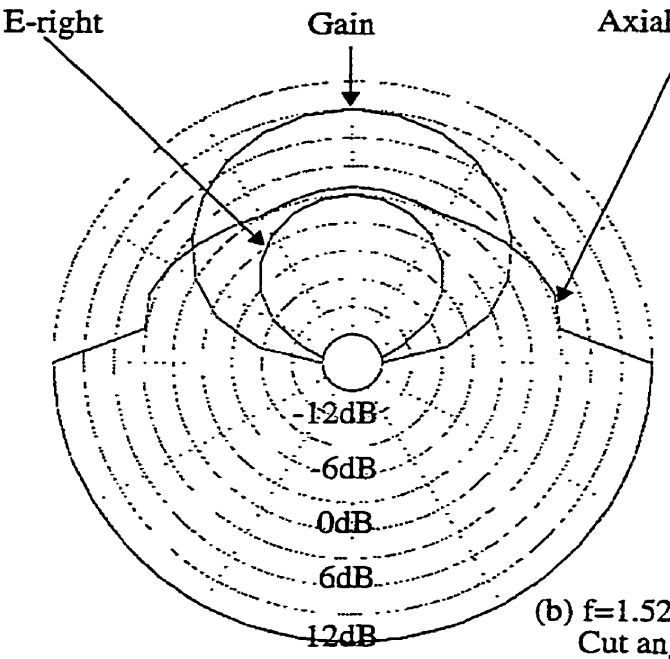

(b) f=1.525 GHz
Cut angle=45 degree

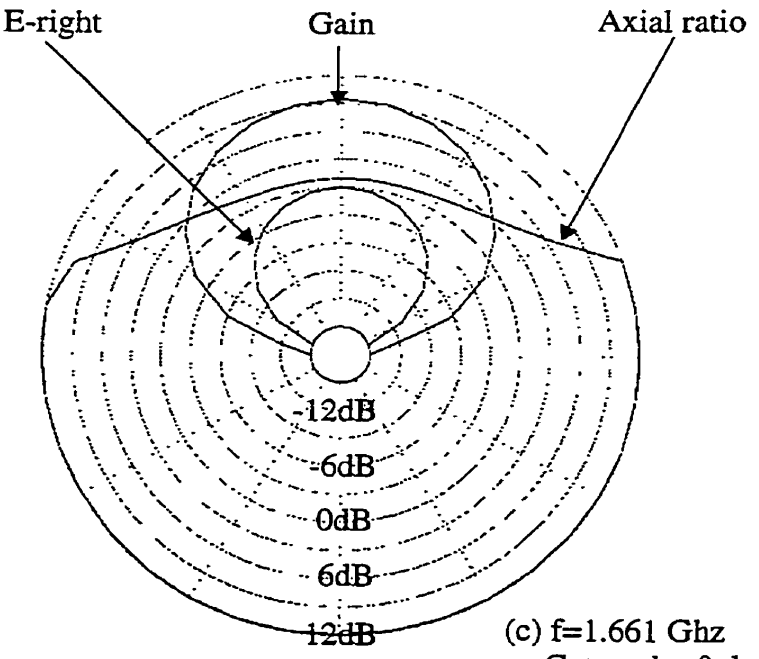

(c) f=1.661 Ghz
Cut angle=0 degree

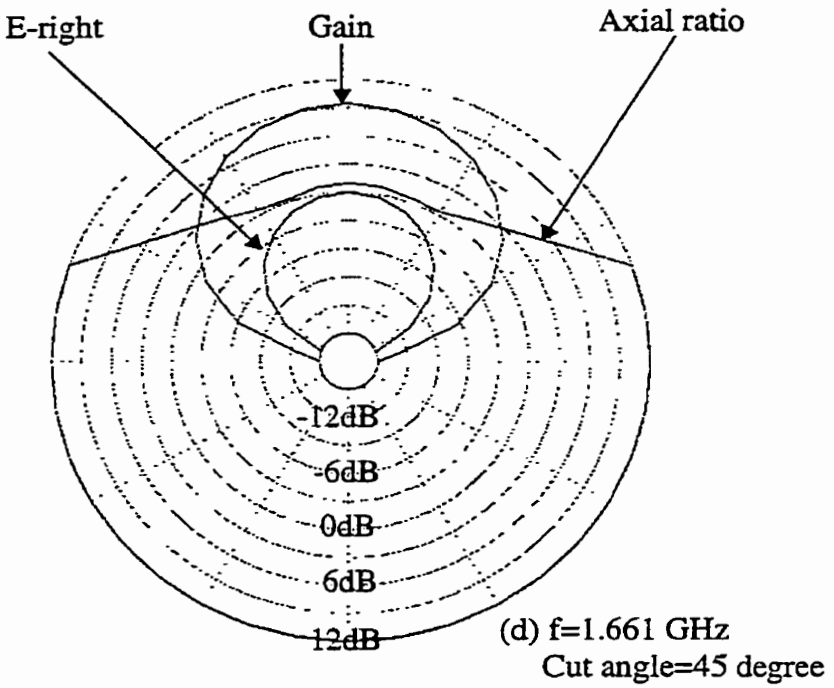

Figure 5.22 Calculated gain, axial ratio, and right-hand circular polarization radiation pattern for the antenna shown in Figure 5.13. $f_m = 5GHz$. *The maximum of the radiation pattern is in the direction to the antenna.*

Figures 5.22 (a) to (d) show the calculated gain, the axial ratio, and the right-hand circular polarization radiation pattern for the antenna shown in Figure 5.13 for $f_m = 5GHz$. A cut angle of $0°$ corresponds to a radiation pattern measured in the plane defined by the direction normal to the patch antenna and the orientation of Microstrip 4 shown in Figure 5.13. When the cut angle is $45°$, the plane in which the radiation pattern was measured was obtained from the above plane by rotating it around the antenna normal direction. The 3-dB beam width is about $67°$ at 1.525 GHz and $64°$ at 1.661 GHz. This can be easily understood because when the frequency increases, the electric length of the same antenna will increase, resulting into a higher gain and a narrower beamwidth. The axial ratio tends to increase by 0.5 dB to 1 dB when the direction moves away from the boresight of the antenna to the boundary of the beam defined by the 3-dB beamwidth. The left-hand radiation pattern is not shown in the figures, but is at least 13 dB lower than that of the right-hand radiation pattern over the 3-dB beamwidth.

5.6 Sample patch antenna realization and the measured results

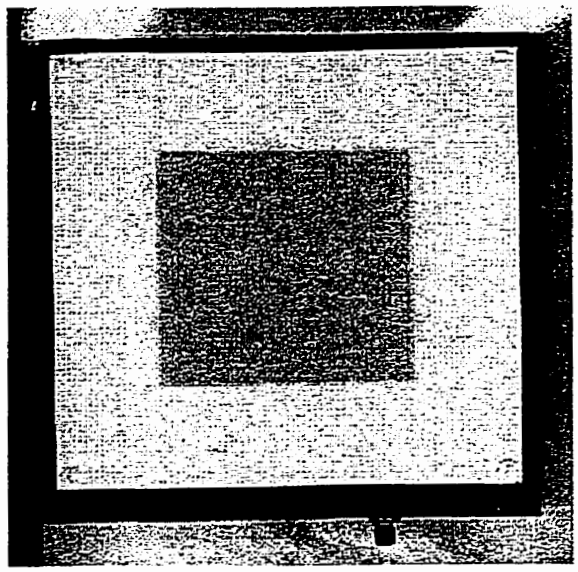

Figure 5.23 Electromagnetically-coupled patch antenna designed under the guidance of the Ensemble simulations.

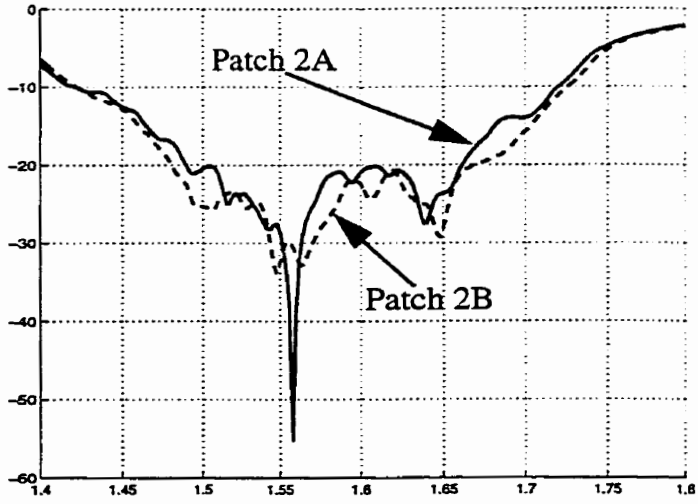

Figure 5.24 Measured return loss in dB vs. frequency in GHz.

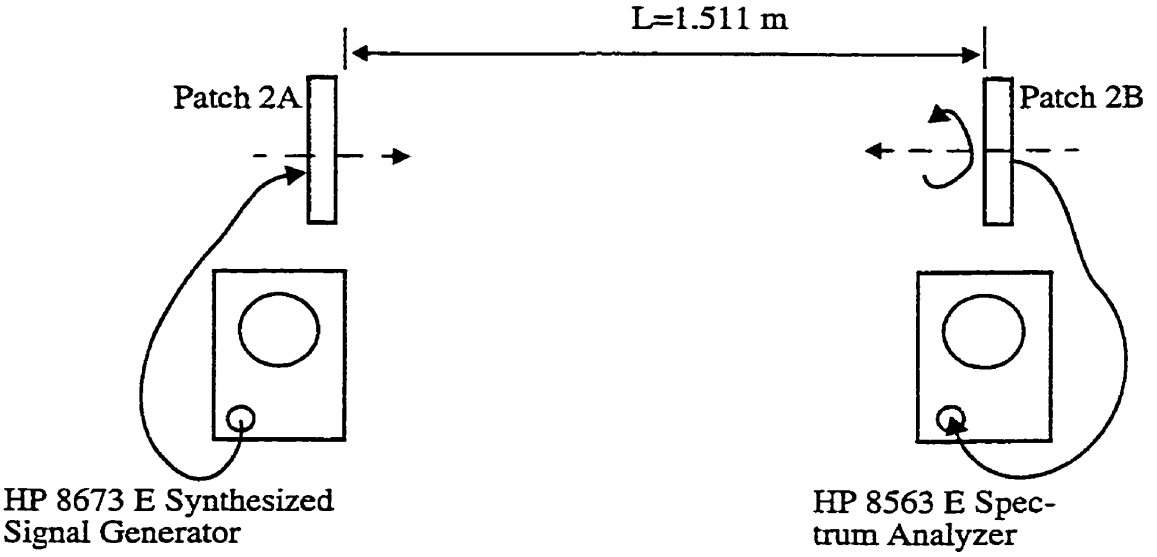

Figure 5.25 Test setup for gain and axial ratio measurement.

Figure 5.23 is a photo of a sample electromagnetically-coupled patch antenna designed in the last section. The width of the gap between the two layers is set to be10 mm by 4 plastic rods located between the top patch and the lower patch. Figure 5.24 shows the measured return losses vs. frequency for two such antennas, Patch 2A and Patch 2B. As we can see from the figure, except for some minor differences, their return loss curves are almost the same in the whole band from 1.525 GHz to 1.661 GHz. A maximum return loss of -19.52 dB was measured at 1.661 GHz.

The gain and axial ratio in the boresight direction of the antennas are measured by placing the two antennas opposite to each other, as shown in Figure 5.25. The measured gain and axial ratio are averaged ones because the two antennas are assumed identical. In the measurements, Patch 2A is fixed upright to a pole while Patch 2B is rotating around its axis. The microwave signal from a HP 8673 E Synthesized Signal Generator is fed through a coaxial line to Patch 2A and the power received by Patch 2B is guided through another coaxial line to a HP 8563 E Spectrum Analyzer. At each frequency, the maximum received power P_r at the spectrum analyzer and its variation Δp are read while Patch 2B is rotating. The received reference power $P_{r0}(dBm)$ is

measured by removing the two antennas and connecting the two coaxial cables together. The measured data are shown Table 5.1.

Table 5.1 Measured and calculated data for gain and axial ratio measurements.

f(GHz)	1.491	1.508	1.525	1.542	1.559	1.576	1.593
$-P_{r0}(dBm)$	33.67	33.83	34.00	34.17	34.00	34.00	34.00
$\Delta p(dB)$	0.48	0.30	0.33	0.70	0.85	1.05	1.00
$-P_r(dBm)$	56.53	56.70	57.50	56.08	56.80	55.98	56.37
G(dB)	8.32	8.36	8.10	8.94	8.54	9.00	8.85
AR(dB)	2.91	2.30	2.41	3.54	3.91	4.36	4.25

Table 5.1 (continued).

f(GHz)	1.610	1.627	1.644	1.661	1.678	1.695
$-P_{r0}(dB)$	34.17	34.00	34.17	34.33	34.17	34.17
$\Delta p(dB))$	1.08	0.52	0.75	0.93	2.04	3.80
$-P_r(dB)$	55.62	56.45	57.52	58.10	58.83	58.53
G(dB)	9.36	8.90	8.50	8.33	7.93	8.13
AR(dB)	4.41	3.03	3.66	4.09	6.19	8.72

The gains and axial ratios can be calculated from the measured data. The received power is

$$P_r = \frac{P_t}{(4\pi L)^2} G A_{eff} A_c \tag{5.28}$$

where P_t is the power output of the signal generator, L is the distance between the two antennas, A_{eff} the effective area of the antenna and A_c the total loss of the two coaxial cables.The gain can be calculated from A_{eff}, the effective area of the antenna,

$$G = 4\pi A_{eff}/\lambda^2 \tag{5.29}$$

where λ is the wavelength in free space.

When there is no antennas and the two cables are directly connected, we have

$$P_{r0} = P_t A_c . \tag{5.30}$$

From (5.28), (5.29) and (5.30), using L=1.511 m, the gain can be calculated

$$G(dB) = \frac{P_r(dBm) - P_{r0}(dBm)}{2} + 18.01 + 10\log f(GHz) \tag{5.31}$$

where f is the frequency at which the gain is measured.

In (5.7), choosing the "+" sign because both Patch 2A and Patch 2B are of right-hand polarization and assuming $A_E = A_A = A$, the ratio of the mismatch factors for $\theta = 0°$ and $\theta = 90°$ gives Δp:

$$\Delta p = \frac{(1 + A^2)^2}{4A^2}, \tag{5.32}$$

and the axial ratio can be calculated as

$$AR(dB) = 10\log\left(\frac{2}{\Delta p} - 1 + \frac{2}{\Delta p}\sqrt{1 - \Delta p}\right). \tag{5.33}$$

The calculated gain and axial ratio are also shown in Table 5.1, according to the measured data for each frequency.

As shown in Table 5.1, the averaged gains are typically higher than 8.0 dB. The axial ratio is low at lower frequencies and increases with frequency. In the band from 1.525 GHz to 1.661 GHz, the averaged gain is between 8.10 and 9.36 dB and the axial ratio is between 2.41 dB and 4.41 dB. The measured gains are typically lower than the simulated gain by about 1 dB. We attribute these lower gains to the loss of the feeding circuit and of the patch antennas. Ensemble does not appropriately account for copper and dielectric losses in the calculation. The axial ratio is about 1 dB higher than calculated. We believe that this is mainly because of error in the width of the gap between the two patches in each sample antenna. This gap was assumed to be 10 mm in the simulations and an error of $\pm 0.5mm$ was measured in both sample antennas because of the deformation of the substrate which is relatively thin. From Figures 5.4 and 5.5, the increase

of the axial ratio from 3 dB to 4 dB will decrease the polarization mismatch factor by at most 0.17 dB.

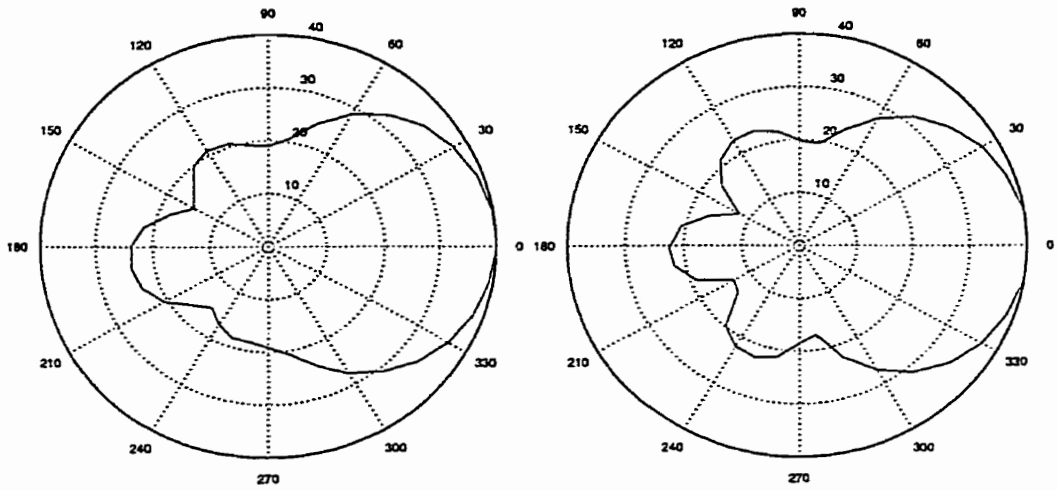

Figure 5.26 Typical measured right-hand circularly-polarized field radiation patterns of Patch 2A.

The right-hand circularly polarized field radiation pattern of Patch 2A was measured by using Patch 2B as the test antenna. Typical radiation patterns are shown in Figure 5.26. From the figures we can read that the typical 3-dB beamwidth is about 60° . The measured beam is a little narrower than the simulated ones shown in Figure 5.22 because here the polarization mismatch factor is included in the radiation patterns.

5.7 The measured results from a patch antenna with improved axial ratio

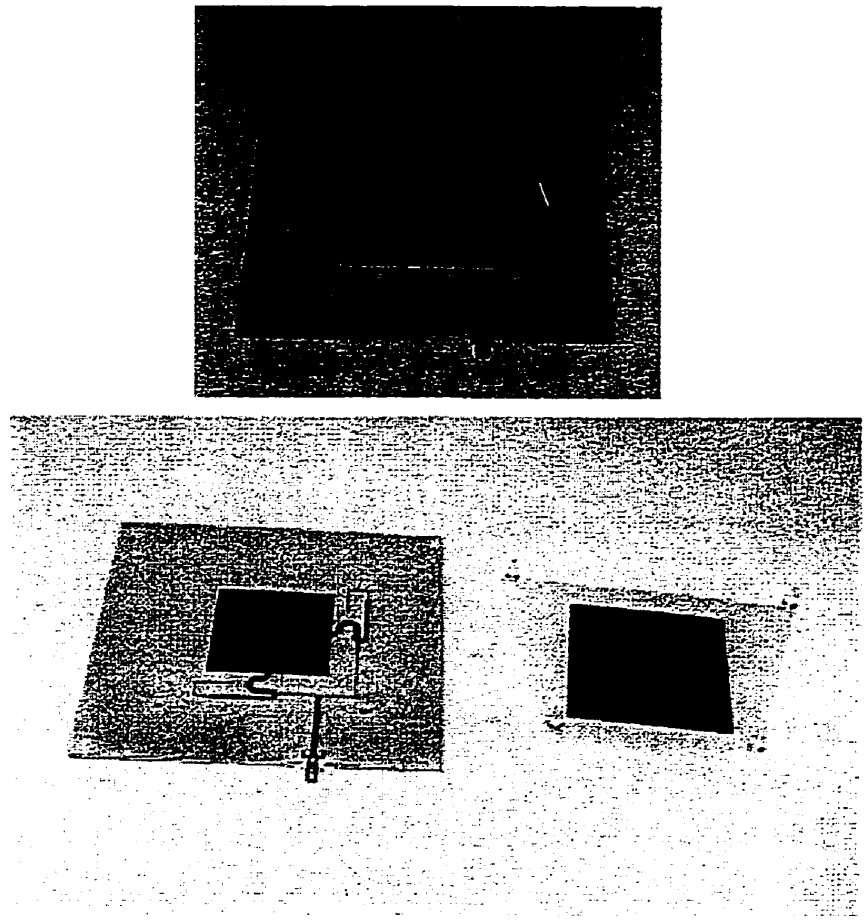

Figure 5.27 An electromagnetically-coupled patch antenna with improved axial ratio.

The axial ratio of Patch 2A and 2B described in the last section is 2.41dB to 4.41 dB in the band from 1.525 GHz to 1.661 GHz. We also designed a patch antenna with improved axial ratio. In order to do this, after Step 2 in the last section, a compound half-wavelength open stub as described in Section 2.5 is added in shunt to the circuit, in order to tune off the imaginary part of the impedance shown in Figure 5.12. As a result, the impedance of the single-feed antenna has a smaller imaginary part. The axial ratio is thus improved. Figure 5.27 shows such an antenna

in its assembled state and decomposed state. Please note the compound half-wavelength open stubs used in each feed.

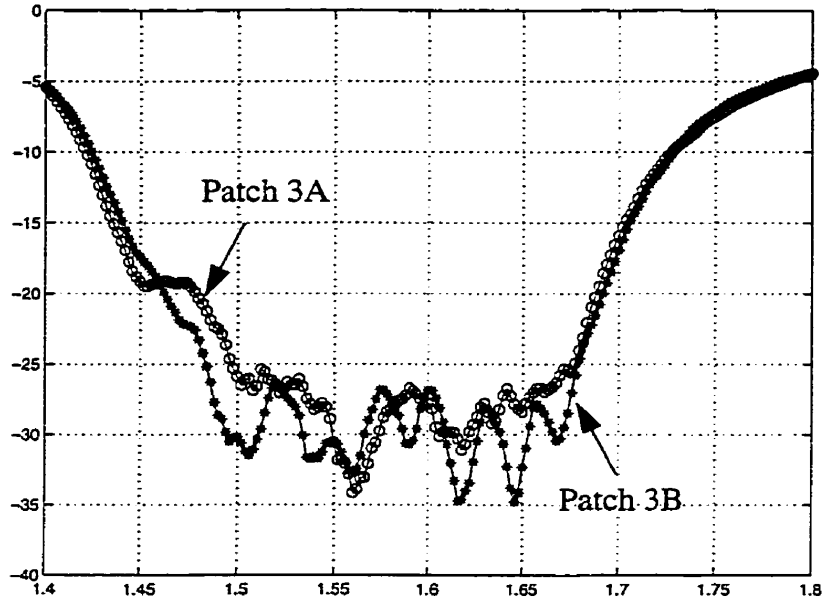

Figure 5.28 Measured return losses in dB vs. frequency in GHz for Patch 3A and Patch 3B.

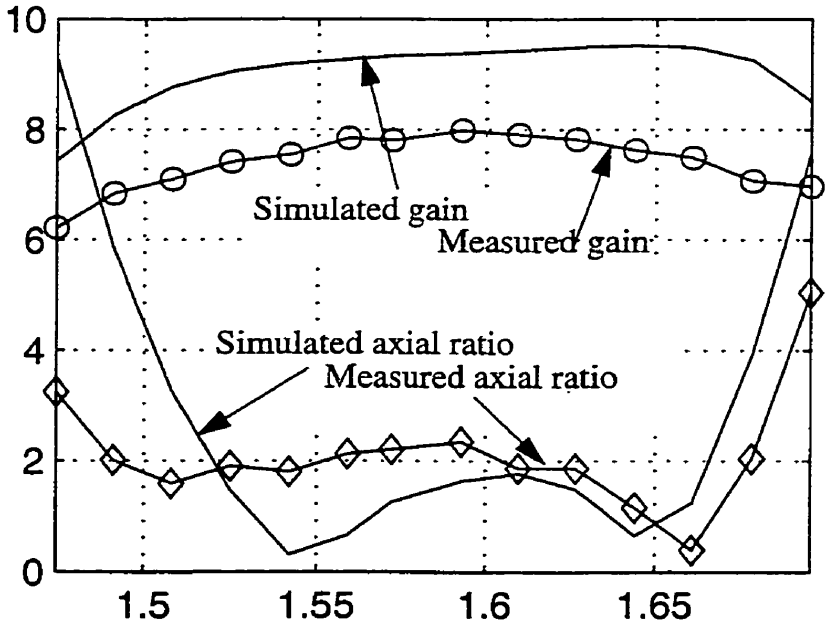

Figure 5.29 The simulated and measured gain and axial ratio in dB vs. frequency in GHz for Patch 3A.

The return losses of two such sample antennas, Patch 3A and Patch 3B, are shown in Figure 5.28. As can be expected, adding the tuning stubs also leads to improved return losses. For both sample antennas, reflection coefficient is lower than -26.01 db from 1.525 GHz to 1.661 GHz.

The averaged gains and axial ratios of Patch 3A and Patch 3B were measured in their boresight direction, using the same method described in the last section. The measured gains and axial ratios of Patch 3A are shown in Figure 5.29 The measurements were carried out at a distance of 2.10 m between the two antennas. Also shown are the simulated gains and axial ratios. It can be seen that, in the band from 1.525 GHz to 1.661 GHz, the simulated axial ratio was lower than 2.35 dB in the boresight direction, which happens at 1.525 GHz. The measured axial ratios were lower than 2.4 dB and the bandwidth was improved. Although the axial ratios were improved considerably from Patch 2A and 2B, the measured gains were lower by 1 to 2 dB than the simulated ones in the band. At the center frequency, the measured gain was about 8.00 dB and the lowest gain in the band was 7.42 dB which appeared at 1.525 GHz. We found in the test that the loss in the added tuning stubs was the main reason for such lower gains.

5.8 Discussion and conclusion

In this chapter we presented a method for economical electronically-coupled antenna design and measured results from sample antennas. First we derived the polarization mismatch factor as a function of the axial ratio of an incident electromagnetic wave and that of a receiving antenna. This provided us a measure to evaluate the effect of the axial ratio of a receiving antenna on its received signal level. Second, we proposed a simple circuit which is capable of delivering equal phase-controlled power into two resistive loads, which is constituted in our case by the dual-feed antenna under design, fed orthogonally. Third, assuming the power fed into each port to the dual-feed antenna are specified, we derived formulae to show the effect of the difference of the phases of the orthogonal electrical fields radiated from the antenna on the axial ratio. A step-by-step method for the design of electromagnetically-coupled patch antenna design was then presented. The method works with the input impedance, phase and amplitude of the radiation field, gain and axial ratio obtained from Ensemble simulations. This method was explained in the design of a sample antenna.

Following the simulations, two sample antennas, Patch 2A and 2B were fabricated and measured. Averaged gains from 8.10 dB to 9.36 dB and axial ratios from 2.41 dB to 4.41 dB were measured in the boresight direction of the antennas for frequencies from 1.525 GHz to 1.661 GHz. The return losses were lower than -19.52 dB.

In order to improve the axial ratio, another antenna using two compound half-wavelength open stubs in the power dividing circuit was also designed. The axial ratio was lower than 2.4 dB, return loss lower than -26.01 dB, and the gain was between 7.42 dB and 8.00 dB. Although we achieved some improvement in axial ratio, the gain is considerably lower because of the added tuning circuit. From Figures 5.4 and 5.5, an improvement of axial ratio from 4.4 dB to 2.4 dB will lead to at most a 0.38 dB increase in the polarization mismatch factor. Consequently, Patch 3A and 3B will receive a 0.3dB to 1.0 dB lower power than Patch 2A and 2B. In our application, Patch 2A and 2B are preferred.

CHAPTER 6

An electronically-scanned antenna array with quasi-hemispheric coverage

6.1 Introduction

A typical mechanically-scanned antenna available from the market covers elevation angles from 15° to 60°. For such an antenna and a geo-stationary satellite through which a communication is to be made, there is an area on the surface of the earth from which the antenna cannot "see" the satellite. Refer to Figure 6.1 and suppose that the geo-stationary satellite is above a certain point P on the Equator of the Earth: the elevation angle of the satellite to a terminal, which is at point T with the same longitude as point P, is θ_E. The latitude is related to the elevation angle by

$$\phi = \cos^{-1}\left(\frac{R}{H+R}\cos\theta_H\right) - \theta_E, \tag{6.1}$$

where R=6370 km is the radius of the earth and H=35700 km is the height of the geo-stationary satellite above the surface of the Earth. Using the Inmarsat-2F2 satellite which has a longitude

of $98°W$, as an example, from (6.1) an elevation angle of $60°$ would correspond to a latitude of $26.2°$. The arc distance from Point P to the terminal at point T on the surface of the earth can be calculated to be about 2913 km. In a real three-dimensional case this means that, for the area with a radius of 2913 km around point P ($Longitude = 98°W$ and $Latitude = 0°$), communication will be difficult or impossible using such a mechanically scanned antenna.

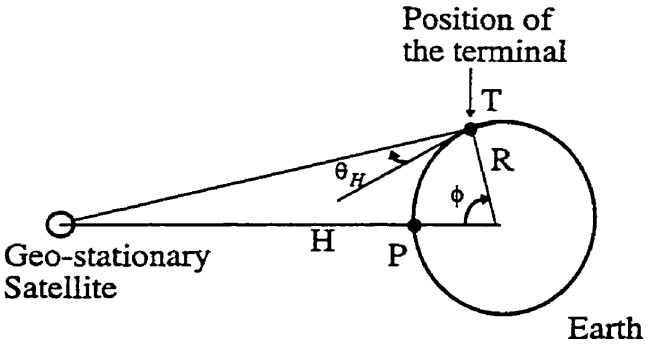

Figure 6.1 The elevation angle of a geo-stationary satellite to a terminal.

In order to solve this problem, a global electronically-scanned antenna array covering elevation angles from $20°$ to $90°$ is proposed and implemented. Figure 6.2 shows a functional block diagram of the array. It is composed of a No.9 channel and of a sub-array with 8 patch antennas. The No.9 channel or the sub-array are activated by a pre-switch. When the sub-array is activated and the No.9 channel deactivated, the 3/8-channel beam controller acts as described previously in Chapter 4 and 24 beams can be formed horizontally. The elevation coverage of the sub-array is then from $20°$ to $60°$. To cover the higher elevation angles from $60°$ to $90°$, the No.9 channel should be activated, and the beam controller de-activated.

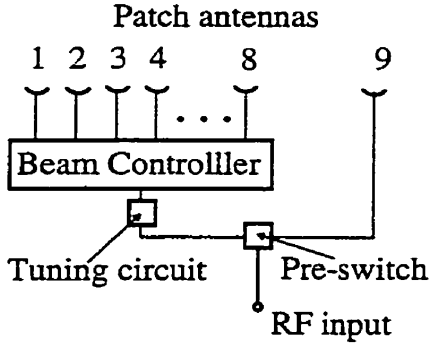

Figure 6.2 Functional block diagram of the global electronically-scanned array.

In this chapter the configuration of this global electronically-scanned antenna array prototype with quasi-hemispherical coverage will be described. In Section 6.2, the configuration and performance of the pre-switch sub-circuit, which included the pre-switch in series with a tuning circuit, will be presented. In Section 6.3, the detailed configuration of the array will be given. In Section 6.4, we will provide measured results from the prototype. In Section 6.5, several aspects in which the performance of the antenna array can be improved, will be addressed. In the last section are some conclusions.

6.2 The pre-switch sub-circuit

The choice of the top antenna or of the sub-array is made by a pre-switch, which is shown in Figure 6.3. It is composed of a 2-channel switch and of a tuning circuit whose design has already been discussed in Section 4.2.

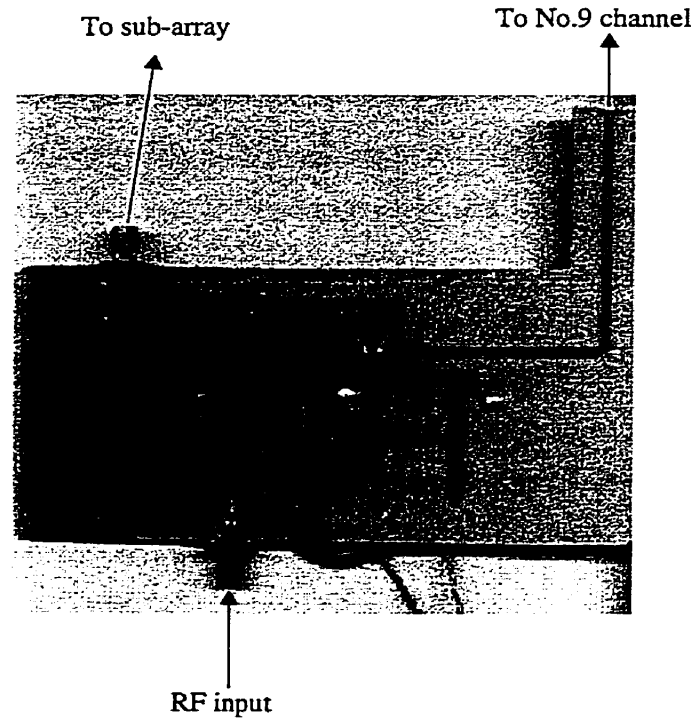

Figure 6.3 A power pre-switch and a tuning circuit integrated together.

The power input from the lower SMA connector is divided into two channels, in each of which a HSMP 4890 diode is used to activate or deactivate the channel. The left channel leads to the

sub-array through another SMA connector while the right channel leads to the No.9 channel. In the left channel, between the upper SMA connector and the PIN diodes, are two compound half-wavelength open stubs in parallel, which act as a tuning circuit. In operation, the two diodes are always biased in opposite states, allowing activation of only one channel.

Such a circuit was also designed under the guidance of simulations. It was then connected to a beam controller described in Chapter 4. The whole circuit was then measured for frequencies from 1.525 GHz to 1.661 GHz. When the No.9 channel was deactivated, the whole circuit acted like the beam controller together with the tuning circuit whose performance can be found in Section 4.3, except that the maximum overall insertion loss was 2.31 dB instead of 2.08 dB. This 0.23 dB extra loss was caused by the No.9 channel. Although it has been deactivated, it still dissipated and leaked some power. The power leaked into the No.9 channel was found to be at least 27.30 dB lower than the input power and the return loss lower than -12.36 dB from 1.525 GHz to 1.661 GHz. When the No.9 channel was activated, the insertion loss was lower than 0.67 dB, the return loss lower than -16.69 dB and the power leaks to any channel of the beam controller was at least 32.74 dB lower than the input power.

6.3 The configuration of the array

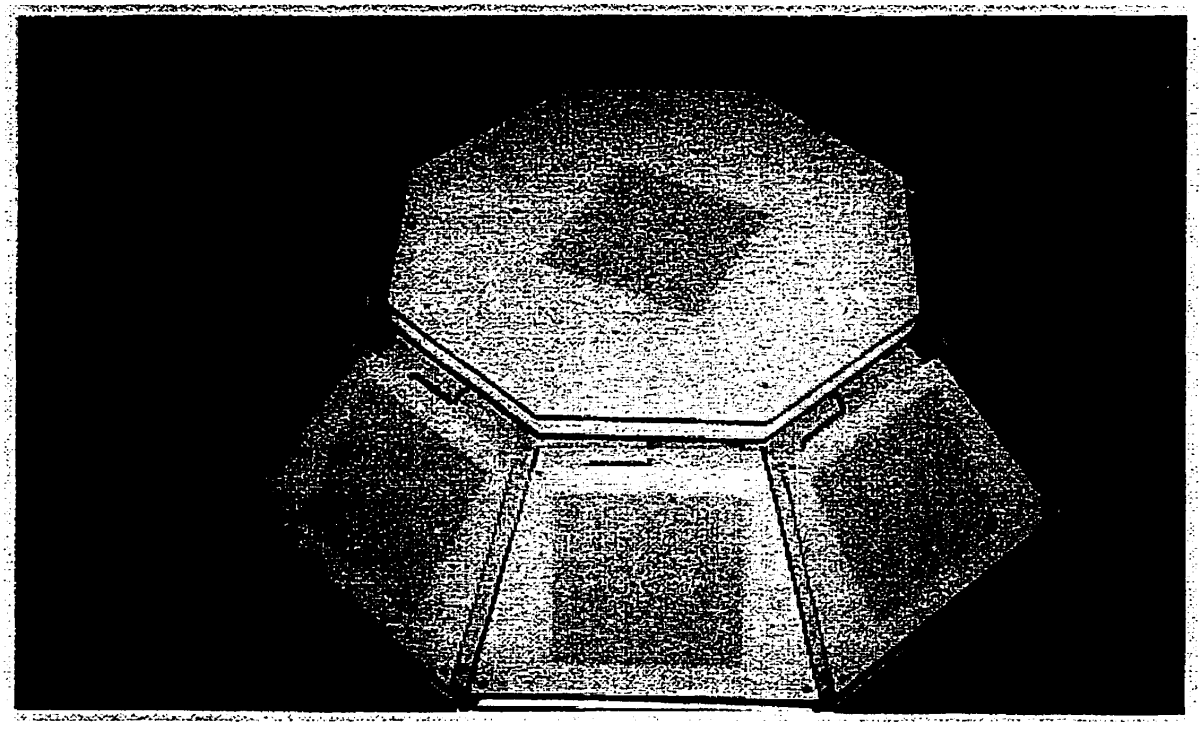

Figure 6.4 A global electronically-scanned antenna array prototype with quasi-hemispherical coverage.

The global array, as shown in Figure 6.4, is realized by adding a top patch antenna on the top of the sub-array. The overall configuration is a truncated octagon cone with an inclination angle of 35°, which is required for the antenna to have an elevation angle coverage from 20° to 60°. The beam controller is an octagon-shaped planar circuit with a side length of 89.5 mm. Each facet of the cone is a trapezoid with an upper side of 89.5 mm and a lower side of 143 mm and a height of 115 mm. The patch antenna used in the array was the same as Patch 3A described Section 5.6, which has a gain from 7.42 dB to 8.0 dB and an axial ratio lower than 2.35 dB in the operation bands. The top substrate and lower substrate of each patch antenna were trimmed to an appropriate trapezoidal shape with an upper side of 92 mm, a lower side of 140 mm and a height of 100 mm, to fit the facet of the cone. The boundary of the top substrate is 5 mm from the upper boundary of the facet. The top substrate of each patch antenna is supported by four

plastic pins which guarantee the upper substrate and the lower substrate in the patch antenna be aligned and which set a 10 mm gap between the top patch and the lower patch.

Each patch antenna in the sub-array was connected to one channel of the beam controller. A 125° microstrip transition, as shown in Figure 6.5, was used to transfer power from one channel of the beam controller to the feed of a patch antenna. In the operation band from 1.525 GHz to 1.661 GHz, the return loss of such a bend was measured to be lower than -30 dB.

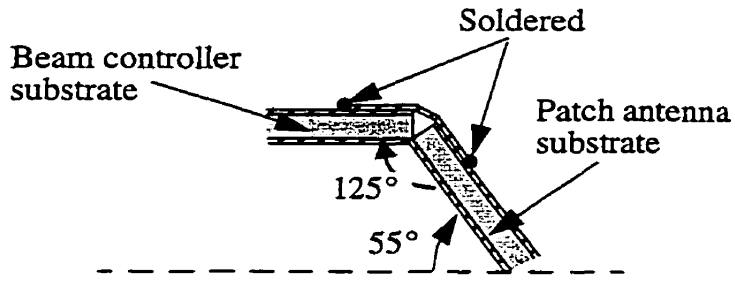

Figure 6.5 Simple microstrip transition to connect a beam controller channel to a patch antenna.

The hollow space underneath the antenna array provides enough place for the pre-switch sub-circuit and for the electronic circuits for controlling the beam. The microstrip on the right side of the pre-switch sub-circuit shown in Figure 6.3 penetrates through the beam controller plane and connects to the top patch through a microstrip transition similar to that shown in Figure 6.5, except that the angle is 90° instead of 125°. The reflection of such a bend was measured to be lower than -26 dB in the operation band. The antenna is finally fed by a coaxial cable at the input port of the pre-switch sub-circuit. The overall dimensions of the antenna are: top diameter: 23.4 cm, base diameter 37.6 cm and the height 12.0 cm.

6.4 Measured results from the array prototype

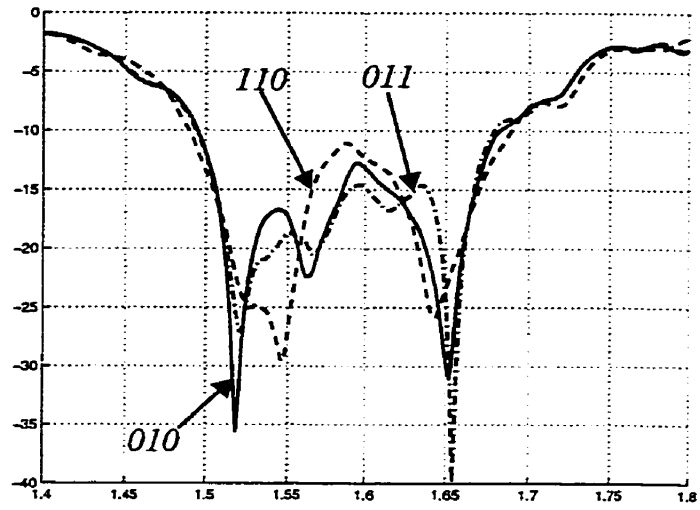

Figure 6.6 The measured return loss in dB vs. frequency in GHz for the global antenna array prototype with its top antenna deactivated.

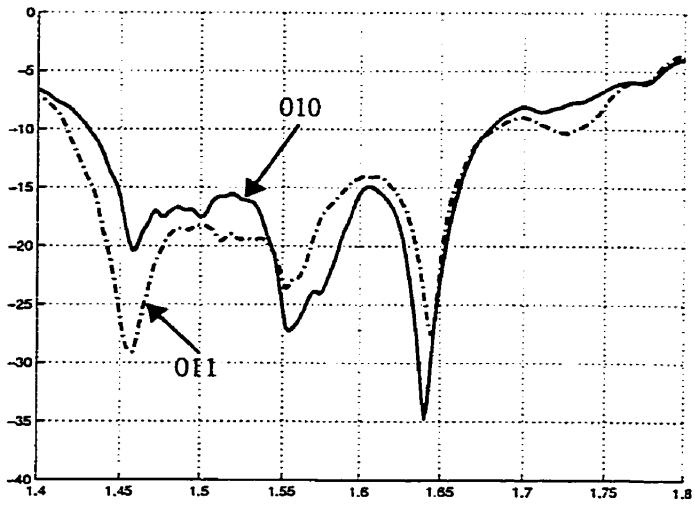

Figure 6.7 The measured return loss in dB vs. frequency in GHz for the global antenna array prototype with its top antenna activated.

The return losses for different beams were measured by properly biasing the PIN diodes and typical curves are shown in Figures 6.6 and 6.7. Return losses lower than -14.5 dB were measured in the receiving band (1.525 GHz to 1.559 GHz) and in the transmitting band (from 1.627 GHz to 1.661 GHz). The highest return loss was -11.1 dB for frequencies from 1.525 GHz to 1.661 GHz.

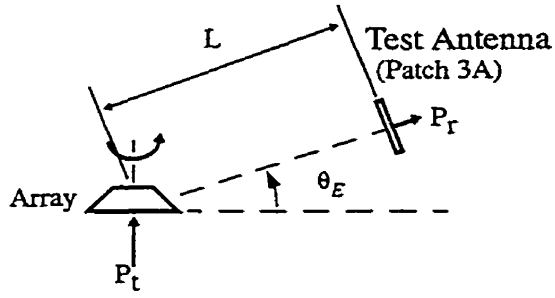

Figure 6.8 Test setup for array gain measurements.

The test setup for array gain measurements is shown in Figure 6.8. Following the same procedures as in Chapter 5, the gain of the array G_A, the gain of the test antenna G_T, the distance between the two antennas L, the frequency f and the transmission coefficient from the array to the test antenna S_{21} are linked by the relation:

$$G_A(dB) = S_{21}(dB) + 32.44 + 20\log f(GHz) + 20\log L(m) - G_T(dB). \qquad (6.2)$$

Rotating the array around its axis and measuring the transmission coefficient S_{21}, its gain vs. the horizontal angle θ_H could be measured.

It should be mentioned that in obtaining (6.2) the polarization mismatch factor has been assumed to be 1. This assumption is usually not true and consequently the array gain obtained from (6.2) is a little lower than its real value, by the polarization mismatch factor between the array and the test antenna.

Figure 6.9 is a schematic top view of the antenna array, used to show the beam number denomination and the definition of the zero degree for the horizontal angle. Please note that as illustrated by the hypothetical radiation patterns, the 110 beams are represented by dashed lines, the 010 beams by solid lines and the 011 beams by dash-dotted lines. A 010 beam and the two beams at its both sides are generated by the patch antenna, which faces the same horizontal direction as that of the 010 beam, and the two patch antennas at its both sides. For example, beams 1, 2, and 3 are formed by activating channels 8, 1, 2 in the sub-array with different combinations of the phase states in each of the three channels.

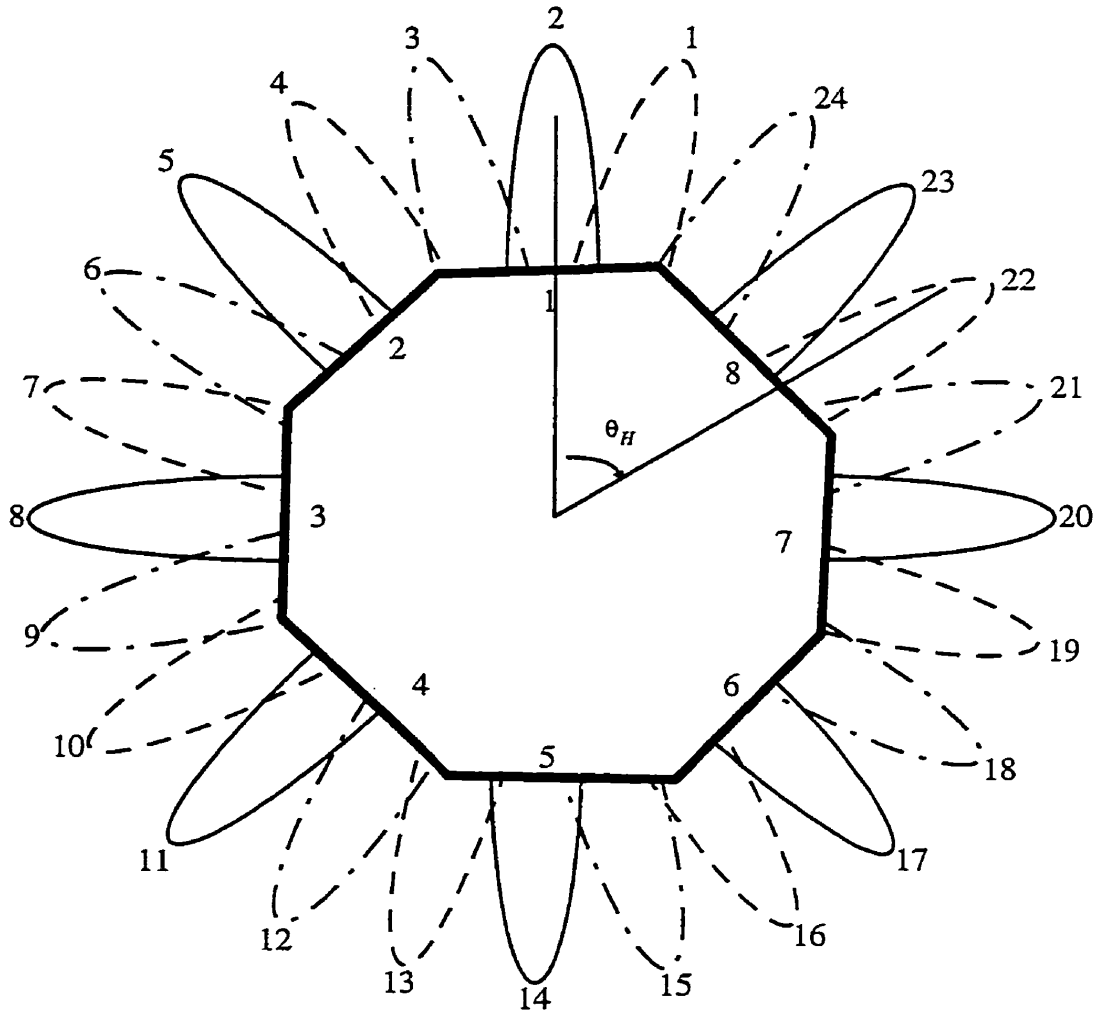

Figure 6.9 The definition of the number for each beam and the horizontal angles.

The gain of the antenna array was measured vs. the horizontal angles at two frequencies, 1.525 GHz and 1.661 GHZ, and at three elevation angles, $\theta_E = 20°$, $\theta_E = 45°$, and $\theta_E = 60°$, and the results are shown in Figure 6.10 (a) to (f).

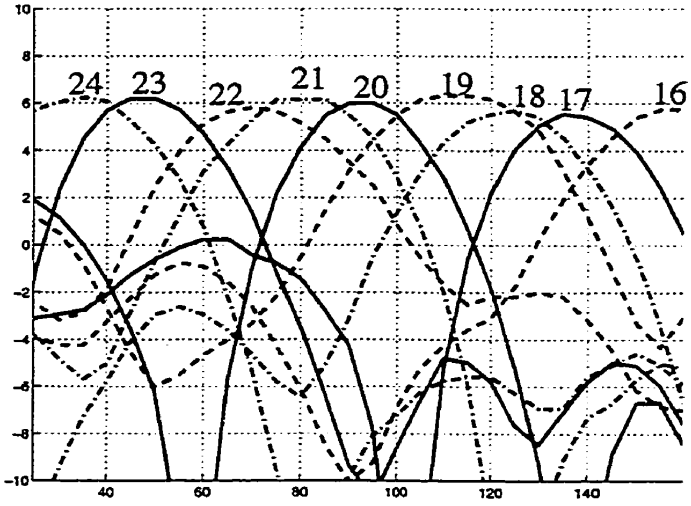

(a): Beams No.16 to 24 of the sub-array for f=1.525 GHz and $\theta_E = 20°$.

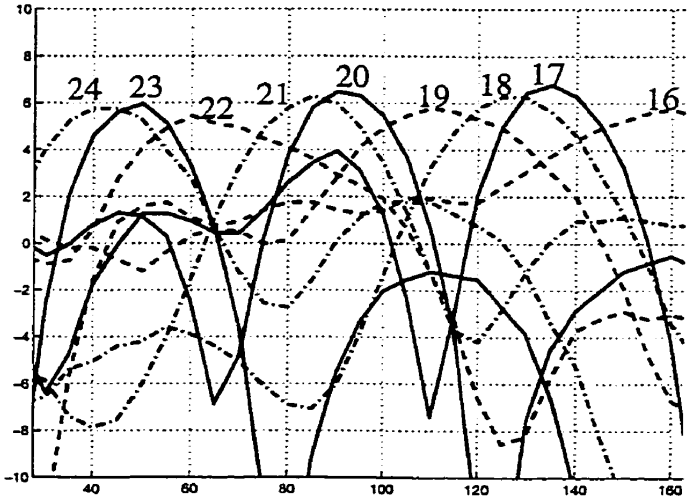

(b): Beams No.16 to 24 of the sub-array for f=1.661 GHz and $\theta_E = 20°$.

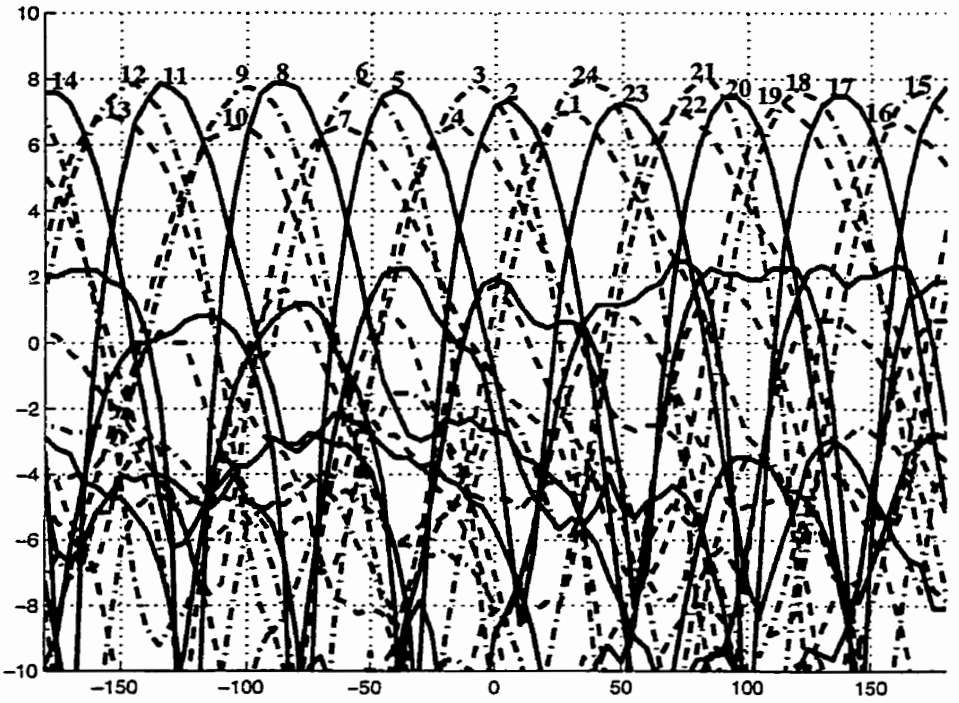

(c): All beams of the sub-array for f=1.525GHz and $\theta_E = 45°$.

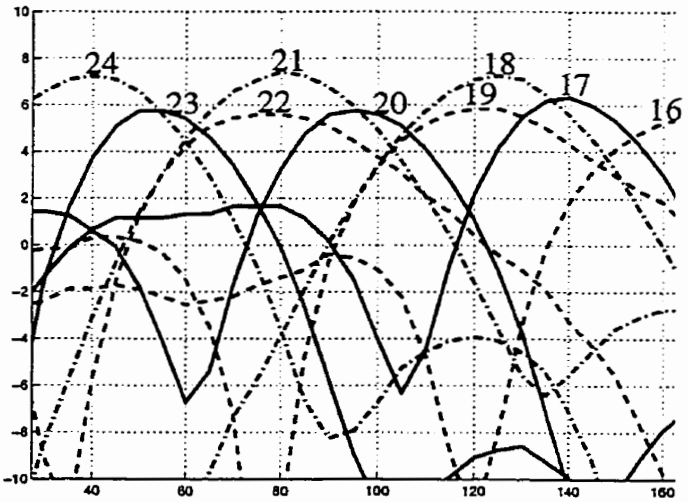

(d): Beams No.16 to 24 of the sub-array for f=1.661 GHz and $\theta_E = 45°$.

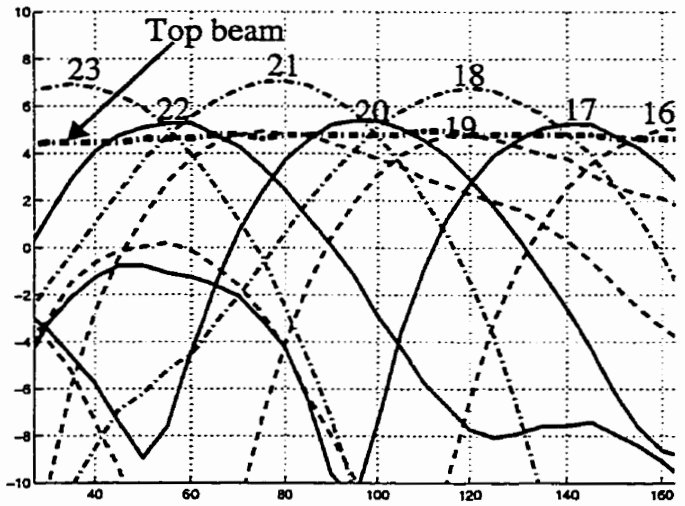

(e): The top beam and beams No.16 to 24 of the sub-array for f=1.525 GHz, $\theta_E = 60°$.

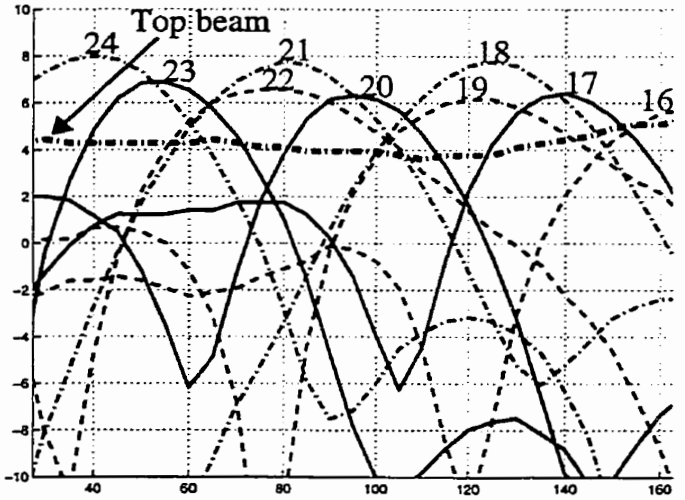

(f): The top beam and beams No.16 to 24 of the sub-array for f=1.661 GHz and $\theta_E = 60°$.

Figure 6.10 Measured gain in dB vs. horizontal angle θ_H *in degree for the global antenna array. The solid curves correspond to the 010 beams, dashed curves to the 110 beams and dash-dotted beams to the 011 beams.*

From Figure 6.10 (a) to (f) we can see that the lowest gain for elevation angles from 20° to 60° when the sub-array was activated was 4.6 dB which was measured in the horizontal direction of $\theta_H = 72°$ at 1.661 GHz and at an elevation angle of 20°. The highest gain measured was about 8 dB. Figures 6.10 (e) and (f) also show the measured gain at an elevation angle of 60° when the top antenna was activated. For elevation angles from 60° to 90°, the gain of the top antenna

was found to increase to 8.08 dB and 6.42 dB for frequencies of 1.525 GHz and 1.661 GHz, respectively. The beam of the top antenna together with that of the sub-array guaranteed a gain higher than 4.6 dB in the overlapped directions.

6.5 Discussion

The measured radiation patterns from the global array prototype when its sub-array was activated were a little different from the expected ones. As can be seen from Figure 6.10, the maximum gains of the 24 beams are different from each other by at most 2 dB. Each beam was also somewhat deflected away from its expected position shown in Figure 6.9. In general, the three beams formed by certain three adjacent channels had different gains, which tended to increase from the 110 beam, to the 010 beam and to the 011 beam and all the beams were deflected in an anti-clockwise direction.

The squint radiation pattern for each unit patch antenna was found responsible for these undesired radiation patterns of the sub-array. In order to form the sub-array, the lower substrate of each unit patch antenna was cut to a trapezoidal shape. This modification to the ground layer, was found to affect the field from the antenna. Some variation of the maximum gains from beam to beam could also have arisen from a deformed aluminum frame. The inclination angle was found to change slightly from facet to facet, causing the inclination angles of the unit antennas to change from one to another by certain amount.

To improve the performance of the array, the lower substrate of each patch antenna can be increased by some amount to decrease the squint in the radiation pattern for each unit antenna. The sacrifice for this is an increase in the size of the array. The second improvement we can make is through the use of a more rigid frame for the antenna array to ensure a uniform inclination angle for each unit antenna. Finally, as mentioned in Section 6.3, the patch antennas used in the array were of the model of Patch 3A. We can use patch antennas of the model of Patch 2A, which has a higher gain, to form the array for increased gain.

6.6 Conclusions

In this chapter we presented the configuration of a global electronically-scanned array prototype with a quasi-hemispherical coverage. As shown by the measurements, the array covered elevation angles from $\theta_E = 20°$ to $\theta_E = 90°$ with a gain higher than 4.6 dB and the measured return loss was lower than -14.5 dB in the receiving and transmitting bands. The use of our newly designed unit patch antenna with a little larger ground substrate for each unit antenna and a more rigid array frame was suggested for a higher overall gain covering the directions of interest.

CHAPTER 7

Conclusions

In the work described in this thesis, broadband microstrip circuits, antennas and antenna arrays were designed for Inmarsat/Msat mobile communications:

Several techniques for broadband microwave circuit and antenna design were established, i.e., an optimized two-stage quarter-wavelength transformer to match two distinct loads, a three point compromise in choosing the impedance of the feed line for a narrow band circuit or antenna, an optimized shunt half-wavelength open stub to tune off the active part of the input impedance of a narrow band circuit or antenna, and a compound half-wavelength open stub which can be realized with both higher and lower impedances than a conventional one.

For the design of radial switches which can be used in an electronically-scanned array or switched-beam array, criteria were established for broadband design. The criteria were used to guide the design and implementation of a switch prototype with performance parameters substantially improved over switches reported in the literature.

For an electronically-scanned antenna array, the concept of a beam controller was proposed and implemented for a beam-forming network with low return loss, low insertion loss, high isolation between the input and a deactivated channel, and good power-delivering balance between activated channels.

Simple air-spaced electromagnetically-coupled patch antennas were designed for applications in arrays. By working with the simulated input impedances and radiated fields, a step-by-step method using Ensemble simulations was used to design the patch antennas with simple off-set feeding circuit. Patch antennas with higher overall gain and a little higher axial ratio and patch antennas with improved axial ratio and a little lower gain were designed.

A beam controller and 9 patch antennas were integrated into a global electronically-scanned array for Inmarsat/Msat mobile communications. Compared with a commercially available mechanically-scanned antenna, the array covers elevation angle from 20° to 90° and is therefore very attractive to inter-continental fleets who may be anywhere on the earth. By scanning electronically instead of mechanically, the array is much faster in satellite acquisition and tracking. Because there is no moving component in the array, it is inherently more robust. Another advantage with the array is its low DC power consumption. The cost of our array should also be very competitive compared with electronically-scanned arrays or switched-beam arrays developed by other groups, due to the use of simple circuits with a small number of PIN diodes.

The array prototype was 37.6 cm in diameter and 12.0 cm in height with a return loss lower than -14.5 dB in both the receiving band (1.525 GHz ~1.559 GHz) and the transmitting band (1.627 GHz ~ 1.661 GHz) and lower than -11.1 dB over the whole band from 1.525 GHz to 1.661 GHz. The measured compound gain, which was defined as the gain of the array less the polarization mismatch factor between the array and an incident wave, was higher than 4.6 dB for all the covered angles.

The array was used for on site satellite communications. There the beam was controlled by a closed-loop electronic controlling circuit developed by other fellow students and colleagues in our laboratory. The controlling circuit switched beam by controlling the bias voltage or current

on each PIN diode in the array while monitoring the received pilot signal from the satellite. In finding the satellite, each of the total beams was turned on sequentially and the beam which gave the highest pilot signal was chosen for communications. In tracking the satellite, should the pilot signal drop because of the rotation of the array with respect to the satellite, the beam on the either side of the present beam was turned on and compared. The beam which gave the higher pilot signal would be chosen as the new beam. This process could be repeated every several tenth of a second.

Under the controlling of such an electronic controlling circuit, on site communication through Msat satellites was demonstrated, together with a Westinghouse Series 1000 Mobile Satellite Telephone System with its mechanically-scanned antenna replaced by our antenna array. Communication was maintained while the array was turned in a way as if the array would be on a car which was making a fast turn.

The overall compound gain achieved thus far was 4.6 dB, which is a little lower than the required 7 dB gain mentioned in Chapter 1. The lowest gain in the covered angles was defined by the minimum gain in the radiation pattern of the array when all its beams were knit together. Because of a relatively small ground plate for each of the 8 tilted patch antennas, the beam of each patch antenna was squint, resulting in lower gains for 110 beams and higher gains for 011 beams compared with that of 010 beams. A little larger ground plate for each patch antenna can be used to avoid a squint beam and thus alleviate the problem and increase the overall gain. The overall gain can also be increased by using a more rigid frame for the antenna array which will guarantee the same inclination angle for all the tilted patch antennas. Our newly designed patch antennas Patch 2A has higher gains than Patch 3A antennas which was used in the present prototype. Using such new patch antennas, the gain of the array can be further increased. With the above three measures we can expect a minimum overall gain of the array of about 6 dB. Another measure which can increase the signal noise ratio is to place the low noise amplifier and duplexer of the receiver under the array. In existing communication products, this amplifier is usually placed 2 to 3 meters away from the antenna with a coaxial cable. Our array is hollow and enough room can be found under it for the electronic controlling circuit and for the low noise amplifier.

After all the measures mentioned above, signal quality comparable to that obtained with existing mechanically-scanned antennas can be expected from our array.

References

[1] J. V. Evans, "Satellite systems for personal communications", IEEE Antennas and Propagation Magazine, Vol. 39, No.3, pp.7-19, 1997.

[2] http://www.acelgroup.ca/glentel/newequipment/index.html

[3] http://www.acelgroup.ca/glentel/equipment/mitsubishi/lmt.htm

[4] P.C. Strickland, "Compact, low profile antennas for MSAT and Mini-M and Std-M Land Mobile satellite communications," International Mobile Satellite Conference, Ottawa, -IMSC'95, pp.340-344.

[5] Charles D. McCarrick, "Mechanically-steered disk antenna for mobile satellite service," International Mobile Satellite Conference, Ottawa, -IMSC'95, pp.345-350.

[6] J. Huang, "Circular polarized Conical Patterns from Microstrip Antennas," IEEE Trans. Antennas and Propagation, Vol.AP-31, No.9, September 1984, pp.991-994.

[7] R. Milne, "A small adaptive array antenna for mobile communications", IEEE AP-S Simp. Digest, June 1985, pp. 797-800.

[8] R. Milne, "An Adaptive Array Antenna for Mobile Satellite Communications," Proc. 2nd Int. Mobile Satellite Conf., JPL Publication 90-7, June 1990, pp.529-534.

[9] http://www.crc.doc.ca/innovation/adapt.html

[10] T. Hori, N. Terada, and K. Kagoshima, "Electronically steerable spherical array antenna for mobile earth station," IEE Int. Antennas and Propagation Conf., 1987, pp.55-58.

[11] M. E. Bialkowski, S. T. Jellett, and R. S. Varnes, "Electronically steered antenna system for the Australian Mobilesat", IEE Proc.-Microw., Antennas, Propag., Vol.143, No.4, pp. 347-352, 1996.

[12] M. E. Bialkowski and N. C. Karmakar, "A two-ring circular phased-array antenna for mobile satellite communications", IEEE Antennas and Propagation Magazine, Vol.41, No.3, pp.14-23, 1999.

[13] S. Ohmori, S. Yamamoto, K. Tanaka, "Phased array tracking antenna system for vehicles," Proceedings of IREECON'91, Sydney 1991, pp.17-20.

[14] J. Aurinsalo, I. Huhtinen, A. Hujanen, A. Jongejans, I. Marttila, R. Mutanen, I. Pitkanen, P. Rinous, T. Salminen, S. Tallqvist, M-N. Travers, "Steerable L-band antennas for land mobile terminals," 44th IEEE Vehicular Technology Conference, Stockholm, pp.600-604, 1994.

[15] P. Lahaie and M. Lecours, "Analysis and measurements of reflection phase shifters at 1.5 and 18.5 GHz", ANTEM'98 Symposium on Antennas and Electromagnetics, Ottawa, August 1998, pp. 163-167.

[16] S. Damphousse, M. Lecours, and C. Vergnolle, "Design of a low-cost MIC Antenna Array Network at Microwave Frequencies", ANTEM Symposium on Antennas and Electromagnetics, Montreal, August 1996, pp 563-567.

[17] S. Damphousse, "Réalisation de déphaseurs numériques a 9.71 GHz pour les réseaux adaptatifs d'antennes plaques", thèse de Maîtrise, Université Laval, 1996.

[18] T. Breahna, "Conception d'antennes microruban à bande élargie en technologie micro-ruban pour une antenne réseau à balayage électronique", Thèse de Maîtrise, Université Laval, 1999.

[19] M. Lecours, M. Pelletier, P. Lahaie, T. Breahna, Q. Wang, G.-Y. Delisle, R. Daviault and M. Lefebvre., "Experimental results with a circular electronically steered antenna for mobile satellite communications", Sixth International Mobile Satellite Conference, Ottawa, June 1999, pp.388-392.

[20] Q. Wang, M. Lecours, and C. Vergnolle, "Optimization of switches for radial satellite antenna array applications", Sixth International Mobile Satellite Conference, Ottawa, June 1999, pp.393-397.

[21] Q. Wang, M. Lecours, and C. Vergnolle, "Criteria for wide- band radial switch design", IEEE Transactions on Microwave Theory and Techniques, accepted for publication, Nov., 1999.

[22] Q. Wang, "Test results from an electromagnetically-coupled, circularly-polarized patch antenna at 1.6 GHz for mobile satellite communications", Internal Report, LRTS, Department of Electrical and Computational Engineering, Laval University, March 15, 1999.

[23] Q. Wang and M. Lecours, "Beam controller for electronically-scanned antenna array applications", submitted to IEEE Transactions on Microwave Theory and Techniques, Dec., 1999.

[24] R. S. Varnes and M. E. Bialkowski, "A switched radial power divider/combiner for a mobile satellite antenna application", Microwave Journal, pp.22-36, Nov., 1996.

[25] T. Edwards, "Foundations for Microstrip Circuit Design", John Wiley & Sons, New York, 1991, p. 13. ISBN 0-471-93062-8.

[26] P. S. Hall and C. M. Hall, " Coplanar corporate feed effects in microstrip patch array design, " IEE Proceedings, Pt.H, Vol. 135,No.3, 1988, pp.180-186.

[27] http://www.paratek.com/index.htm

[28] "Handbook for electronics engineering technicians", pp.11-19, Edited by Milton Kaufman, Arthur Seidman, and Perry J. Sheneman, McGraw-Hill Book Company, 1984. ISBN 0-07-033408-0.

[29] Robert A. Sainati, "CAD of microstrip antennas for wireless applications", p.140, Artech House, Boston, 1996, ISBN 0-89006-562-4.

[30] Bharathi Bhat and Shiban K. Koul, "Stripline-like transmission lines for microwave integrated circuits", p.675, Wiley Eastern Limited, New Delhi, 1989.

[31] N. C. Karmakar and M. E. Bialkowski, "Circularly polarized aperture-coupled circular microstrip patch antennas for L-band applications", IEEE Transactions on Antennas and Propagation, Vol.47, no.5, pp.933-940, May 1999.

[32] W. L. Stutzman and G. A. Thiele, "Antenna Theory and Design", p.66, John Wiley & Sons, New York, 1981. ISBN 0-471-00458-X.